EFFICIENT DESIGN METHODS FOR MULTIRATE FILTER BANKS AND THEIR APPLICATIONS

by

Hua Xu

M. Eng , Southeast University, 1991

A Dissertation Submitted in Partial Fulfillment of the
Requirements for the Degree of

DOCTOR OF PHILOSOPHY

in the Department of Electrical and Computer Engineering

We accept this dissertation as conforming
to the required standard

Dr. A. Antoniou, Co-supervisor, Dept. of Elect. and Comp. Eng.

Dr. W.-S. Lu, Co-supervisor, Dept. of Elect. and Comp. Eng.

Dr. P. Agathoklis, Departmental Member, Dept. of Elect. and Comp. Eng.

Dr. P. Fisher, Outside Member, Dept. of Health Information Sci.

Dr. M. O. Ahmad, External Examiner (Concordia University)

Supervisors: Drs. A. Antoniou and W.-S. Lu.

Abstract

Over the last decade, multirate digital signal processing techniques have found many applications in speech and image compression, the digital audio industry, statistical and adaptive signal processing, numerical solution of differential equations, and in many other fields. Research activity in the area of multirate signal processing has been growing quickly and is producing a large amount of new literature in the design of multirate digital filter banks, multidimensional multirate systems, wavelet representations, and their applications in audio and image compression etc.

This thesis is dedicated to the design of multirate filter banks and their applications in audio and image compression, and it consists of three parts. Part I is concentrated on the design of 1-D filter banks. Several methods are proposed for the design of two-channel QMF banks with near-perfect reconstruction. The methods have improved design efficiency and lead to QMF banks with satisfactory performance. Low-delay QMF banks, which are highly desired in real-time applications, are also considered. A null-space projection method is then proposed to design perfect reconstruction QMF banks with either linear-phase responses or low reconstruction delays. On the design of multi-channel cosine-modulated QMF banks, an efficient method is proposed which can be used in the design of both conventional and low-delay QMF banks. Part II is devoted to studies on nonseparable 2-D filter banks where the design of four-channel hexagonal QMF banks and two-channel diamond-shaped QMF banks are investigated, leading to several efficient design methods. Part III describes applications of the 1-D and 2-D filter banks designed by the design methods developed in Parts I and II of the thesis in audio and image compression. Some comparisons are made with the current international standards.

Examiners:

Dr. A. Antoniou, Co-supervisor, Dept. of Elect. and Comp. Eng.

Dr. W.-S. Lu, Co-supervisor, Dept. of Elect. and Comp. Eng.

Dr. P. Agathoklis, Departmental Member, Dept. of Elect. and Comp. Eng.

Dr. P. Fisher, Outside Member, Dept. of Health Information Sci.

Dr. M. O. Ahmad, External Examiner (Concordia University)

To my parents, my wife Qin, and my new-born baby Jason.

Acknowledgements

The author would like to thank his supervisors, Professors A. Antoniou and W.-S. Lu of the Department of Electrical and Computer Engineering, for their encouragement, patience and advice during the course of this research, and for their help in the preparation of this thesis.

Financial assistance provided by Professors A. Antoniou and W.-S. Lu's research grants from Micronet, NCE Program, and NSERC is also gratefully acknowledged.

Contents

List of Tables

List of Figures

List of Abbreviations

1-D	one-dimensional
2-D	two-dimensional
APU	additions per unit
BFGS	Broyden-Fletcher-Goldfard-Shanno
bpp	bits per pixel
DCT	discrete cosine transform
DWT	discrete wavelet transform
FIR	finite-duration impulse response
HDTV	high-definition television
IIR	infinite-duration impulse response
ISO	International Standard Organization
JPEG	Joint Picture Expert Group
MFLOPS	floating-point operations in millions
MPEG	Moving Picture Expert Group
MPU	multiplications per unit
NI	number of iterations
PCRE	peak complex recosntruction error
PRE	peak reconstruction error
QMF	quadrature mirror filter
SNR	signal-to-noise ratio
SNR_s	signal-to-noise ratio with a step input
SNR_r	signal-to-noise ratio with a random input
STFT	short-time Fourier transform
SVD	singular value decomposition

Chapter 1

Introduction

Multirate digital signal processing techniques find applications in speech and image compression, the digital audio industry, statistical and adaptive signal processing, the numerical solution of differential equations, and in many other fields. The discipline also fits naturally with certain special classes of time-frequency representations such as the short-time Fourier transform and the wavelet transform, which are useful in analyzing the time-varying nature of signal spectra.

Over the last decade, there has been a tremendous growth of activity in the area of multirate signal processing, perhaps triggered by the first book in this field [1]. Particularly impressive is the amount of new literature in multirate digital filter banks, multidimensional multirate systems, and wavelet representations.

In the thesis several new methods which could be used in the design of a wide range of one-dimensional (1-D) and two-dimensional (2-D) filter banks are investigated and some of the filter banks designed are used in audio and image compression.

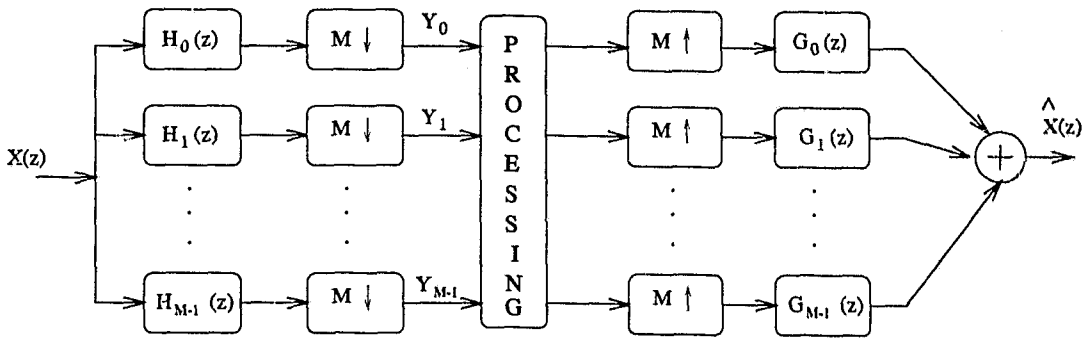

Figure 1.1: A general multirate filter bank system.

1.1 Filter Banks and Design Considerations

1.1.1 Multirate Filter Bank

Fig. 1.1 shows the block diagram of a general multirate filter bank system, in which the spectrum of the input signal, $x(n)$, is divided into frequency bands using filters with impulse responses $h_m(n)$ in the analysis filter bank. These channel signals are then *maximally decimated* individually at a rate of $M:1$ which results in the aliased channel outputs

$$Y_m(e^{j\omega}) = \frac{1}{M}\sum_{r=0}^{M-1} X(e^{j(\frac{\omega}{M}-\frac{2\pi r}{M})})H_m(e^{j(\frac{\omega}{M}-\frac{2\pi r}{M})}) \qquad (1.1)$$

For most applications the filters in the analysis filter bank have uniform passband. Therefore, the set of decimated signals, $\{y_m(n)\}$, form a critically sampled *time-frequency* representation of the original signal, $x(n)$.

In the absence of any processing, like quantization and coding, the output signal $\hat{x}(n)$ is simply a reconstructed version of the input, $x(n)$. The reconstruction is accomplished by *up-sampling* the channel signals to their original sampling rate, then passing each signal through a synthesis filter with impulse responses $g_m(n)$,

and summing the results. The resulting reconstruction equation is given by

$$\hat{X}(e^{j\omega}) = \sum_{m=0}^{M-1} \frac{1}{M} \sum_{r=0}^{M-1} X(e^{j(\omega-\frac{2\pi r}{M})}) H_m(e^{j(\omega-\frac{2\pi r}{M})}) G_m(e^{j\omega}) \tag{1.2}$$

For ideal bandpass filters, it is simple to show that Eqn. (1.2) results in an exact reconstruction of the input signal. For such system, the aliasing terms, (i.e., terms involving $r \neq 0$), are zero which modifies (1.2) to

$$\hat{X}(e^{j\omega}) = X(e^{j\omega}) \sum_{m=0}^{M-1} \frac{1}{M} H_m(e^{j\omega}) G_m(e^{j\omega}) = X(e^{j\omega}) \tag{1.3}$$

if

$$\sum_{m=0}^{M-1} \frac{1}{M} H_m(e^{j\omega}) G_m(e^{j\omega}) = 1 \tag{1.4}$$

Since ideal filters are not realizable, in practice the channel signals are always aliased. However, in a filter bank environment it is possible to choose proper filters to cancel the aliasing and achieve analysis/synthesis systems that achieve exact reconstruction even though all the individual channel signals are aliased.

1.1.2 Design Problems

The system in Fig. 1.1 can be considered to be a hierarchical. At the lowest level there are the individual filters which typically consist of lowpass, bandpass, and highpass filters. At the second level the analysis filters are considered collectively as the analysis filter bank and the synthesis filters are considered collectively as the synthesis filter bank. At the third level, the analysis filter bank and synthesis filter bank are viewed as a so-called *analysis/synthesis* system which is formed by directly connecting the analysis outputs to the synthesis inputs without any processing in between. The final level in the hierarchy is the complete system in which processing

or coding of the analysis outputs is considered. In the rest of the section, design considerations and constraints for each of the levels are described.

A. Filters

For the filters in the analysis filter bank, the stopband, passband, and transition band characteristics of the individual filters must be constrained to control the magnitude, phase, and aliasing distortion of the channel signals. For the filters in the synthesis filter bank, in addition to the reconstruction issues, exactly the same properties must be addressed so as to control the effects of the processing distortion in the reconstructed signal. If the computational complexity is a critical issue, the type of filters to be used, like finite-duration impulse response (FIR) filter or infinite-duration impulse response (IIR) filter, the parameter sensitivity of the filters, and implementation structure must also be considered during the design.

B. Filter Banks

Since the total set of channel signals constitutes a time-frequency representation, it is important to ensure that the union of frequency bands of analysis filters or synthesis filters covers the entire baseband. In addition, the realization of the filter bank needs to be efficient.

C. Analysis/Synthesis System

The goal of the analysis/synthesis system in the absence of channel processing is to reconstruct the input signal at the output. Therefore, the distortion due to aliasing, and the system distortions in magnitude and phase responses must be minimized.

D. Complete System

The complete system explicitly includes the analysis and synthesis filter banks, and the processing on decimated multirate signals such as quantization and coding.

The final goal of the design is to maximize the system performance in the actual processing environment and reject the distortion introduced by the processing.

In this thesis, primary attention will be given to the first three design issues. Complete systems with coding mechanism are used in Chapter 8 when applications of the analysis/synthesis systems are addressed.

1.2 Review of the Previous Work

Most of the work on maximally decimated analysis/synthesis systems has been developed based on the earlier work on the frequency-domain processing of speech [2] and on filter bank for TDM/FDM conversion [3]. An early theoretical framework for signal analysis and reconstruction was formulated by Portnoff [4] using the short-time Fourier transform (STFT). This work provided insight with respect to the narrowband-wideband nature of the time-frequency representation, the filter constraints for reconstruction, and the relationships between discrete-time and continuous-time analogues. However, the question of how to design realizable maximally decimated time-frequency systems able to exactly reconstruct the input was still unanswered.

In 1976, Crochiere et al. [5] introduced the subband coder as a new technique for coding speech waveforms. In this method the speech is split into four non-uniform frequency bands each of which is modulated to the baseband. The signal in each channel is then lowpass filtered and decimated. The dual process is applied for reconstruction. Filters of 125 taps are used to reject the aliasing distortion.

1.2.1 Quadrature-Mirror Filter Bank

Almost at the same time, Croisier et al. [6] proposed a two-band filter bank system now known as quadrature mirror filter (QMF) bank which consists of two analysis filters and two synthesis filters. Certain frequency-domain relationships must be satisfied for the filters to cancel the aliasing. If linear-phase FIR filters are used, there will be no phase distortion in the output signal. However, the non-unity magnitude, which introduces magnitude distortion, still has to be minimized in the design. A remarkable feature of QMF banks is that they can be implemented using the efficient polyphase structure [7] where multiplications and additions can be shared between the lowpass and highpass filtering. The two-channel QMF bank system can be cascaded in a tree structure to perform a variety of multi-band spectral decompositions and its use in an octave-band structure for the subband coder has substantively improved the speech quality [8].

The problem of designing QMF banks have been a subject for research since the middle of 70's. Johnston [9] designed a family of QMF banks by minimizing a weighted stopband-ripple/system reconstruction error. The results have been widely used as a standard set of QMF banks for many years since their publication in 1980. Later, Barnwell [10] proposed a QMF structure using IIR filters where either phase or magnitude distortion could be eliminated. In [11] a time-domain algorithm was proposed for the design of QMF banks which involves calculation of the eigenvalues and eigenvectors of a matrix in each step of an iterative procedure. Recently, Chen and Lee [12] introduced an iterative algorithm that improves design efficiency over the design methods using conventional minimization.

1.2.2 Filter Banks with Perfect Reconstruction

In the design methods mentioned above, the overall amplitude distortion is minimized but not completely eliminated, which leads to near-perfect reconstruction QMF banks. Smith and Barnwell [13] [14] , and Mintzer [15] proposed methods for the design of filter banks that yield perfect reconstruction of the input signals. These filters were termed conjugate quadrature filters or CQF's [14]. In addition, Smith and Barnwell [16] [17] developed the so-called AC-matrix formulation for analyzing multi-band filter banks. In particular, necessary and sufficient conditions for N-band perfect reconstruction filter banks were obtained.

Based on certain polyphase representations [7] of the filter involved, Vetterli [18] and by Vaidyanathan [19] proposed a variation of the AC matrix formulation. Vaidyanathan reported a paraunitary structure for the polyphase matrix which, although was only sufficient to ensure perfect reconstruction, greatly simplified the design procedure. Later, improvements to the original scheme were reported [20] [21]. Recently, a Lagrange multiplier approach was proposed by Horng and Willson on the design of two-channel perfect-reconstruction linear-phase FIR filter banks [22].

1.2.3 Cosine-Modulated QMF Bank

For uniform multi-band systems it was shown that satisfactory performance of the filter bank can be achieved by only canceling the major aliasing components in the reconstructed signal [23] - [26]. The major benefit of this approach, however, was the improvement in computational efficiency. This is because each individual filter

in the bank is represented as a cosine-modulation of the baseband filter in the form

$$h_k(n) = h_0(n) \cos\left(\frac{\pi nk + \phi}{N}\right) \tag{1.5}$$

By exploiting redundant arithmetic present among the bandpass filters, these partial aliasing cancellation filter banks (often called pseudo-QMF banks or cosine-modulated QMF banks) achieve their enormous efficiency over tree structured QMFs in multi-band decomposition. One of the most important applications of cosine-modulated filter banks is in the Moving Picture Expert Group (MPEG) audio compression scheme [27].

Several methods for the design of multi-channel cosine-modulated QMF banks have been proposed. In [26][28][29], near-perfect reconstruction filter banks were designed by minimizing a weighted objective function which is a fourth-order function of the coefficients of the prototype filter. In [30] a spectral factorization approach for the design of pseudo-QMF banks without using optimization was proposed. In [31] a lattice structure that leads to a perfect reconstruction filter bank was presented. In [32] an extended lapped transform is described which also achieves perfect reconstruction filter bank. Recently, in [33] a method for the design of near-perfect reconstruction QMF banks was proposed. It appears that this approach can achieve high stopband attenuation and very low aliasing and amplitude distortions.

1.2.4 Low-Delay Filter Banks

The reconstruction delay is an important issue in real-time applications and to date there are relatively few results available on the design of low-delay filter banks. For many popular filter banks such as two-channel QMF banks and multi-channel cosine-modulated QMF banks, the reconstruction delay is fixed to be $N - 1$ where N is

the filter length. When high order filters are needed in order to achieve satisfactory performance, or in a tree structure where two-channel filter banks are cascaded, long reconstruction delays are unavoidable, which is highly undesired for real-time applications.

In [34] [35], a time-domain design method is studied for the design of low-delay two-channel filter banks. Some interesting observations and useful comparisons were made and low-delay tree-structure systems were constructed using the obtained low-delay two-channel filter banks. For the design of low-delay cosine-modulated QMF banks, a class of generalized cosine-modulated filter banks has been proposed in [36] whose reconstruction delay is not fixed but could be chosen among several values. Some preliminary results were also reported in [37] on low-delay cosine-modulated filter banks through designing several filter banks with various-lengths but a fixed reconstruction delay.

1.2.5 2-D Filter Banks

Since 1984, research on 2-D subband coding schemes has also been intensive. Vetterli [38] was the first to propose two-band nonseparable QMF banks with quincunx decimation lattices, in which the aliasing terms are completely cancelled. Using linear-phase filters with certain restrictions on the order of filters, it was shown that the reconstructed signal coincides with the input signal up to a constant factor and a spatial shift. A separable 2-D QMF bank where 1-D QMFs operate first on the rows and then on the columns of 2-D inputs or vice versa was also proposed in [38]. In 1986 Woods and O'Neil [39] constructed a 2-D subband image coder using a separable 2-D QMF bank and reported that the subband coder has improved the signal-to-noise ratio (SNR) and that the subjective performance compared to that

obtained by using the adaptive discrete-cosine transform (DCT). Smith et al. [40] and Ramstad [41] suggested several 2-D perfect reconstruction recursive filter banks based on separable filters. In [42] both recursive and nonrecursive filter banks were investigated.

In a separable 2-D QMF bank the frequency spectrum of the input signal is split into central lowpass, horizontal highpass, vertical highpass, and diagonal highpass bands in which the diagonal highpass band contains a mixture of the two orientations. To avoid this problem, a nonseparable four-band hexagonal QMF bank based on hexagonal sampling was proposed by Simoncelli and Adelson [43] where the analysis and synthesis filters have a similar structure to that of 1-D QMF banks. It has been shown that aliasing in the system output is cancelled and amplitude distortion can be minimized through the design. Another important class of nonseparable 2-D filter banks is the class of two-band diamond-shaped filter banks, in which the frequency spectrum is split into diamond-shaped lowpass and four-corner highpass bands. This type of filter banks has been applied for image and video compression in high-definition television (HDTV) coding and the results obtained appear to be satisfactory [44][45]. Most existing methods for the design of nonseparable 2-D diamond-shaped filter banks are based on the application of transformations to 1-D prototype filters [45] - [47].

In the area of generalized multidimensional bank design, Viscito and Allebach [48] extended the theory of perfect reconstruction filter banks to arbitrary downsampling lattices introduced in [49][50]. The scheme of [48] is based on the concept of the multidimensional polyphase transfer matrix. It was shown that if the analysis polyphase matrix is formed by cascading constant coefficient matrices with diagonal shift matrices between them, its inverse can be readily evaluated. The synthesis

filters are then derived from this matrix inverse. In [51], a theory of multirate operations on arbitrary multidimensional lattices and a numerical optimization method for designing the multidimensional filter banks are proposed.

1.3 Scope of the Thesis

This thesis consists of three parts. Part I, comprising Chapters 2 to 5, is concentrated on several methods for the design of 1-D filter banks; Part II (Chapter 6) is devoted to studies on the design of 2-D filter banks; Part III, comprising Chapters 7 and 8, describes applications of the 1-D and 2-D filter banks designed in Parts I and II of the thesis in audio and image compression.

The major concern of Chapter 2 is the design of near-perfect two-channel QMF banks from the frequency domain. First an improved version of the iterative method, originally proposed in [12], is described. A simple and explicit formula for the precise evaluation of integrals involved in the objective function is derived. As will be shown in the design examples, this significantly reduces the design complexity. To achieve low reconstruction delay in a QMF bank, a generalized two-channel QMF bank is proposed, whose reconstruction delay is adjustable, leading to low-delay filter banks.

Chapter 3 is concerned with the design of QMF banks from the time domain. A new approach is described in which the perfect reconstruction condition is formulated in the time-domain instead of in the frequency domain as in Chapter 2. An iterative method similar to that in Chapter 2 is used to reduce the design complexity. For the purpose of designing low-delay QMF banks, a time-domain perfect reconstruction condition is derived which can be minimized efficiently by the iterative method.

Chapter 4 describes a null-space projection method for the design of two-channel perfect reconstruction QMF banks. In the proposed method two filters, i.e., the analysis lowpass filter and the synthesis lowpass filter, need to be designed. The analysis lowpass filter is first designed by a conventional FIR filter design method. It is then followed by solving a constrained optimization problem using the null-space project method to obtain the synthesis lowpass filter. The proposed method is used in the design of two-channel perfect reconstruction QMF banks with normal and low reconstruction delays.

Chapter 5 describes several methods for the design of cosine-modulated QMF banks, which have been widely used in many applications due to their high design efficiency and implementation efficiency. In order to design conventional cosine-modulated QMF banks, a new iterative algorithm is proposed that greatly improves the design efficiency and leads to filter banks with high stopband attenuation and low aliasing and amplitude distortions. A general version of the algorithm is then developed, which can be used to design low-delay cosine-modulated QMF banks. This algorithm is based on a weighted objective function that depends on the error between the actual frequency response and that of a linear-phase ideal filter. Artifacts that can occur in the amplitude responses of the analysis and synthesis filters when designing low-delay filter banks can be reduced significantly by simply adding one more error component to the objective function.

Although separable 2-D filter banks are easy to implement, the class of non-separable 2-D filter banks are believed to be more adequate for use in many image processing related applications. In Chapter 6 several design methods for the design of four-channel hexagonal QMF banks and two-channel diamond-shaped QMF banks are proposed. It will be demonstrated that the hexagonal filter banks de-

signed using the proposed methods are superior to that described in [43] in terms of design efficiency and system performance. The problem of designing diamond-shaped QMF banks is solved by using some iterative methods. Unlike the existing methods, no 1-D to 2-D transformation is required in our designs. The proposed methods show high design efficiency and design flexibility.

In Chapter 7 a 32-band filter bank is designed using the iterative method proposed in Chapter 5 and comparisons of the filter banks designed with the current MPEG filter bank are made. In order to reduce the reconstruction delay of the MPEG audio codec, a cosine-modulated QMF bank whose reconstruction delay is about half of that in the current MPEG filter bank is designed and implemented using an efficient polyphase structure. Some sample sound signals are used to test the designed filter bank.

In Chapter 8, subband coding of images is studied. A two-stage subband coding system is constructed using diamond-shaped filter banks, the DCT transformation, and Huffman coding. In addition, the Daubechies wavelet transform is used in a separable 2-D multi-stage subband coding system. Comparisons of the wavelet transform method with the current Joint Picture Expert Group (JPEG) coding scheme are conducted using sample images.

Chapter 2

Improved Iterative Methods for the Design of QMF Banks

2.1 Introduction

The importance of quadrature-mirror-filter (QMF) banks in subband coding has been widely recognized and various analysis, design, and implementation issues pertaining to these filters have been intensively studied since the mid 70's. The quadrature mirror structure of QMF banks leads to the complete cancellation of interband aliasing due to the overlapping filter responses. If the filters involved have symmetrical impulse responses of finite duration (FIR), no phase distortion will occur and, therefore, the design can be focused on selecting filter parameters so as to minimize the system's amplitude distortion.

Like the design of conventional digital filters, the design of QMF banks can be accomplished by using least-squares and minimax methods. In [52], the reasoning of using the least-squares criterion for telecommunication applications has been clarified. On the other hand, in [12][53][54] it has been shown that minimax design can be accomplished if an adequately updated weighting function is included in a

least-squares objective function. In either the non-weighted or weighted case, the least-squares objective function is a fourth-order function of the design parameters. Hence the design is a typical unconstrained, *nonquadratic* optimization problem. Recently, an iterative design method has been proposed by Chen and Lee [12] in which the least-squares objective function is modified by assigning a set of appropriate values, which form a vector $\mathbf{h}$, to a part of the design parameters in such a way as to obtain a *quadratic* and globally convex objective function. Upon obtaining the global minimum point, say $\mathbf{f}$, the value of $\mathbf{h}$ is updated accordingly and is then re-assigned to the same part of the design parameters. This procedure is repeated until $\mathbf{f}$ and $\mathbf{h}$ become identical. Since in each iteration $\mathbf{f}$ can be formulated in closed form and only a few iterations are needed for convergence when a good initial $\mathbf{h}$ is used, the algorithm is efficient and good performance is achieved in the filter bank. In the method described two integrals are involved in the objective function, which are evaluated by discretization. This gives rise to two problems. First, the solution obtained actually minimizes the discretized version of the objective function rather than the objective function itself. This can degrade the performance of the QMF bank designed. Second, in order to reduce the performance degradation the density of sample points needs to be high, which leads to increased computational complexity. In this chapter, we describe an improved version of the above algorithm in which the integral discretization is avoided by deriving a simple and explicit formula for the precise evaluation of the two integrals. As a result, filter banks with better performance can be designed with considerably reduced computational complexity. Design examples are demonstrated to show the proposed algorithm and comparisons are made in terms of design efficiency.

For real-time or quasi-real-time applications, filter banks with low reconstruc-

tion delay are highly desired. Unfortunately, in conventional QMF banks the filter length N is required to be fairly high in order to achieve satisfactory performance. Consequently, the reconstruction delay, which is $(N-1)$ sampling periods, can become too long. A time-domain approach to the design of analysis/synthesis systems with low reconstruction delays was proposed in [34]. In this chapter, we propose a two-channel low-delay QMF bank, and the iterative algorithm mentioned above is extended to the design of low-delay QMF banks, first in a discretization version and then in an improved version in which simple and explicit expressions are derived for the precise evaluation of the objective function. This increases the computational efficiency during the design and improves the quality of the filter banks designed. Design examples are illustrated and comparisons are made with designs from [34] in terms of design efficiency, performance of the resulting filter banks, implementation aspects, etc. By employing the proposed method, a family of two-channel low-delay QMF banks were designed which could be used in different kinds of applications.

From experiments, it is found that the iterative method can achieve filter banks of good performance with high design efficiency. To investigate the method further, some analysis has been done concerning such aspects as the choice of initial points and convergence speed.

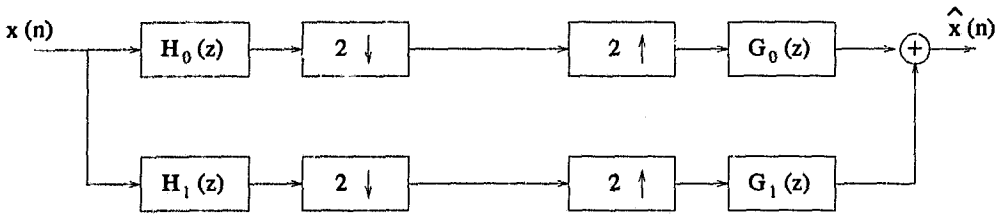

Figure 2.1: A two-band filter bank.

2.2 Design of Conventional QMF Banks

2.2.1 Objective Function

Consider the two-band filter bank depicted in Fig. 2.1. The input-output relation is given by

$$\begin{aligned}\hat{X}(z) = &\tfrac{1}{2}[H_0(z)G_0(z) + H_1(z)G_1(z)]X(z) \\ &+\tfrac{1}{2}[H_0(-z)G_0(z) + H_1(-z)G_1(z)]X(-z)\end{aligned} \tag{2.1}$$

where the second term on the right-hand side represents aliasing due to the decimation operation. By assuming that $H_1(z) = H_0(-z)$, $G_0(z) = H_0(z)$, and $G_1(z) = -H_0(-z)$, which, in general, are referred to as *quadrature-mirror* relationships, we obtain a QMF bank in which the aliasing term is completely eliminated, and (2.1) becomes

$$\hat{X}(z) = \tfrac{1}{2}\,[H_0^2(z) - H_0^2(-z)]X(z) \tag{2.2}$$

If FIR filters with symmetrical impulse responses are used in the QMF bank, which is referred to as the *conventional* QMF bank, then the frequency response of filter H_0 can be expressed as

$$H_0(e^{j\omega}) = M_h(\omega)\; e^{-j\omega(N-1)/2} \tag{2.3a}$$

where

$$M_h(\omega) = 2\,\mathbf{h}^T\mathbf{c}(\omega) \tag{2.3b}$$

$$\mathbf{h} = [\, h_0 \;\; h_1 \;\; \cdots \;\; h_{N/2-1} \,]^T \tag{2.3c}$$

$$\mathbf{c}(\omega) = [\, \cos{(N-1)\omega/2} \;\; \cdots \;\; \cos{\omega/2} \,]^T \tag{2.3d}$$

and N is the length of the filter, which is assumed to be even. From (2.2) and (2.3), the perfect reconstruction condition of the QMF bank assumes the form

$$T(\omega) \equiv M_h^2(\omega) + M_h^2(\omega+\pi) = 1 \tag{2.4}$$

and the system delay is $(N-1)$ sampling periods. In order to design a filter bank satisfying (2.4), an objective function is defined as

$$E = E_1 + \alpha E_2 \tag{2.5a}$$

where

$$E_1 = \int_0^{\pi} [T(\omega) - 1]^2 d\omega \tag{2.5b}$$

and

$$E_2 = \int_{\omega_s}^{\pi} M_h^2(\omega) d\omega \tag{2.5c}$$

The parameter α is a positive weight that can be used to control the stopband attenuation for H_0 and ω_s is the stopband edge.

2.2.2 Improved Iterative Algorithm

The basic idea in the iterative algorithm [12] is that instead of directly minimizing the objective function in (2.5a), which is a fourth-order function of parameter vector **h**, one minimizes the modified objective function

$$E' = E_1' + \alpha E_2' \tag{2.6a}$$

where

$$E_1' = \int_0^{\pi} [T'(\omega) - 1]^2 d\omega \tag{2.6b}$$

$$E_2' = \int_{\omega_s}^{\pi} M_f^2(\omega) d\omega \tag{2.6c}$$

$$T'(\omega) = M_h(\omega) M_f(\omega) \; + \; M_h(\omega + \pi) M_f(\omega + \pi) \tag{2.6d}$$

$$M_f(\omega) = 2 \; \mathbf{f}^T \mathbf{c}(\omega) \tag{2.6e}$$

$$\mathbf{f} \; = [\; f_0 \; f_1 \; \cdots \; f_{N/2-1} \;]^T \tag{2.6f}$$

under the assumption that coefficient vector $\mathbf{h}$ is *fixed* with respect to the minimization. Obviously, as a function of $\mathbf{f}$, the modified objective function E' is *quadratic* and globally convex and, therefore, its minimum can be obtained easily. Having obtained the minimum point of E', say $\mathbf{f}$, vector $\mathbf{h}$ is updated using a linear combination of $\mathbf{f}$ and $\mathbf{h}$ as

$$\mathbf{h} := (1 - \tau)\mathbf{h} + \tau \mathbf{f} \tag{2.7}$$

where τ is a smoothing parameter between 0 and 1. With an appropriate choice of τ, which is found to be in a vicinity of 0.5, $\mathbf{f}$ will quickly converge to $\mathbf{h}$ and an optimal design parameter vector results. In the approach in [12], discretization is used to evaluate E_1' and E_2'. An alternative approach is to derive a closed-form and explicit formulation of E' as a quadratic function of $\mathbf{f}$ without discretizing E_1' and E_2'. As will be shown, this formulation in conjunction with the iterative procedure described above leads to improved computation efficiency and performance in the designed filter bank.

From (2.6b) and (2.6d), E_1' can be written as

$$E_1' = 4\mathbf{f}^T \mathbf{U} \mathbf{f} \; - \; 8\pi \mathbf{h}^T \mathbf{f} \; + \; \pi \tag{2.8}$$

where

$$\mathbf{U} = \int_0^{\pi} [M_h(\omega)\mathbf{c}(\omega)+M_h(\omega+\pi)\mathbf{c}(\omega+\pi)][M_h(\omega)\mathbf{c}(\omega)+M_h(\omega+\pi)\mathbf{c}(\omega+\pi)]^T \, d\omega \quad (2.9)$$

with $\mathbf{c}(\omega)$ given by (2.3d) and

$$M_h^2(\omega) = 4 \sum_{n=0}^{N/2-1} \sum_{m=0}^{N/2-1} h_n h_m \cos\left[\left(n - \frac{N-1}{2}\right)\omega\right] \cos\left[\left(m - \frac{N-1}{2}\right)\omega\right] \quad (2.10)$$

From (2.3), (2.9) and (2.10) straightforward but somewhat extensive analysis shows that the $(i,\ j)th$ entry of matrix $\mathbf{U}$ in (2.9) is given by

$$u_{ij} = \pi \sum_{n=0}^{N/2-1} \sum_{m=0}^{N/2-1} h_n h_m \left\{\sum_{l=1}^{8} [1+(-1)^{k_l'}]\delta(k_l)\right\}, \quad 1 \le i,\ j \le N/2 \quad (2.11)$$

where

$$\delta(k_l) = \begin{cases} 1\ , & k_l = 0 \\ 0\ , & \text{otherwise} \end{cases}$$

$$k_1 = \beta+\gamma+\xi+\eta, \quad k_2 = \beta+\gamma+\xi-\eta$$

$$k_3 = \beta+\gamma-\xi+\eta, \quad k_4 = \beta+\gamma-\xi-\eta$$

$$k_5 = \beta-\gamma+\xi+\eta, \quad k_6 = \beta-\gamma+\xi-\eta$$

$$k_7 = \beta-\gamma-\xi+\eta, \quad k_8 = \beta-\gamma-\xi-\eta$$

$$\beta = n - \frac{N-1}{2}$$

$$\gamma = m - \frac{N-1}{2}$$

$$\xi = \frac{N+1}{2} - i$$

$$\eta = \frac{N+1}{2} - j$$

$$k_1' = m-j+1, \quad k_2' = m+j-N$$

$$k_3' = k_1', \quad k_4' = k_2'$$
$$k_5' = -k_2', \quad k_6' = -k_1'$$
$$k_7' = -k_2', \quad k_8' = -k_1'$$

Now from (2.6c),

$$E_2' = 4\mathbf{f}^T \left[\int_{\omega_s}^{\pi} \mathbf{c}(\omega)\mathbf{c}^T(\omega)\, d\omega\right] \mathbf{f}$$
$$= 4\mathbf{f}^T \mathbf{U}_s \mathbf{f} \tag{2.12}$$

where the $(i,\ j)th$ entry of $\mathbf{U}_s$ is given by

$$u_{ij}^{(s)} = \int_{\omega_s}^{\pi} \cos\left[\left(i-1-\frac{N-1}{2}\right)\omega\right] \cos\left[\left(j-1-\frac{N-1}{2}\right)\omega\right]\, d\omega$$
$$= \begin{cases} (\pi-\omega_s)/2 - \sin[(2i-N-1)\omega_s]/(4i-2N-2)\ , & i=j \\ \sin[(i-j)\omega_s]/(2j-2i) - \sin[(i+j-N-1)\omega_s]/(2i+2j-2N-2)\ , & i\neq j \end{cases} \tag{2.13}$$

Equation (2.13) was also used in [11] in a time-domain formulation of the design problem. Note that matrix $\mathbf{U}_s$ is *independent* of $\mathbf{h}$ and can be pre-calculated as long as the filter length N and stopband edge ω_s are specified.

The objective function E' can now be expressed as

$$E' = 4\mathbf{f}^T\mathbf{Q}\mathbf{f} \ - \ 8\pi\mathbf{h}^T\mathbf{f} \ + \ \pi \tag{2.14}$$

where

$$\mathbf{Q} = \mathbf{U} \ + \ \alpha\mathbf{U}_s \tag{2.15}$$

From (2.9) and (2.12) it follows that matrix $\mathbf{Q}$ is positive definite and, therefore, with a fixed $\mathbf{h}$ the global minimum of E' is given by

$$\mathbf{f} = \pi\mathbf{Q}^{-1}\mathbf{h} \tag{2.16}$$

On the basis of the preceding analysis, an iterative algorithm can now be constructed as follows:

Algorithm 2.1

Step 1 Use a conventional method (e.g., the window method) to design a linear phase, lowpass, FIR filter of length N with stopband edge ω_s, and use the coefficient vector of the filter obtained as the initial $\mathbf{h}$.

Step 2 Use (2.11) to compute matrix $\mathbf{U}$.

Step 3 Form matrix $\mathbf{Q}$ using (2.15), and compute $\mathbf{f}$ in (2.16).

Step 4 If $\| \mathbf{h} - \mathbf{f} \| < \epsilon$, where ϵ is a prescribed tolerance, output $\mathbf{f}$ as the design result and stop. Otherwise, update $\mathbf{h}$ using (2.7) with a τ close to 0.5 and repeat from Step 2.

A remark on the evaluation of matrix $\mathbf{U}$ is appropriate at this point. From (2.9) it is clear that $\mathbf{U}$ is symmetric, and so only $N(N+2)/8$ entries of $\mathbf{U}$ need to be calculated. For each entry of $\mathbf{U}$, $\sum_{l=1}^{8} [1+(-1)^{k_l}]\delta(k_l)$ is a simple combination of eight *delta* functions, each of which is very sparse and easy to determine. Consequently, designs using Algorithm 2.1 can be accomplished very quickly.

2.2.3 Design Examples

Two FIR QMF banks have been designed by using Algorithm 2.1. The parameters used in the two designs, which will be referred to as Examples 2.1 and 2.2, are $N = 32, \alpha = 1$, $\omega_s = 0.6\pi$, $\tau = 0.7$, $\epsilon = 10^{-3}$, and $N = 80, \alpha = 1$, $\omega_s = 0.55\pi$, $\tau = 0.7$, $\epsilon = 10^{-3}$, respectively. The initial $\mathbf{h}$ was $[\ 0\ 0\ \cdots\ 0\ \frac{1}{2}\ ]^T$. For comparison purposes the method of Chen and Lee [12] was applied to design two FIR QMF banks with the same design parameters and initial $\mathbf{h}$. The comparisons were made in terms of

- Number of floating-point operations in millions (MFLOPS)
- the minimum stopband attenuation

$$A_a = \min_{\omega_s \le \omega \le \pi} \left[-20 \log_{10} |H_0(e^{j\omega})| \right]$$

- the peak-to-peak passband ripple

$$A_p = \max_{0 \le \omega \le \omega_p} \left[20 \log_{10} |H_0(e^{j\omega})| \right] - \min_{0 \le \omega \le \omega_p} \left[20 \log_{10} |H_0(e^{j\omega})| \right]$$

where ω_p is the passband edge,

- Peak reconstruction error

$$\text{PRE} = \max_{\omega} \left| 20 \log_{10} \left[|H_0^2(\omega) - H_0^2(\omega + \pi)| \right] \right|$$

- Signal-to-noise ratio

$$\begin{aligned} \text{SNR} &= 10 \log_{10} \left(\frac{\text{energy of the signal}}{\text{energy of the reconstruction noise}} \right) \\ &= 10 \log_{10} \left\{ \frac{\Sigma\ x^2(n)}{\Sigma\ [x(n) - \hat{x}(n + k_d)]^2} \right\} \end{aligned}$$

where k_d is the reconstruction delay.

Both the proposed method and the method of [12] were programmed using MATLAB (version 4.1) and run on a Sun SPARC station. The number of frequency sampling points was set to $8N$ when implementing the method of [12], where N is the filter length. The results are summarized in Table 2.1 where SNR_s and SNR_r denote the SNR with a step input and a random input, respectively. The amplitude responses of filter H_0 designed by the proposed method and the method of [12] with two sets of design parameters specified above are depicted in Fig. 2.2 (a) and

Table 2.1: Comparisons of the proposed method with the method of Chen-Lee.

	Example 2.1		Example 2.2	
	Proposed	Chen-Lee	Proposed	Chen-Lee
MFLOPS	0.62	2.55	8.11	36.83
A_a (dB)	35.20	36.81	44.69	45.19
A_p (dB)	0.0124	0.0139	0.0042	0.0045
PRE (dB)	0.0148	0.0154	0.0091	0.0093
SNR_s (dB)	84.1	83.6	83.9	82.7
SNR_r (dB)	69.1	68.4	76.5	74.8

(b), respectively. As can be observed from the design results, the proposed method shows consistent improvement over the method of [12] especially in terms of design efficiency where the computation complexity can be reduced by as much as 75%.

2.3 Design of Low-Delay QMF Banks

2.3.1 General Two-Channel QMF Bank

In Sec. 2.2.1, the impulse responses of the filters in a QMF filter bank are assumed to be symmetrical so that they are of linear phase with group delay $(N-1)/2$, where N is the length of the filter. This gives a filter bank that has linear phase response and the reconstruction delay is fixed at $(N-1)$ sampling period. Unlike the conventional QMF bank, here we consider a QMF bank which imposes no symmetry constraints on the impulse responses of the filters. From [55] we know that optimization methods can be used to design FIR filters with group delay less than $(N-1)/2$. Suppose that we have designed a lowpass FIR filter H_0 with group delay $k_d/2 < (N-1)/2$ where

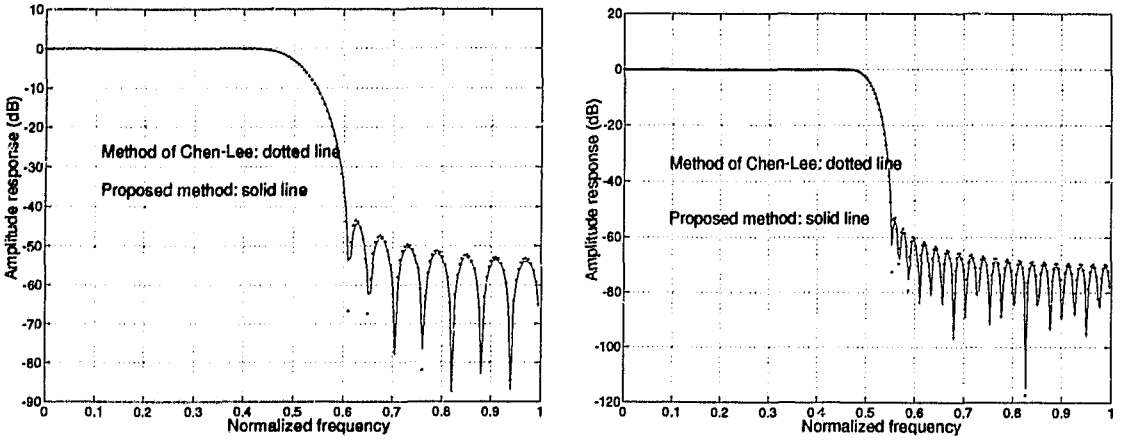

(a) (b)

Figure 2.2: (a) Amplitude responses of the filters in Example 2.1. (b) Amplitude responses of the filters in Example 2.2.

k_d is assumed to be an odd number, then its frequency response can be expressed as

$$H_0(e^{j\omega}) = |H_0(e^{j\omega})|e^{-j\omega k_d/2}$$

So with the same quadrature-mirror relationship among analysis and synthesis filters assumed as in a conventional QMF bank, the aliasing term in the output is cancelled and the frequency response of the filter bank is given as

$$\begin{aligned} H_0^2(e^{j\omega}) - H_0^2(e^{j(\omega+\pi)}) &= |H_0(e^{j\omega})|e^{-j\omega k_d} + |H_0(e^{j(\omega+\pi)})|e^{-j[(\omega+\pi)k_d+\pi]} \\ &= \left[|H_0^2(e^{j\omega})| + |H_0^2(e^{j(\omega+\pi)})|\right] e^{-j\omega k_d} \end{aligned} \tag{2.17}$$

Therefore, if

$$|H_0^2(e^{j\omega})| + |H_0^2(e^{j(\omega+\pi)})| = 1$$

for all $0 \leq \omega \leq \pi$, the perfect reconstruction will be achieved while the reconstruction delay is $k_d < N-1$, which is less than that in a conventional QMF bank, and it

can be made *small* if k_d is *small*. The QMF bank obtained can be referred to as a two-channel low-delay QMF bank and its perfect reconstruction condition in the z domain can be expressed as

$$H_0^2(z) - H_0^2(-z) = z^{-k_d}$$

Based on the above analysis, a design method can be developed in which a weighted objective function is formed as

$$E = \sum_{i=1}^{2} w_i E_i \tag{2.18}$$

with

$$E_1 = \sum_{\omega} |H_0^2(e^{j\omega}) - H_0^2(e^{j(\omega+\pi)}) - e^{-j\omega k_d}|^2$$
$$E_2 = \sum_{\omega} |H_0(e^{j\omega}) - H_I(e^{j\omega})|^2$$

where w_i for $i = 1, 2$ are weights and $H_I(e^{j\omega})$ is the frequency response of an ideal lowpass filter with group delay $k_d/2$.

The minimization of the objective function in the above design procedures can be achieved by optimization. We have employed a quasi-Newton optimization algorithm based on the Broyden-Fletcher-Goldfard-Shanno (BFGS) updating formula and the inexact line search described in [55] to perform the optimization. The number of variables is N. A fortran program has been written to implement the algorithm.

A filter bank was designed with filter length $N = 32$ and system delay $k_d = 9$, which is referred as Example 2.3. First the coefficients of filter H_0 are determined by minimizing the objective function given in Eqn. (2.18) and then three other analysis and synthesis filters are obtain through the quadrature-mirror relation as

Table 2.2: SNR for Example 2.3.

k_d	SNR_s (dB)	SNR_r (dB)
9	78.87	75.99

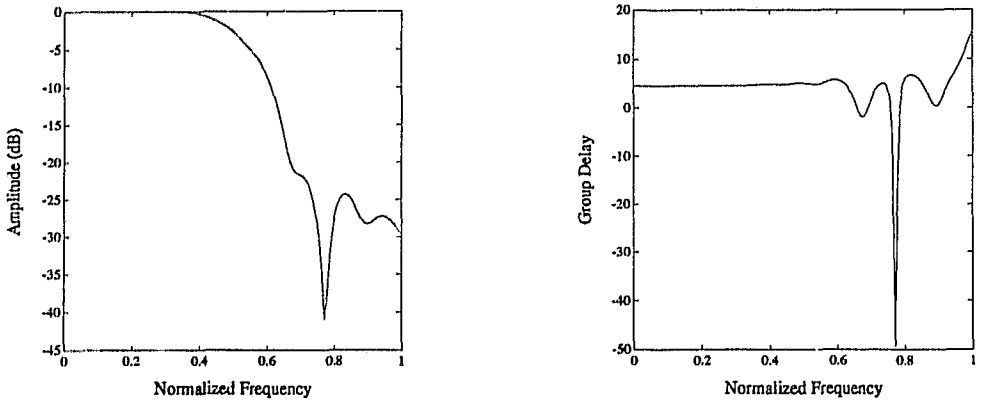

(a) (b)

Figure 2.3: Example 2.3 (a) Amplitude response of H_0. (b) Group delay of H_0.

in a conventional QMF bank. The amplitude response and group delay characteristic of filter H_0 are shown in Fig. 2.3 (a) and (b), respectively. It is observed that in the passband the group delay characteristic is flat. The SNR values for the obtained filter bank are listed in Table 2.2.

2.3.2 Iterative Method

In Sec. 2.3.1, a two-channel QMF bank is considered whose reconstruction delay could be lower than that in a conventional QMF bank. Since the objective function involved in the design is usually highly nonlinear, its minimization with standard

optimization methods is usually quite time-consuming and sensitive to the initial points. In this section, we propose an iterative algorithm for the design of two-channel low-delay QMF banks.

The objective function involved in the design can be rewritten as

$$E = E_1 + \alpha E_2 \tag{2.19}$$

where

$$E_1 = \sum_{0 \le \omega \le \pi} |H_0^2(e^{j\omega}) - H_0^2(e^{j(\omega+\pi)}) - e^{-j\omega k_d}|^2$$
$$E_2 = \sum_{\omega_s \le \omega \le \pi} |H_0(e^{j\omega})|^2$$

and $\alpha > 0$ is a weighting constant. Term E_1 deals with the perfect reconstruction condition and $k_d < N-1$ is the system delay. Term E_2 deals with the intra-band aliasing where ω_s is the stopband edge.

Instead of minimizing directly the above objective function with respect to the coefficients of H_0, an iterative method, which is an extension of that in [12], is adopted. The error components E_1 and E_2 in (2.19) are changed to

$$E' = E_1' + \alpha E_2' \tag{2.20}$$
$$E_1' = \sum_{0 \le \omega \le \pi} |H_0(e^{j\omega})Q_0(e^{j\omega}) - H_0(e^{j(\omega+\pi)})Q_0(e^{j(\omega+\pi)}) - e^{-j\omega k_d}|^2$$
$$E_2' = \sum_{\omega_s \le \omega \le \pi} |Q_0(e^{j\omega})|^2$$

where

$$Q_0(e^{j\omega}) = \sum_{l=0}^{N-1} q_0(l) e^{-j\omega l}$$

is the transfer function of a lowpass filter Q_0, whose coefficient vector is $\mathbf{v} = [q_0(0)\ q_0(1)\ \cdots\ q_0(N-1)]^T$. It is assumed that at the start of the iteration process the coefficient vector of H_0, $\mathbf{u} = [h_0(0)\ h_0(1)\ \cdots\ h_0(N-1)]^T$, is known and so

$H_0(e^{j\omega})$ is known. Let $\mathbf{\Omega} = \{\omega_1, \omega_2, \ldots, \omega_s, \ldots, \omega_L\}$ be the set of sampling points and construct the matrices

$$\mathbf{U}_t(\mathbf{\Omega}) = \begin{bmatrix} 1 & e^{-j\omega_1} & \cdots & e^{-j\omega_1(N-1)} \\ \vdots & & & \vdots \\ 1 & e^{-j\omega_s} & \cdots & e^{-j\omega_s(N-1)} \\ \vdots & & & \vdots \\ 1 & e^{-j\omega_L} & \cdots & e^{-j\omega_L(N-1)} \end{bmatrix} \tag{2.21a}$$

$$\mathbf{U}_s = \begin{bmatrix} 1 & e^{-j\omega_s} & \cdots & e^{-j\omega_s(N-1)} \\ \vdots & & & \vdots \\ 1 & e^{-j\omega_L} & \cdots & e^{-j\omega_L(N-1)} \end{bmatrix} \tag{2.21b}$$

$$\mathbf{H}(\mathbf{\Omega}) = \text{diag}[H_0(e^{j\omega_1}), \ldots, H_0(e^{j\omega_s}), \ldots, H_0(e^{j\omega_L})] \tag{2.21c}$$

$$\mathbf{U} = \mathbf{H}(\mathbf{\Omega})\mathbf{U}_t(\mathbf{\Omega}) - \mathbf{H}(\mathbf{\Omega}+\pi)\mathbf{U}_t(\mathbf{\Omega}+\pi) \tag{2.21d}$$

E' in (2.20) can be expressed in the form

$$E' = (\mathbf{U}\mathbf{v} - \mathbf{I})^H(\mathbf{U}\mathbf{v} - \mathbf{I}) + \alpha(\mathbf{U}_s\mathbf{v})^H(\mathbf{U}_s\mathbf{v}) \tag{2.22}$$

where $\mathbf{I} = [e^{-j\omega_1 k}\ e^{-j\omega_2 k}\ \cdots\ e^{-j\omega_L k}]^T$ and superscript H denotes complex conjugate transposition. E' in (2.22) is a quadratic function of the coefficients in $\mathbf{v}$. It can be shown that this function has a global minimum point given by the closed-form solution

$$\mathbf{v} = (\text{Re}\ [\mathbf{U}^H\mathbf{U} + \alpha\mathbf{U}_s{}^H\mathbf{U}_s])^{-1} \cdot \text{Re}\ ([\mathbf{U}^H\mathbf{I}]) \tag{2.23}$$

where Re $[\cdot]$ is the real part of $[\cdot]$. After obtaining $\mathbf{v}$, a linear formula is adopted to update $\mathbf{u}$ as

$$\mathbf{u} := (1-\tau)\mathbf{u} + \tau\mathbf{v} \tag{2.24}$$

and the above process is repeated until $\| \mathbf{u} - \mathbf{v} \|$ is less than a prescribed tolerance.

A step-by-step procedure based on the above methods is as follows:

Algorithm 2.2

Step 1 Set the weighting constant α, the smoothing parameter τ, and the stopping criterion ϵ and initialize the coefficients of vector $\mathbf{u}$.

Step 2 Calculate the matrices expressed in (2.21).

Step 3 Obtain coefficient vector $\mathbf{v}$ using (2.23).

Step 4 If $|| \mathbf{u} - \mathbf{v} || < \epsilon$, terminate the process; otherwise, update coefficient vector $\mathbf{u}$ using (2.24) and go to step 2.

By using the proposed iterative design method, filter banks with low reconstruction delays were designed. Two design examples are presented here. The filter length in these two design examples is 32. The first design example, referred to as Example 2.4, was to design a filter bank with system reconstruction delay $k_d = 9$. Fig. 2.4 (a) is the amplitude response of the prototype filter H_0 and (b) is its group delay plot. In the second example, which is referred to as Example 2.5, a filter bank with system delay $k_d = 15$, was designed. Fig. 2.5 (a) is the amplitude response of the prototype filter H_0 and (b) is its group delay plot. From these plots, it is observed that the filters achieved have fairly good passband and stopband characteristics and in the passband have nearly linear phase responses, which are desired in many applications. For the above two examples, the SNR values and the number of iterations (NI) used in the designs are listed in Table 2.3. Compared with the example in Sec. 2.3.1, it is observed that by using the iterative algorithm, design efficiency is improved and filter banks with better performance are obtained.

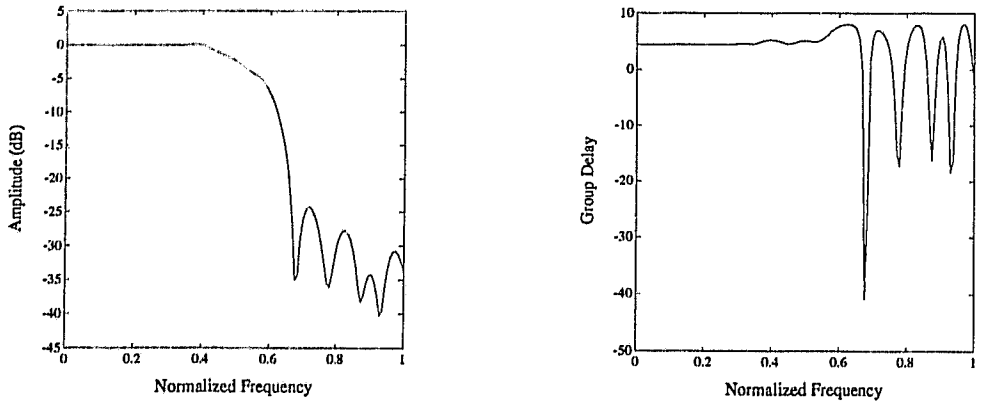

(a) (b)

Figure 2.4: Example 2.4 (a) Amplitude responses of H_0. (b) Group delay of H_0.

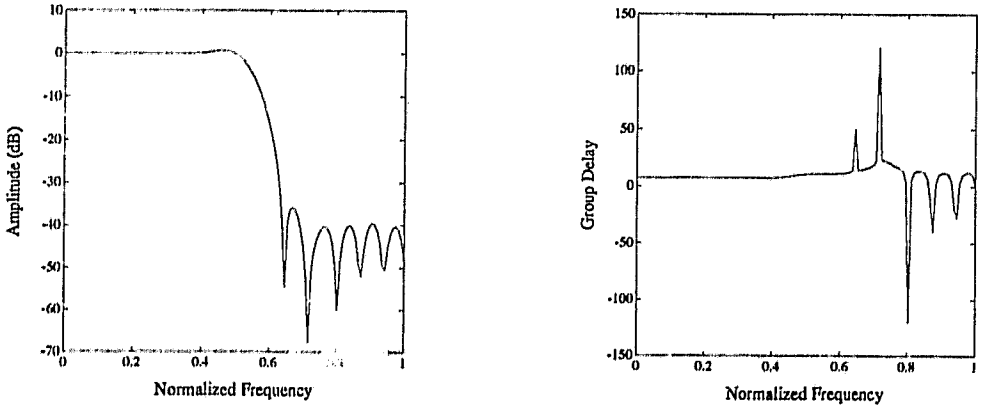

(a) (b)

Figure 2.5: Example 2.5 (a) Amplitude response of H_0. (b) Group delay of H_0.

Table 2.3: Results for Examples 2.4 and 2.5.

	k_d	NI	SNR_s (dB)	SNR_r (dB)
Example 2.4	9	15	81.84	74.05
Example 2.5	15	10	82.31	76.85

2.3.3 Equiripple Complex Reconstruction Error

Using Algorithm 2.2, the magnitude of the complex reconstruction error defined as

$$e_r(\omega) = H_0^2(e^{j\omega}) - H_0^2(e^{j(\omega+\pi)}) - e^{-j\omega k_d} \tag{2.25}$$

will be minimized. However, it is not equiripple in general. In what follows it will be shown that if a weighted objective function in the form of

$$E'_w = E'_{1w} + \alpha E'_{2w} \tag{2.26a}$$

$$E'_{1w} = \sum_{0\le\omega\le\pi} W(\omega)\,|H_0(e^{j\omega})Q_0(e^{j\omega}) - H_0(e^{j(\omega+\pi)})Q_0(e^{j(\omega+\pi)}) - e^{-j\omega k_d}|^2 \tag{2.26b}$$

$$E'_{2w} = \sum_{\omega_s\le\omega\le\pi} |Q_0(e^{j\omega})|^2 \tag{2.26c}$$

is adopted and the weighting $W(\omega)$ is chosen adequately, equiripple complex reconstruction error can be achieved.

Since E'_w in (2.26a) can be written as

$$E'_w = (\mathbf{Uv} - \mathbf{I})^H \hat{\mathbf{W}}(\mathbf{Uv} - \mathbf{I}) + \alpha(\mathbf{U}_s\mathbf{v})^H(\mathbf{U}_s\mathbf{v})$$

where $\mathbf{U}$, $\mathbf{U}_s$ are given by (2.21) and $\hat{\mathbf{W}}$ is defined as

$$\hat{\mathbf{W}} = \text{diag}\,[\,W(\omega_1),\ \ldots,\ W(\omega_s),\ \ldots,\ W(\omega_L)\,]$$

Hence if

$$\mathbf{v} = (\text{Re}\,[\mathbf{U}^H\hat{\mathbf{W}}\mathbf{U} + \alpha\mathbf{U}_s{}^H\mathbf{U}_s])^{-1} \cdot \text{Re}\,([\,\mathbf{U}^H\hat{\mathbf{W}}\mathbf{I}\,]) \tag{2.27}$$

the minimum of E'_w is achieved. Then a process similar to that in Algorithm 2.2 is repeated until $|| \mathbf{u} - \mathbf{v} || < \epsilon$.

To obtain equiripple complex reconstruction error, the weighting $W(\omega)$ should be updated based on the weighted least squares (WLS) algorithm proposed in [53]. Suppose that $W_k(\omega)$ is the weighting function used in the kth iteration, then the weighting used in the $(k+1)$th iteration is expressed as

$$W_{k+1}(\omega) = W_k(\omega)v_k(\omega) \tag{2.28}$$

where $v_k(\omega) > 0$ is selected such that $v_k(\omega_i) > v_k(\omega_j)$ if $|e_{rk}(\omega_i)| > |e_{rk}(\omega_j)|$ where $e_{rk}(\omega)$ denotes the values of $e_r(\omega)$ defined in (2.25) at the kth iteration. This ensures that in the next iteration $|e_r(\omega_i)|$ will decrease at the expense of increasing $|e_r(\omega_j)|$. The criterion of choosing $v_k(\omega)$ is as follows: Compute the magnitude of the complex reconstruction error $e_{rk}(\omega)$ at the kth iteration. Let the Jth extremal value of $|e_{rk}(\omega)|$ be $V_k(J) = |e_{rk}(\omega_J)|$ if $|e_{rk}(\omega_{J+1})| < |e_{rk}(\omega_J)|$ and $|e_{rk}(\omega_{J-1})| < |e_{rk}(\omega_J)|$ are satisfied where ω_J is defined as the Jth extremal frequency of the reconstruction error. For any nonband-edge extremal point, let $V_k(J) = 0.1\text{MIN}[V_k(J-1), V_k(J+1)]$ if $V_k(J) < 0.1\text{MIN}[V_k(J-1), V_k(J+1)]$ where $\text{MIN}(u, v)$ denotes the smaller of u and v. An envelop function $B_k(\omega)$ is then formed by joining together all the extremal points of the same frequency band of interest with straight lines, i.e., for $\omega_J < \omega < \omega_{J+1}$

$$\begin{aligned} B_k(\omega) = &[(\omega - \omega_J)/(\omega_{J+1} - \omega_J)]V_k(J+1) \\ &+[(\omega_{J+1} - \omega)/(\omega_{J+1} - \omega_J)]V_k(J) \end{aligned}$$

Finally, $v_k(\omega)$ is constructed as

$$v_k(\omega) = \frac{L\{B_k(\omega)\}^\theta}{\sum_{i=1}^{L}[W_k(\omega_i)\{B_k(\omega_i)\}^\theta]} \tag{2.29}$$

where parameter θ affects the convergence rate and is chosen to be 1.5 in our designs.

Since the purpose of the design procedure is to achieve equiripple magnitude of the complex reconstruction error, the process could be terminated if

$$\frac{[\max(V) - \min(V)]}{\max(V)} \leq \kappa \tag{2.30}$$

where κ is a prescribed positive constant and $\max(V)$ and $\min(V)$ are the maximum and minimum values of the magnitude of the complex reconstruction error at all extremal frequencies.

The steps that need to be taken to accomplish the design of low-delay QMF banks with equiripple reconstruction error are summarized as follows:

Algorithm 2.3

Step 1 Design a lowpass, FIR filter of length N with stopband edge ω_s and group delay $k_d/2$, and use the coefficient vector of the filter obtained to initialize $\mathbf{u}$. The initial weighting is set $W(\omega) = 1$.

Step 2 Use (2.21b) to compute matrix $\mathbf{U}_s$.

Step 3 Form matrix $\mathbf{U}$ using (2.21d) and compute $\mathbf{v}$ using (2.27).

Step 4 If $\| \mathbf{u} - \mathbf{v} \| < \epsilon$ where ϵ is the prescribed tolerance, go to Step 5. Otherwise, update $\mathbf{u}$ using (2.24) with a τ close to 0.5 and repeat from Step 3.

Step 5 If termination condition (2.30) is satisfied, output $\mathbf{u}$ as the design result and stop. Otherwise, update $W(\omega)$ using equations (2.28) - (2.30) and repeat from Step 3.

It should be pointed out that, the algorithm not only leads to designs of low-delay QMF banks with equiripple complex reconstruction error, it can also be used to design linear phase QMF banks with equiripple amplitude response if $k_d = N - 1$ and initial $\mathbf{u}$ contains symmetrical coefficients.

Table 2.4: Results for Examples 2.6 and 2.7.

	Example 2.6	Example 2.7
NI	23	11
PCRE	2.4223×10^{-4}	$1.4627\times^{-4}$
SNR_r (dB)	73.20	77.32

Two low-delay QMF banks with equiripple complex reconstruction error were designed by using the proposed algorithm. The performance of the designs are evaluated in terms of NI, the peak complex reconstruction error PCRE= $\max_{\omega} |e_r(\omega)|$ where $e_r(\omega)$ is defined in (2.25), and SNR. In Example 2.6 a filter bank with the specifications $N = 32$, $k_d = 15$, $\alpha = 0.01$, $\omega_s = 0.7\pi$, $\tau = 0.5$, $\kappa = 0.02$, $\epsilon = 10^{-4}$ was designed. The results are summarized in Table 2.4. The amplitude responses of the analysis filters obtained and the magnitude of the complex reconstruction error are depicted in Fig. 2.6(a) and (b), respectively. Example 2.7 shows a filter bank with design specifications $N = 44$, $k_d = 21$, $\alpha = 0.1$, $\omega_s = 0.65\pi$, $\tau = 0.5$, $\kappa = 0.02$ $\epsilon = 10^{-4}$. The results are listed in Table 2.4. The amplitude responses of the analysis filters and the magnitude of the complex reconstruction error are shown in Fig. 2.7(a) and (b), respectively.

From Table 2.4 and the figures, it is observed the filters obtained have satisfactory frequency responses, and that the magnitude of the complex reconstruction errors are made equiripple.

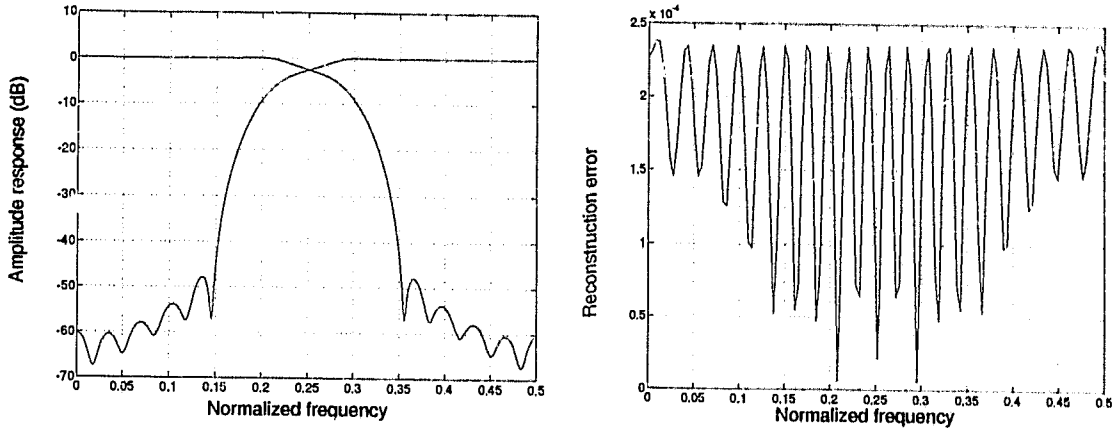

(a) (b)

Figure 2.6: Example 2.6 (a) Amplitude responses of the analysis filters. (b) Magnitude of the complex reconstruction error.

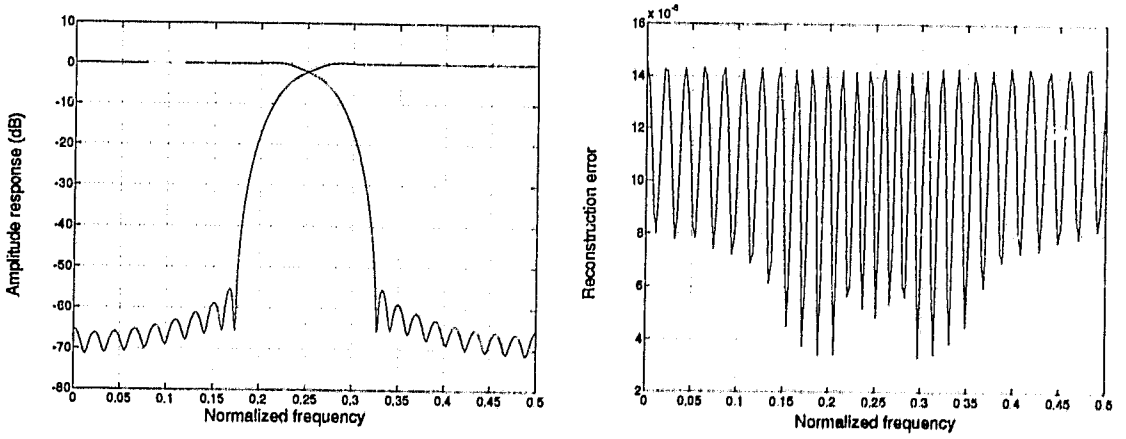

(a) (b)

Figure 2.7: Example 2.7 (a) Amplitude responses of the analysis filters. (b) Magnitude of the complex reconstruction error.

2.3.4 Improved Iterative Method

From Sec. 2.3.2 it is observed that in the design of two-channel low-delay QMF banks, the iterative method has high efficiency compared with that using a standard unconstrained optimization method. However, it can be noticed that discretized versions of the objective function is used which first will degrade the evaluation of the error components and second will increase the amount of calculations since a large density of sample points is required. In this section, an improved iterative method is proposed in which the integral discretization is replaced by a simple and explicit formula of the precise computation of the integrals involved in forming the objective functions.

Again the design problem amounts to finding the coefficients of H_0 that minimize

$$E_L = E_{L1} + \alpha E_{L2} \tag{2.31a}$$

with $\alpha > 0$, where E_{L1} and E_{L2} are given by

$$E_{L1} = \int_0^{\pi} |H_0^2(e^{j\omega}) - H_0^2(e^{j(\omega+\pi)}) - e^{-jk_d\omega}|^2 \, d\omega \tag{2.31b}$$

$$E_{L2} = \int_{\omega_s}^{\pi} |H_0(e^{j\omega})|^2 \, d\omega \tag{2.31c}$$

Note that in this case, filter H_0 does not have a symmetrical impulse response and, therefore, the frequency response should be expressed as

$$H_0(e^{j\omega}) = \mathbf{h}_L^T \mathbf{c}_L(\omega) \tag{2.32a}$$

where

$$\mathbf{h}_L = [\, h_0 \; h_1 \; \cdots \; h_{N-1} \,]^T \tag{2.32b}$$

$$\mathbf{c}_L(\omega) = [\, 1 \;\; e^{-j\omega} \; \cdots \; e^{-j(N-1)\omega} \,]^T \tag{2.32c}$$

The iterative algorithm here is based on a modified objective function

$$E'_L = E'_{L1} + \alpha E'_{L2} \tag{2.33a}$$

where

$$E'_{L1} = \int_0^{\pi} |H_0(e^{j\omega})F_0(e^{j\omega}) - H_0(e^{j(\omega+\pi)})F_0(e^{j(\omega+\pi)}) - e^{-jk_d\omega}|^2 d\omega \tag{2.33b}$$

$$E'_{L2} = \int_{\omega_s}^{\pi} |F_0(e^{j\omega})|^2 d\omega \tag{2.33c}$$

and $\mathbf{h}_L$ is fixed; $F_0(e^{j\omega})$ is given by

$$F_0(e^{j\omega}) = \mathbf{f}_L^T \mathbf{c}_L(\omega) \tag{2.33d}$$

$$\mathbf{f}_L = [\, f_0 \;\; f_1 \;\cdots\; f_{N-1} \,]^T \tag{2.33e}$$

After some fairly extensive manipulation, (2.32) and (2.33) give

$$E'_L = \mathbf{f}_L^T \mathbf{Q}_L \mathbf{f}_L \;-\; 2\, \mathbf{h}_L^T \mathbf{S} \mathbf{f}_L \;+\; \pi \tag{2.34}$$

where

$$\mathbf{Q}_L = \mathbf{R} + \alpha \mathbf{R}_s \tag{2.35a}$$

$$\mathbf{R} = \mathrm{Re} \int_0^{\pi} [H_0(e^{j\omega})\mathbf{c}_L(\omega) - H_0(e^{j(\omega+\pi)})\mathbf{c}_L(\omega+\pi)] \cdot [H_0(e^{j\omega})\mathbf{c}_L(\omega) - H_0(e^{j(\omega+\pi)})\mathbf{c}_L(\omega+\pi)]^H \, d\omega \tag{2.35b}$$

Entry $(i,\ j)$ of $\mathbf{R}$ is given by

$$r_{ij} = 2\pi \sum_{n=0}^{N-1} \sum_{m=0}^{N-1} h_n h_m [1 + (-1)^{j+m}] \delta(-i + j - n + m) \tag{2.35c}$$

where $\delta(\cdot)$ is the delta function defined in (2.11),

$$\mathbf{R}_s = \mathrm{Re} \int_{\omega_s}^{\pi} \mathbf{c}_L(\omega)\mathbf{c}_L^H(\omega) \, d\omega$$

$$= \begin{bmatrix} \pi-\omega_s & -\sin\omega_s & -\frac{1}{2}\sin 2\omega_s & \cdots & -\frac{1}{N-1}\sin(N-1)\omega_s \\ -\sin\omega_s & \pi-\omega_s & -\sin\omega_s & \cdots & -\frac{1}{N-2}\sin(N-2)\omega_s \\ \vdots & & \ddots & & \vdots \\ -\frac{1}{N-1}\sin(N-1)\omega_s & \cdots & \cdots & \cdots & \pi-\omega_s \end{bmatrix} \tag{2.35d}$$

and

$$\mathbf{S} = \mathrm{Re}\int_0^{\pi}[\mathbf{c}_L(\omega)\mathbf{c}_L^T(\omega) - \mathbf{c}_L(\omega+\pi)\mathbf{c}_L^T(\omega+\pi)]e^{jk_d\omega}d\omega$$

$$= 2\pi \begin{bmatrix} 0 & \cdots & \cdots & 1 & 0 & \cdots & 0 \\ 0 & & 1 & 0 & \cdots & \cdots & 0 \\ \vdots & \iddots & \iddots & & & & \vdots \\ 1 & \iddots & & & & & \\ 0 & & & & & & \\ \vdots & & & & & & \vdots \\ 0 & \cdots & & & & \cdots & 0 \end{bmatrix} \tag{2.35e}$$

Evidently, $\mathbf{S}$ has unity entries on the $(k_d+1)th$ northeast-to-southwest sub-diagonal.

From (2.35a), (2.35b) and (2.35d), we observe that $\mathbf{Q}_L$ is a positive definite symmetric matrix and, therefore, for a given $\mathbf{h}_L$ the global minimum of E_L' is achieved if

$$\mathbf{f}_L = \mathbf{Q}_L^{-1}\mathbf{S}\mathbf{h}_L \tag{2.36}$$

Note that matrices $\mathbf{R}_s$ and $\mathbf{S}$ are *independent* of $\mathbf{h}_L$, and can be pre-calculated as long as filter length N, stopband edge ω_s, and reconstruction delay k_d are specified.

An algorithm for the design of a QMF bank with reconstruction delay k_d is as follows:

Algorithm 2.4

Step 1 Use a least-squares method to design a lowpass, FIR filter of length N with passband edge ω_p, stopband edge ω_s, i.e., minimizing a quadratic objective function

$$E_i = \int_0^{\omega_p} |H_0(e^{j\omega}) - e^{-j\omega k_d/2}|^2 \, d\omega + \int_{\omega_s}^{\pi} |H_0(e^{j\omega})|^2 \, d\omega$$

with respect to coefficients of H_0 and take it as initial $\mathbf{h}_L$.

Step 2 Use (2.35c) to compute matrix $\mathbf{R}$.

Step 3 Use (2.35a), (2.35d) and $\mathbf{R}$ obtained from Step 2 to form matrix $\mathbf{Q}_L$; then use (2.36) to compute $\mathbf{f}_L$.

Step 4 If $|| \mathbf{h}_L - \mathbf{f}_L || < \epsilon$, where ϵ is a prescribed tolerance, output $\mathbf{f}_L$ as the design result and stop. Otherwise, update $\mathbf{h}_L$ as

$$\mathbf{h}_L := (1 - \tau)\mathbf{h}_L + \tau \mathbf{f}_L \tag{2.37}$$

with a τ close to 0.5, and repeat from Step 2.

We note from (2.35b) and (2.35c) that $\mathbf{R}$ is symmetric and each entry is a linear combination of *delta* functions, which are very sparse and easy to determine. Consequently, the algorithm can be easily implemented.

We conclude this section with a remark on the issue of undesirable artifacts in the transition region of H_0. It has been observed [34] that the artifacts become more apparent when a very low reconstruction delay k_d is required. An effective approach to this problem is to modify the objective function to include an additional term $\alpha_1 E'_{L3}$, i.e.,

$$E'_L = E'_{L1} + \alpha E'_{L2} + \alpha_1 E'_{L3} \tag{2.38}$$

where

$$\alpha_1 E'_{L3} = \alpha_1 \int_{\omega_{t1}}^{\omega_{t2}} |F_0(e^{j\omega}) - e^{-jk_d\omega/2}|^2 \, d\omega \tag{2.39}$$

and $[\omega_{t1},\ \omega_{t2}]$ is an interval in the transition region where the artifacts occur. It can be readily shown that with this modification the design algorithm, i.e., Algorithm 2.4, can still be used with modifications of (2.34)-(2.36) as follows

$$E'_L = \mathbf{f}_L \mathbf{Q}_L \mathbf{f}_L - 2(\mathbf{h}_L^T \mathbf{S} + \alpha_1 \mathbf{b}^T)\mathbf{f}_L + \pi + \alpha_1(\omega_{t2} - \omega_{t1}) \tag{2.40}$$

where

$$\mathbf{Q}_L = \mathbf{R} + \alpha \mathbf{R}_s + \alpha_1 \mathbf{R}_t \tag{2.41}$$

with $\mathbf{R}$ and $\mathbf{R}_s$ given by (2.35c), (2.35d) and

$$\mathbf{R}_t = \begin{bmatrix} \omega_{t2} - \omega_{t1} & \phi(\omega_{t2},\ \omega_{t1},\ 1) & \cdots & \phi(\omega_{t2},\ \omega_{t1},\ N-1) \\ \phi(\omega_{t2},\ \omega_{t1},\ 1) & \omega_{t2} - \omega_{t1} & & \\ \vdots & & \ddots & \\ \phi(\omega_{t2},\ \omega_{t1},\ N-1) & \cdots & \cdots & \omega_{t2} - \omega_{t1} \end{bmatrix}$$

where

$$\phi(\omega_{t2},\ \omega_{t1},\ k) = \frac{1}{k}\left[\sin k\omega_{t2} - \sin k\omega_{t1}\right]$$

$$\mathbf{b} = \mathrm{Re} \int_{\omega_{t1}}^{\omega_{t2}} \mathbf{c}_L(\omega) e^{jk_d\omega/2} \, d\omega$$

$$= \begin{bmatrix} \frac{2}{k_d}\left[\sin\left(\frac{k_d\omega_{t2}}{2}\right) - \sin\left(\frac{k_d\omega_{t1}}{2}\right)\right] \\ \frac{2}{k_d-2}\left\{\sin\left[\left(\frac{k_d}{2}-1\right)\omega_{t2}\right] - \sin\left[\left(\frac{k_d}{2}-1\right)\omega_{t1}\right]\right\} \\ \vdots \\ \frac{2}{k_d-2N+2}\left\{\sin\left[\left(\frac{k_d}{2}-N+1\right)\omega_{t2}\right] - \sin\left[\left(\frac{k_d}{2}-N+1\right)\omega_{t1}\right]\right\} \end{bmatrix}$$

$$\mathbf{f}_L = \mathbf{Q}_L^{-1}(\mathbf{S}\mathbf{h}_L + \mathbf{b}) \tag{2.42}$$

Table 2.5: Comparisons of the proposed method with the method by Nayebi.

	Example 2.8		Example 2.9	
	Proposed	Method of Nayebi	Proposed	Method of Nayebi
k_d	7	7	15	15
MFLOPS	0.96	-	0.96	-
A_a (dB)	29.17	30.00	66.15	36.97
A_p (dB)	0.2804	0.2169	0.0412	0.0537
PRE (dB)	1.7×10^{-3}	3.5×10^{-4}	1.5×10^{-3}	1.2×10^{-3}
SNR_s (dB)	75.6	74.3	77.5	75.8
SNR_r (dB)	76.2	75.1	77.6	77.4

Two QMF banks with low reconstruction delays were designed by using Algorithm 2.4. The design parameters for Example 2.8 were: $N = 32$, $k_d = 7$, $\alpha = 1 \times 10^{-4}$, $\alpha_1 = 5 \times 10^{-6}$, $\omega_s = 0.75\pi$, $\omega_{t1} = 0.3\pi$, $\omega_{t2} = 0.5\pi$, $\tau = 0.5$ and $\epsilon = 10^{-3}$. Those of Example 2.9 were: $N = 32$, $k_d = 15$, $\alpha = 1$, $\alpha_1 = 3 \times 10^{-4}$ $\omega_s = 0.72\pi$, $\omega_{t1} = 0.35\pi$, $\omega_{t2} = 0.45\pi, \tau = 0.5$ and $\epsilon = 10^{-3}$.

For comparison purposes, we refer to the examples presented in [34] which were designed with a time-domain approach. The performance parameters are the same as those defined in Sec. 2.2.3. The results obtained are summarized in Table 2.5. The amplitude responses of the lowpass analysis filters designed by the proposed method and the method of [34] are depicted in Fig. 2.8 (a) and (b), respectively.

As can be observed from Table 2.5, with $k_d = 7$ the performance of the filter banks designed by the proposed method and the method of [34] are nearly the same. However, as the latter design approach proposed is computationally more demanding, increased computation is expected although no figure is specified in

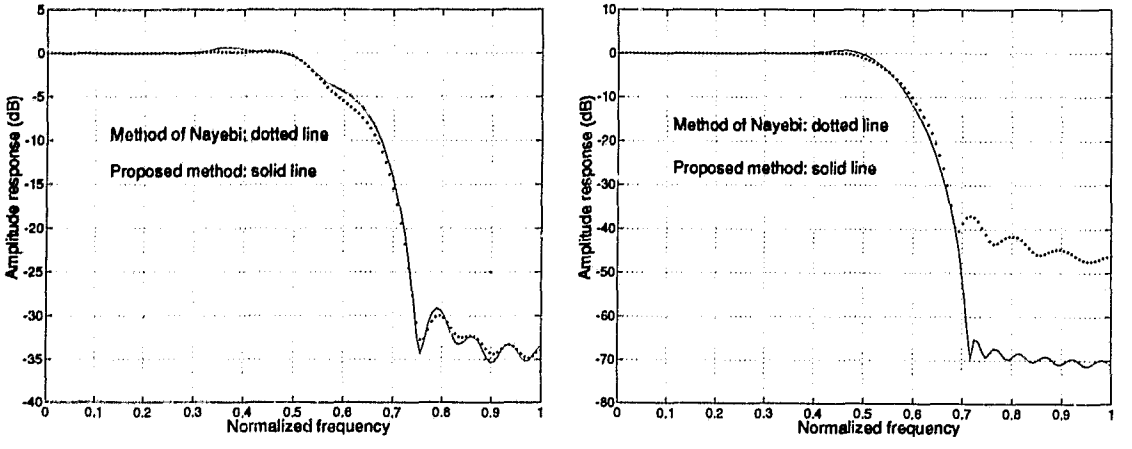

(a) (b)

Figure 2.8: (a) Amplitude responses of the filters in Example 2.8. (b) Amplitude responses of the filters in Example 2.9.

[34]. For the case of $k_d = 15$ the proposed method increased the minimum stopband attenuation by 30 dB. In addition, unlike the low-delay systems proposed in [34], the quadrature mirror structure of the proposed design is amenable to the efficient polyphase-type implementation [29] which requires only $N/2$ additions and $N/2$ multiplications per input, as compared to N additions and N multiplications per input for the low-delay filter banks of [34].

2.3.5 A Case Study

For further analysis and comparison, we used the iterative method introduced in Sec. 2.3.4 to design five two-channel low-delay QMF banks with different filter lengths and delays. The performance of the obtained filter banks were evaluated in terms of PRE and SNR defined in Sec. 2.2.3. The results are listed in Table 2.6. For

Table 2.6: Results for a case study.

Low-delay QMF banks				Conventional QMF banks			
length	delay	PRE (dB)	SNR (dB)	length	delay	PRE (dB)	SNR (dB)
$N = 16$	$k_d = 7$	2.08×10^{-2}	53.09	$N = 8$	$k_d = 7$	6.35×10^{-2}	43.44
$N = 24$	$k_d = 11$	5.5×10^{-3}	65.59	$N = 12$	$k_d = 11$	3.98×10^{-2}	52.69
$N = 32$	$k_d = 15$	1.7×10^{-3}	77.50	$N = 16$	$k_d = 15$	1.91×10^{-2}	59.00
$N = 48$	$k_d = 23$	5.27×10^{-4}	95.55	$N = 24$	$k_d = 23$	8.2×10^{-3}	67.29
$N = 64$	$k_d = 31$	2.87×10^{-4}	98.42	$N = 32$	$k_d = 31$	2.9×10^{-3}	73.51

comparison, corresponding conventional QMF banks with the same reconstruction delays were designed by using the improved iterative method introduced in Sec. 2.2. The results obtained are also listed in Table 2.6.

Graphic displays are depicted in Figs. 2.9 to 2.13. For each design, four plots in solid line are included to show:

(a) amplitude responses of analysis lowpass and highpass filters,

(b) amplitude response of the filter bank,

(c) group delay of filter H_0,

(d) group delay of the filter bank,

For comparison purposes the plots corresponding to the conventional QMF banks are also shown in dotted line.

Several conclusions can be drawn from the design examples, as follows:

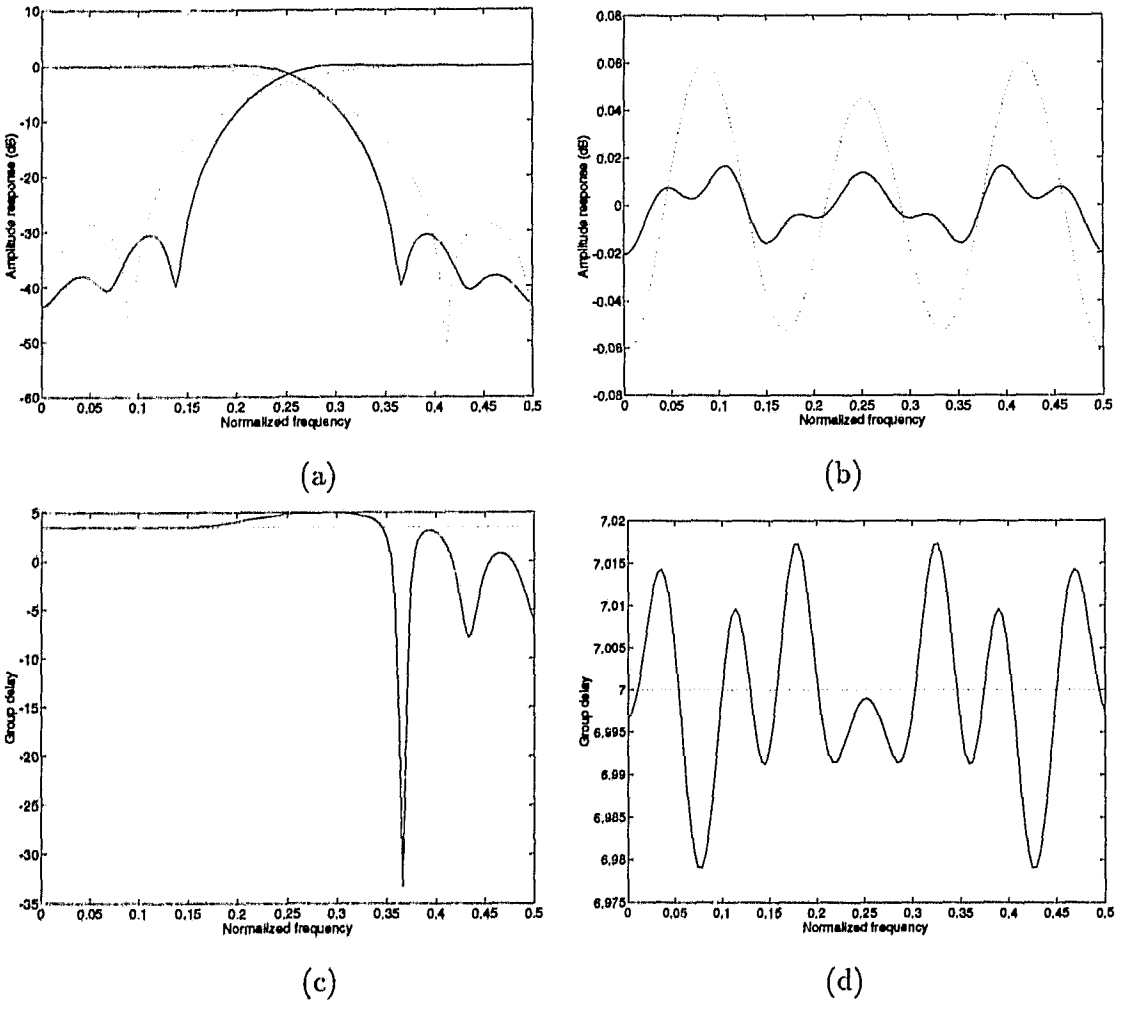

Figure 2.9: Graphic display for $k_d = 7$ (a) Amplitude responses of analysis filters. (b) Amplitude responses of filter banks. (c) Group delay characteristic of H_0. (d) Group delay characteristic of filter banks.

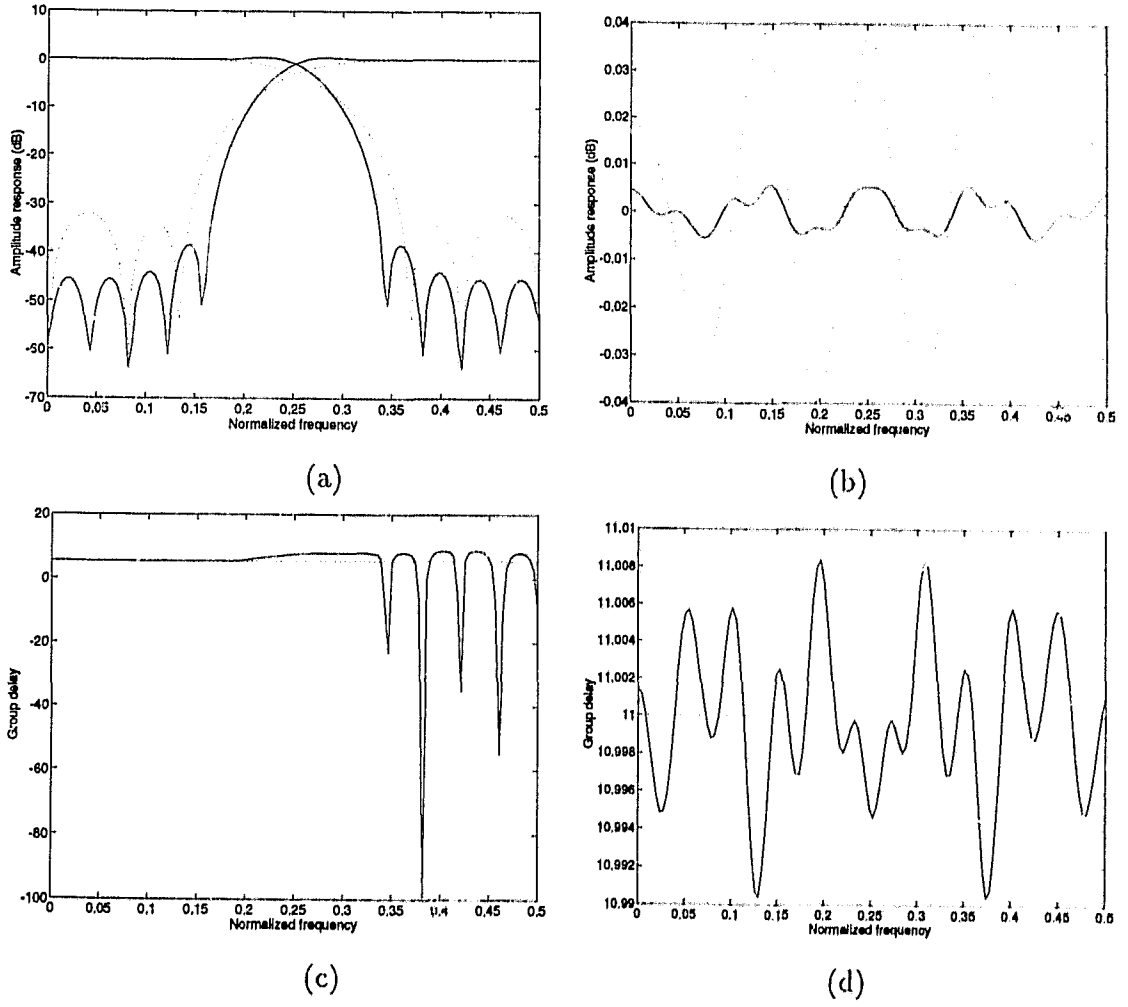

Figure 2.10: Graphic display for $k_d = 11$ (a) Amplitude responses of analysis filters. (b) Amplitude responses of filter banks. (c) Group delay characteristic of H_0. (d) Group delay characteristic of filter banks.

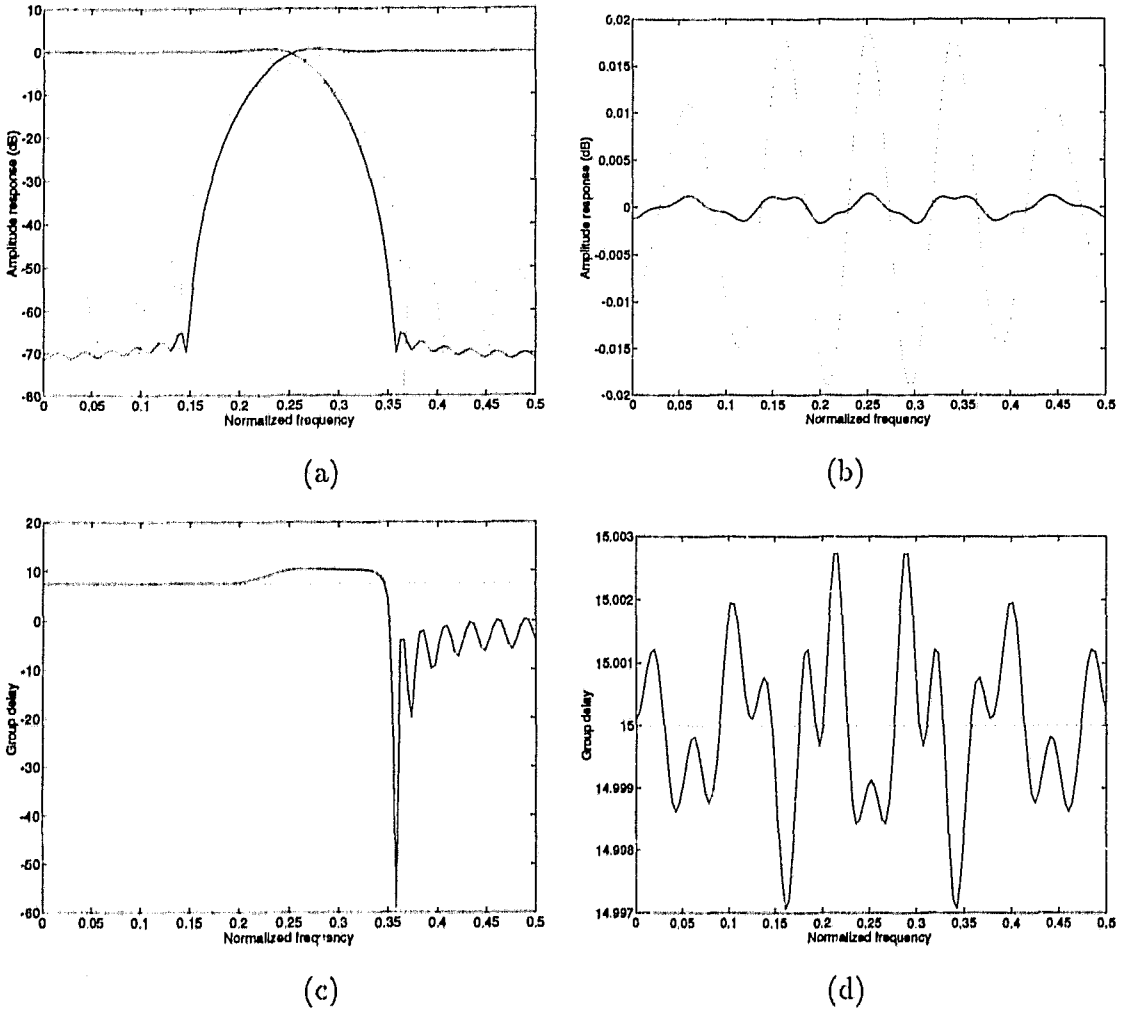

Figure 2.11: Graphic display for $k_d = 15$ (a) Amplitude responses of analysis filters. (b) Amplitude responses of filter banks. (c) Group delay characteristic of H_0. (d) Group delay characteristic of filter banks.

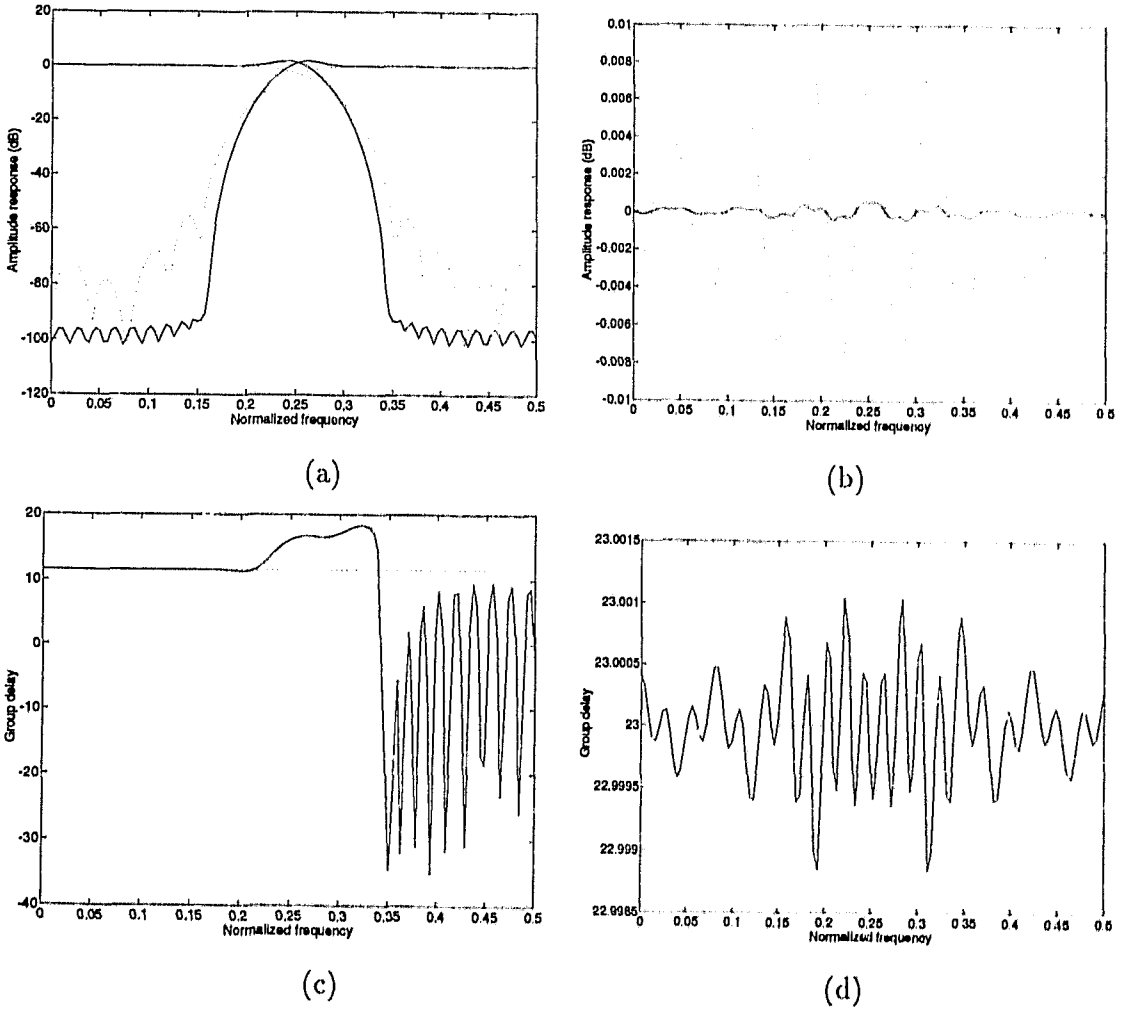

Figure 2.12: Graphic display for $k_d = 23$ (a) Amplitude responses of analysis filters. (b) Amplitude responses of filter banks. (c) Group delay characteristic of H_0. (d) Group delay characteristic of filter banks.

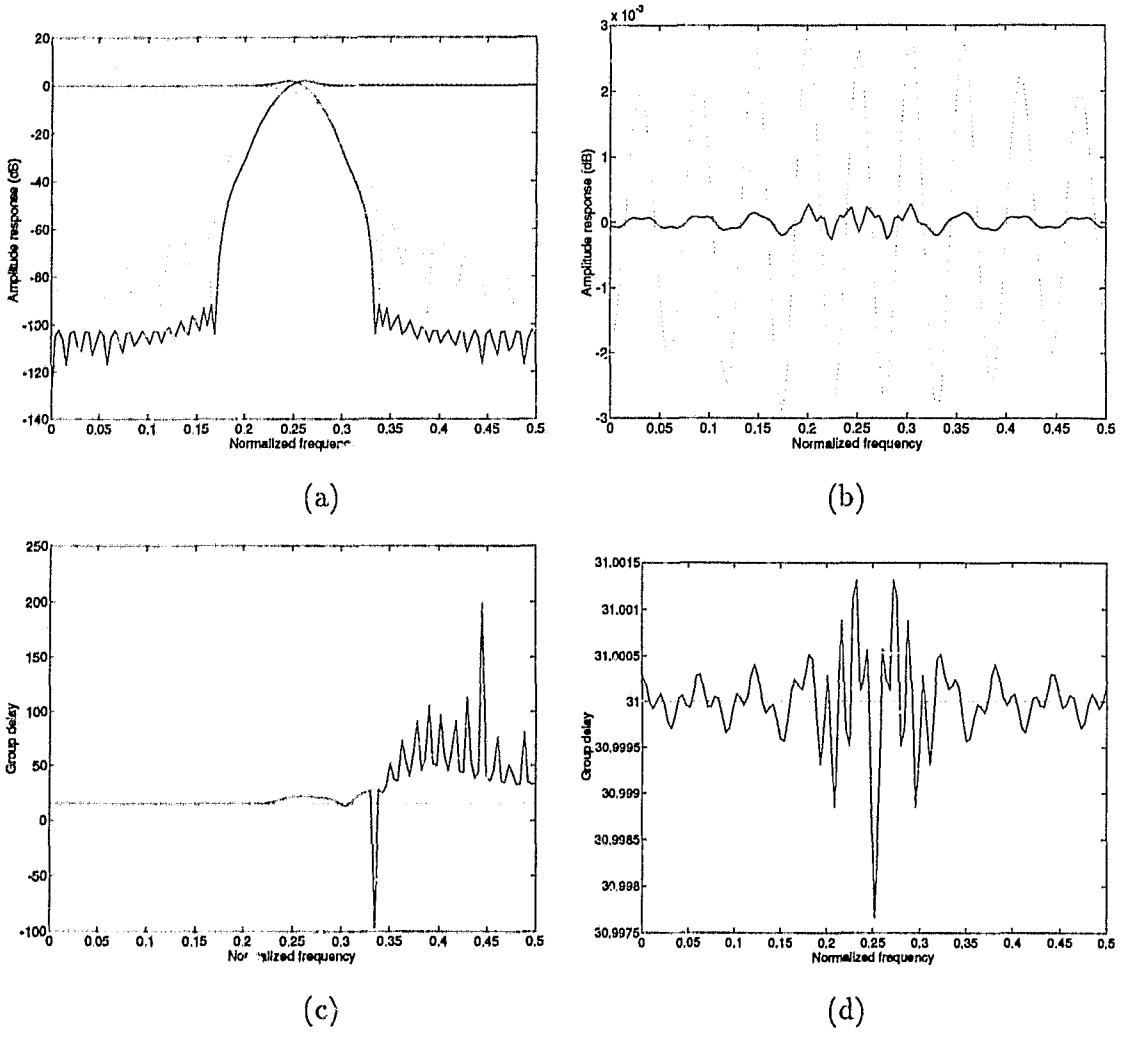

Figure 2.13: Graphic display for $k_d = 31$ (a) Amplitude responses of analysis filters. (b) Amplitude responses of filter banks. (c) Group delay characteristic of H_0. (d) Group delay characteristic of filter banks.

1. The amplitude responses of low-delay QMF banks are better than those of the corresponding conventional QMF banks with the same reconstruction delays. This is because, with a given reconstruction delay, the filter length of a low-delay QMF bank can be made longer than that of a conventional QMF bank.

2. Since the impulse responses of filters in a low-delay QMF bank is not symmetrical in general, the linear phase response is not guaranteed. However, from the plots it is noticed that linear phase response is approximately well in the passband. The phase distortion in the stopband is usually insignificant due to the small gain of the filter in the stopband.

In general low-delay QMF banks are superior than corresponding conventional QMF banks in terms of performances and it is a good choice to use low-delay QMF banks in real-time applications.

2.4 Further Analysis on the Iterative Method

In previous sections an iterative method was proposed for the design of either two-channel conventional QMF banks or two-channel low-delay QMF banks. Compared with the standard optimization methods, the iterative method proposed here has improved design efficiency. In the later chapters, we will see that the iterative method can also be used for the design of multi-channel cosine-modulated QMF banks as well as 2-D QMF banks. In this section several issues such as choosing the initial point, effect of the smoothing parameter τ and effect of the weighting α will be addressed.

2.4.1 The Initial Point

Choosing an initial point is quite important to an iterative method. A good initial point can make the algorithm converge faster and lead to a better design. In the design of two-channel conventional QMF banks, a good initial point can be obtained by designing a linear phase half-band FIR filter with any conventional FIR filter design method such as the window method, the Remez exchange method, etc. [55]; in the design of two-channel low-delay QMF banks, the initial points can be obtained by either minimizing a quadratic least-squares objective function as in Algorithm 2.4, or by first using a conventional method to design a linear phase, lowpass, FIR filter and followed by taking the last $(N+k_d+1)/2$ filter coefficients obtained padded with $(N-k_d-1)/2$ zeros at the end to form the initial point, where N and k_d are the filter length and the desired reconstruction delay, respectively. By doing this the obtained filter will have a group delay of approximately $k_d/2$. In Figs. 2.14 and 2.15, two initial filters are illustrated which were obtained by the above-mentioned two methods.

Although a good initial point is important to the iterative method, our simulation study has indicated that the iterative method is more robust than standard optimization methods in the sense that in the former convergence is less sensitive to the initial point than in a standard optimization method like the BFGS method.

2.4.2 The Effect of Smoothing Parameter τ

From the case study presented in Sec. 2.3.5, we found that the smoothing parameter τ has an effect on the convergence rate. Taking the two designs with $N = 32$, $k_d = 15$ and $N = 24, k_d = 11$ as examples, Fig. 2.16(a) and (b) shows how the numbers of

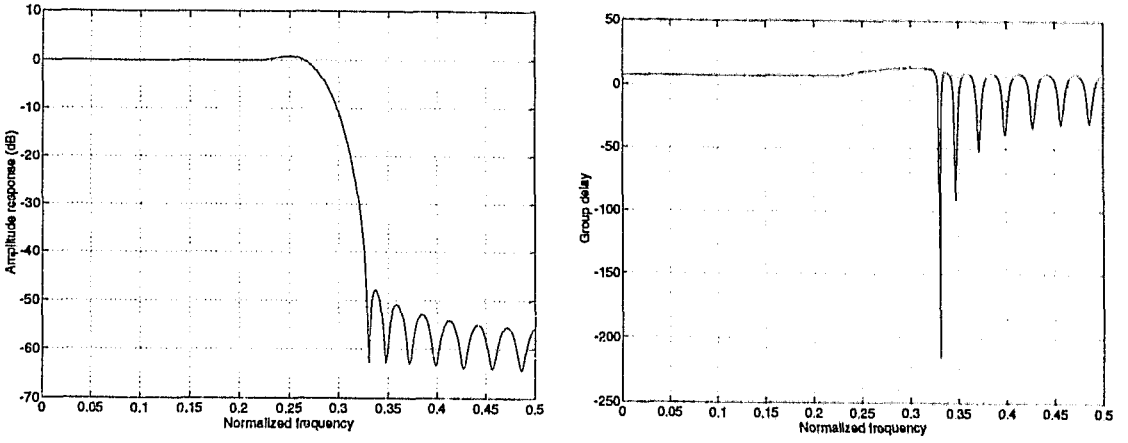

(a) (b)

Figure 2.14: The initial filter ($N = 32$, $k_d = 15$) obtained by the least-squares approach. (a) Amplitude response. (b) Group delay

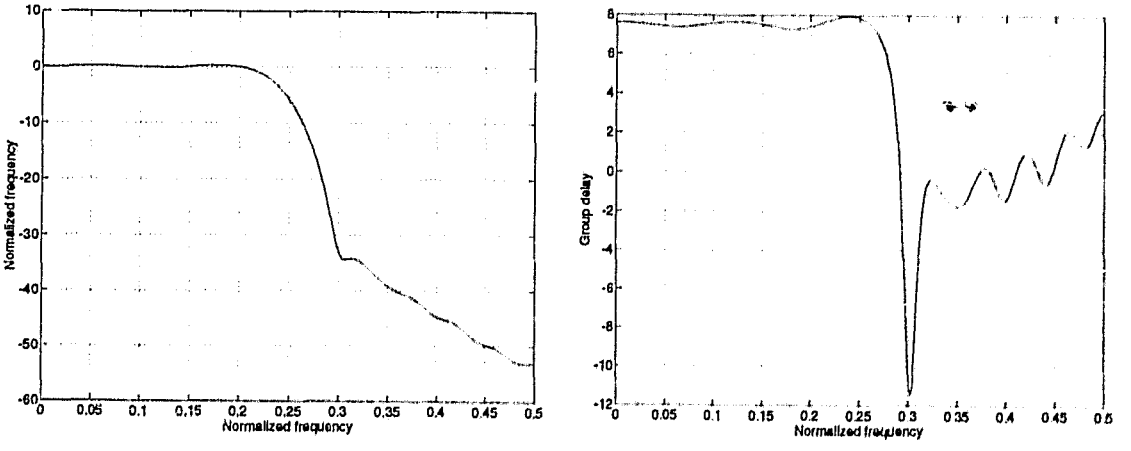

(a) (b)

Figure 2.15: The initial filter ($N = 32$, $k_d = 15$) obtained by the shifting method. (a) Amplitude response. (b) Group delay.

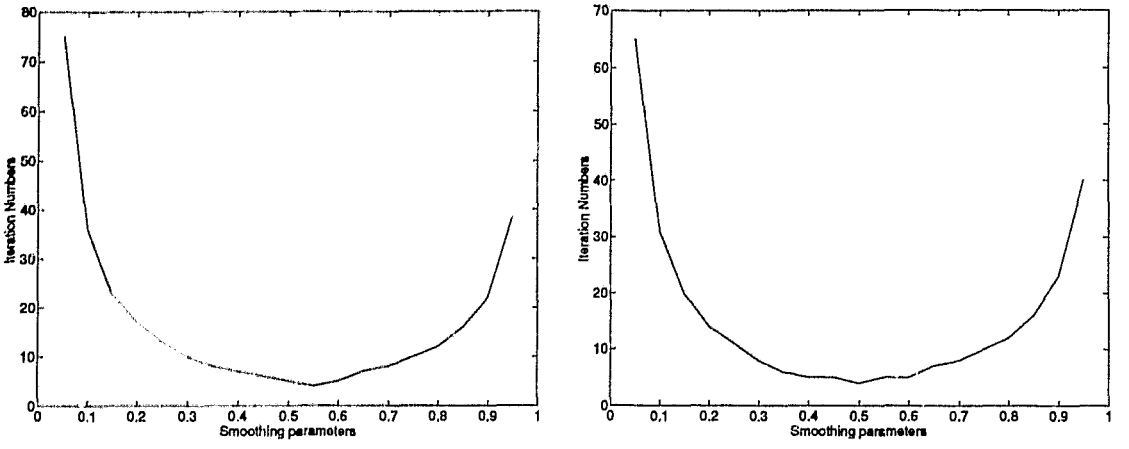

(a) (b)

Figure 2.16: Smooth parameter τ versus iteration numbers. (a) In the experiment when $N = 32$. (b) In the experiment when $N = 24$.

iteration depend on the choice of parameter τ. These two examples as well as many other designs have shown that the iterative design algorithm converges faster when a τ in the vicinity of 0.5 is used.

2.4.3 The Effect of Weighting α

In the iterative method, the objective function to be minimized is a weighted linear combination of two error components, which are related to the prefect reconstruction condition and the intraband aliasing, respectively. By adjusting the weighting α in the design, tradeoff between the reconstruction performance of the filter bank and the frequency response of the individual filters can be achieved. As α increases the stopband edge attenuation of individual filters is increased but the reconstruction error becomes larger as shown in Fig. 2.17.

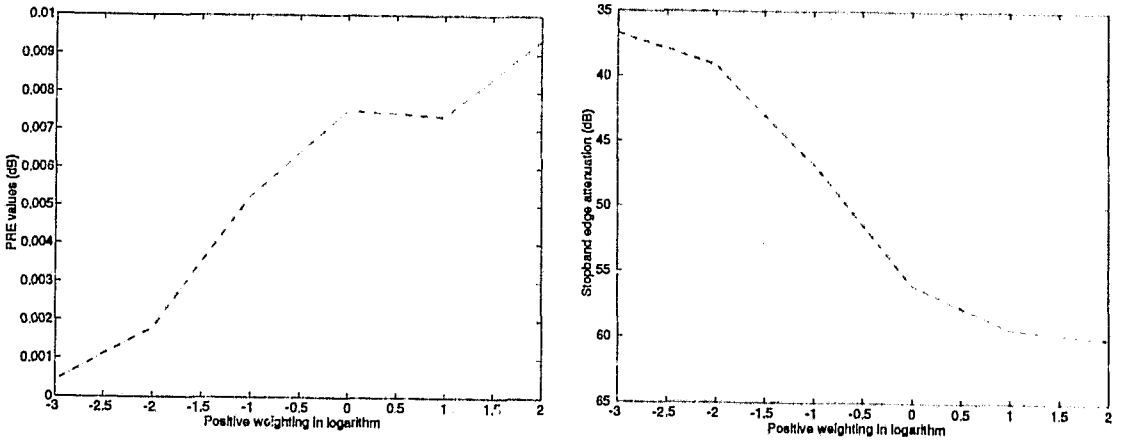

(a) (b)

Figure 2.17: (a) α versus PRE. (b) α versus SEA.

2.5 Conclusion

In this chapter, we have first proposed an improved version of the iterative method for the design of two-channel conventional QMF banks in which a simple and explicit formula for precise evaluation of integrals involved in the objective function is derived. This improvement significantly reduced the design complexity. Later the design of low-delay QMF banks has been considered and several design approaches have been demonstrated for the design of such filter banks. Comparisons have been made with another existing method which shows that the proposed method is superior in terms of design efficiency, performance of the filter banks obtained and implementation. The chapter concludes with some analysis on the iterative method in terms of choosing the appropriate initial points and the smoothing parameter.

Chapter 3

Time-Domain Approaches for the Design of QMF Banks

3.1 Introduction

As mentioned in Chapter 2, two-channel QMF banks have been widely used in one-dimensional (1-D) and two-dimensional (2-D) signal processing. In the design of QMF banks, it is required that the perfect reconstruction condition be satisfied while the intra-band aliasing be eliminated or minimized. Most design methods developed so far involve minimizing an error function directly in the frequency domain to achieve the design requirements, which leads to a nonlinear optimization problem.

In [11] an iterative algorithm for the design of QMF banks was proposed which involves calculating the eigenvalues and eigenvectors of a matrix in each step. In [12], Chen and Lee introduced an iterative procedure to replace the conventional direct minimization of the error function. Compared with the conventional QMF design techniques, this iterative design method requires much less computation and leads to fairly good results. Nevertheless two integrals involved in the objective function are evaluated by discretization, which degrades the performance of the QMF bank

designed and increases the computational complexity in the design. In Chapter 2, we have proposed an improved iterative method which significantly increases the design efficiency. In this chapter, we propose another approach in which the perfect reconstruction condition is formulated in the *time domain*. This also leads to reduced computational complexity in the design. In addition, on comparing with the algorithm of [11] there is no need to calculate eigenvalues and eigenvectors and a linear update formula is adopted which improves the convergence speed. In Section 3.3, this time-domain approach is extended to the design of two-channel low-delay QMF bank.

3.2 Design of Conventional QMF Banks

3.2.1 Problem Formulation

As mentioned in Chapter 2, in a conventional QMF bank filter H_0 has symmetrical impulse response which guarantees that the filter has linear phase response, and perfect reconstruction requires that

$$H_0^2(z) - H_0^2(-z) = z^{-(N-1)} \tag{3.1}$$

where N is the length of filter H_0 and is assumed to be even. The reconstruction delay is $N-1$. Eqn. (3.1) can be expressed in the time-domain by using the convolution as

$$\mathbf{Bh} = \mathbf{m} \tag{3.2}$$

with

$$\mathbf{B} = [\ \mathbf{d}_1 + \mathbf{d}_N \quad \mathbf{d}_2 + \mathbf{d}_{N-1} \quad \cdots \quad \mathbf{d}_{N/2} + \mathbf{d}_{N/2+1}\ ]$$

$$\mathbf{D} = [\ \mathbf{d}_1\ \mathbf{d}_2\ \cdots\ \mathbf{d}_N\ ]$$

$$= 2\begin{bmatrix} h(1) & h(0) & 0 & & \cdots & 0 \\ h(3) & h(2) & h(1) & h(0) & \cdots & 0 \\ \vdots & \vdots & & & & \vdots \\ h(N-1) & h(N-2) & & & \cdots & h(0) \end{bmatrix}$$

$$\mathbf{h} = [\ h(0)\ h(1)\ \cdots\ h(N/2-1)\ ]^T$$

$$\mathbf{m} = [\ 0\ \cdots\ 0\ 1\ ]^T$$

where $h(n)$, for $n = 0,\ 1,\ 2,\ \ldots,\ N/2-1$, is the impulse response of filter H_0.

By considering the design specifications for the frequency response of H_0, the L_2 objective function

$$\Psi = \int_0^{\omega_p} [M_h(\omega) - 1]^2 d\omega + \int_{\omega_s}^{\pi} M_h^2(\omega) d\omega \tag{3.3}$$

can be constructed, where ω_p and ω_s are passband and stopband edges of H_0, respectively, $M_h(\omega) = 2\mathbf{h}^T\mathbf{c}(\omega)$, and $\mathbf{c}(\omega) = [\ \cos(\frac{N-1}{2})\omega\ \cdots\ \cos\frac{1}{2}\omega\ ]^T$.

Taking the perfect reconstruction condition (3.2) into account, the design problem is reduced to minimizing Ψ in (3.3) subject to the constraints in (3.2). Hence the design problem now becomes a constrained optimization problem.

3.2.2 Iterative Approach

Instead of solving the above-mentioned constrained optimization problem directly, which in general is time-consuming, an iterative approach is employed. The objective function in this approach is assumed to be

$$E = E_1 + \alpha E_2 \tag{3.4a}$$

where α is a positive weight. Error component

$$E_1 = (\mathbf{Bf} - \mathbf{m})^T(\mathbf{Bf} - \mathbf{m}) \tag{3.4b}$$

where $\mathbf{B}$ and $\mathbf{m}$ are defined in (3.2), and $\mathbf{f} = [\ f(0)\ f(1)\ \cdots\ f(N/2-1)\ ]^T$, is used to approximate the prefect reconstruction condition in the time-domain. Error component

$$E_2 = \int_0^{\omega_p} [M_f(\omega) - 1]^2 d\omega + \int_{\omega_s}^{\pi} M_f^2(\omega) d\omega \tag{3.4c}$$

where $M_f(\omega) = 2\,\mathbf{f}^T\mathbf{c}(\omega)$ deals with the amplitude response requirement.

The iteration starts by designing a linear phase lowpass filter H_0 and using half of its coefficients to form the initial $\mathbf{h}$. Then E in (3.4a) can be formulated as a quadratic function of $\mathbf{f}$, i.e.,

$$E = \mathbf{f}^T(\mathbf{B}^T\mathbf{B} + 4\,\alpha\mathbf{Q})\,\mathbf{f} + (\alpha\mathbf{b}^T - 2\mathbf{m}^T\mathbf{B})\,\mathbf{f} + \omega_p + 1 \tag{3.5}$$

where

$$\mathbf{Q} = \int_0^{\omega_p} \mathbf{c}(\omega)\mathbf{c}^T(\omega)d\omega + \int_{\omega_s}^{\pi} \mathbf{c}(\omega)\mathbf{c}^T(\omega)d\omega$$

with its $(i,j)th$ entry given by

$$\begin{aligned} q_{ij} = & \int_0^{\omega_p} \cos\left[\left(i-1-\frac{N-1}{2}\right)\omega\right] \cos\left[\left(j-1-\frac{N-1}{2}\right)\omega\right] d\omega \\ & + \int_{\omega_s}^{\pi} \cos\left[\left(i-1-\frac{N-1}{2}\right)\omega\right] \cos\left[\left(j-1-\frac{N-1}{2}\right)\omega\right] d\omega \\ = & \frac{1}{2}\begin{cases} \psi(a_1,\omega_p,\omega_s) + \pi - \omega_s + \omega_p & i = j \\ \psi(a_1,\omega_p,\omega_s) + \psi(a_2,\omega_p,\omega_s) & i \neq j \end{cases} \end{aligned} \tag{3.6a}$$

where

$$\psi(k,\,\omega_p,\,\omega_s) = [\sin(k\omega_p) - \sin(k\omega_s)]/k$$

$$a_1 = i + j - N - 1$$

$$a_2 = i - j$$

and

$$\mathbf{b} = -8 \begin{bmatrix} \sin(\frac{N-1}{2}\omega_p)/(N-1) \\ \sin(\frac{N-3}{2}\omega_p)/(N-3) \\ \vdots \\ \sin(\frac{1}{2}\omega_p) \end{bmatrix} \tag{3.6b}$$

Evidently, $\mathbf{B^T B} + 4\ \alpha\mathbf{Q}$ is positive definite and the global minimum of E is achieved if

$$\mathbf{f} = -\frac{1}{2}(\mathbf{B}^T\mathbf{B} + 4\ \alpha\mathbf{Q})^{-1}(\alpha\mathbf{b} - 2\mathbf{B}^T\mathbf{m}) \tag{3.7}$$

Having obtained $\mathbf{f}$, a linear formula is used to update $\mathbf{h}$

$$\mathbf{h} := (1-\tau)\mathbf{h} + \tau\mathbf{f} \tag{3.8}$$

and the above procedure is repeated until $\| \mathbf{f} - \mathbf{h} \|$ is smaller than a prescribed tolerance.

On the basis of the preceding analysis, an iterative algorithm can now be constructed as follows:

Algorithm 3.1

Step 1 Use a conventional method (e.g., the window method) to design a linear phase, lowpass, FIR filter of length N and use its coefficients to form the initial $\mathbf{h}$.

Step 2 Calculate $\mathbf{Q}$ and $\mathbf{b}$ using (3.6a) and (3.6b).

Step 3 Form $\mathbf{B}$ and $\mathbf{m}$ in (3.2), and compute $\mathbf{f}$ in (3.7).

Step 4 If $\| \mathbf{h} - \mathbf{f} \| < \epsilon$, where ϵ is a prescribed tolerance, output $\mathbf{f}$ as the design result and stop. Otherwise, update $\mathbf{h}$ using (3.8) with a τ close to 0.5 and repeat from Step 3.

3.2.3 Design Examples

In this section a case study is presented to demonstrate the proposed iterative approach. Two design examples are obtained by applying the proposed algorithm and comparisons of the proposed method with the method of Chen and Lee [12] are made in terms of design efficiency and performance of the filter banks obtained.

The parameters used in the two designs, which will be referred to as Examples 3.1 and 3.2, are $N = 32, \alpha = 0.1$, $\omega_p = 0.3\pi$, $\omega_s = 0.6\pi$, $\tau = 0.5$, $\epsilon = 10^{-3}$, and $N = 80, \alpha = 1$, $\omega_p = 0.3\pi$, $\omega_s = 0.55\pi$, $\tau = 0.5$, $\epsilon = 10^{-3}$, respectively. The initial $\mathbf{h}$ was obtained by the window method. For comparison purposes the method of Chen and Lee [12] was applied to design two QMF banks with parameters specified as $N = 32$, $\alpha = 1$, $\omega_s = 0.6\pi$, $\tau = 0.5$, $\epsilon = 10^{-3}$; $N = 80$, $\alpha = 1$, $\omega_s = 0.55\pi$, $\tau = 0.5$, $\epsilon = 10^{-3}$, and using the same initial $\mathbf{h}$ as for the proposed method. The comparison parameters are the same as in Sec. 2.2.3. The number of frequency sampling points was set to $8N$ when implementing the method of [12], where N is the filter length. The results are summarized in Table 3.1. Fig. 3.1 (a) and (b) shows the amplitude response of H_0 and the QMF bank, respectively, for Example 3.1 and Fig. 3.2 (a) and (b) shows those for Example 3.2. As can be observed from the comparisons, the proposed method can achieve almost the same designs as the method of [12] with only about 5 percent of the computation.

Table 3.1: Comparisons of the proposed method and the method by Chen and Lee.

	Example 3.1		Example 3.2	
	Proposed	Chen-Lee	Proposed	Chen-Lee
NI	3	5	3	6
MFLOPS	0.064	1.18	0.85	20.19
A_a (dB)	34.9	35.27	42.5	42.9
A_p (dB)	0.0114	0.0131	0.0068	0.0044
PRE (dB)	0.0145	0.0152	0.0106	0.0091
SNR_s (dB)	82.9	83.4	83.3	82.7
SNR_r (dB)	69.5	67.8	75.3	75.0

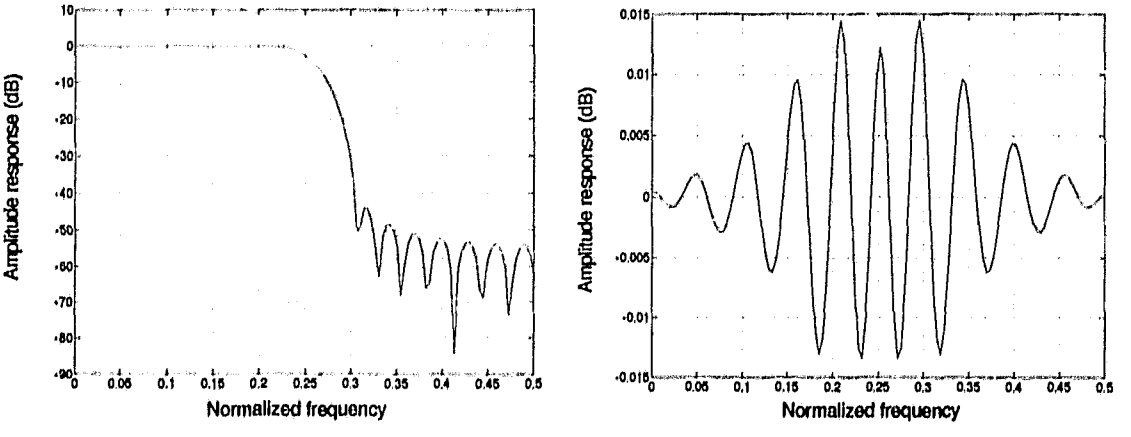

(a) (b)

Figure 3.1: Example 3.1 (a) Amplitude response of filter H_0. (b) Amplitude response of filter bank.

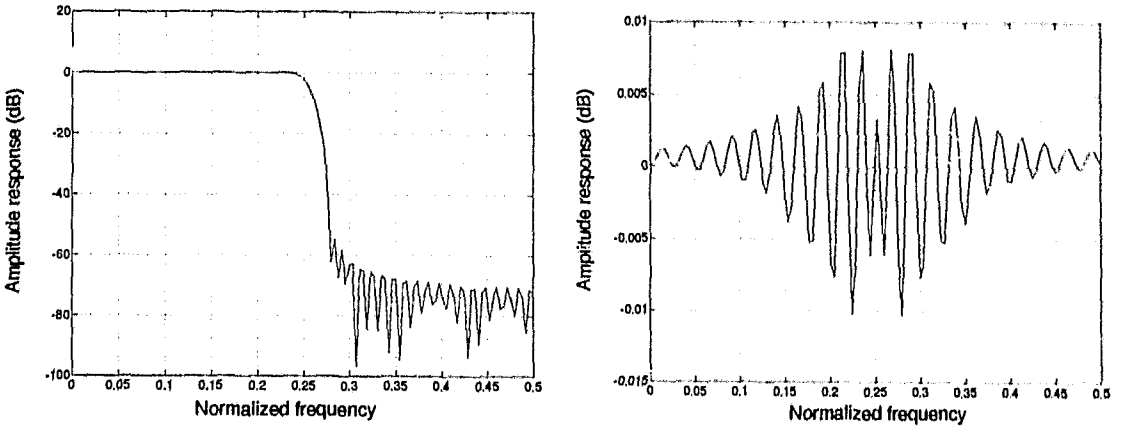

(a) (b)

Figure 3.2: Example 3.2 (a) Amplitude response of filter H_0. (b) Amplitude response of filter bank.

3.3 Design of Low-Delay QMF Banks

3.3.1 Problem Formulation

As shown in Chapter 2, the perfect reconstruction condition in a two-channel low-delay QMF bank becomes

$$H_0^2(z) - H_0^2(-z) = z^{-k_d} \tag{3.9}$$

where $k_d < N-1$ is the system delay. Equation (3.9) can be expressed in the time domain as

$$\mathbf{B}_L \mathbf{h}_L = \mathbf{m}_L \tag{3.10a}$$

where $\mathbf{h}_L = [\, h(0)\ h(1)\ \cdots\ h(N-1)\,]^T$ is the impulse-response vector of H_0, and

$$\mathbf{m}_L = [\, 0\ \cdots\ 0\ 1\ 0\ \cdots\ 0\,]^T \tag{3.10b}$$

where the $[(k_d+1)/2]th$ entry is unity, and $\mathbf{B}_L$ is a $(N-1)\times N$ matrix defined by

$$\mathbf{B}_L = 2\begin{bmatrix} h(1) & h(0) & 0 & \cdots & 0 \\ h(3) & h(2) & h(1) & \cdots & \vdots \\ \vdots & & & & \\ h(N-1) & h(N-2) & \cdots & & h(0) \\ 0 & 0 & h(N-1) & \cdots & h(2) \\ \vdots & & & & \\ 0 & \cdots & & h(N-1) & h(N-2) \end{bmatrix} \tag{3.10c}$$

To meet the design specifications for the frequency response of H_0, the L_2 objective function

$$\Psi = \int_0^{\omega_p} |H_0(e^{j\omega}) - e^{-jk_d\omega/2}|^2 d\omega + \int_{\omega_s}^{\pi} |H_0(e^{j\omega})|^2 d\omega \tag{3.11}$$

can be constructed where ω_p and ω_s are the passband and stopband edges of H_0, respectively.

Taking the perfect reconstruction condition in (3.10a) into account, the design problem is reduced to minimizing Ψ in (3.11) subject to the constraints in (3.10a), which is a constrained optimization problem.

3.3.2 Iterative Approach

As in the design of a conventional QMF bank, an iterative approach is proposed for the design of two-channel low-delay QMF banks in which the objective function is formed as

$$E_L = E_{L1} + \alpha E_{L2} \tag{3.12a}$$

where $\alpha > 0$ is a weighting constant,

$$E_{L1} = (\mathbf{B}_L\mathbf{f}_L - \mathbf{m}_L)^T(\mathbf{B}_L\mathbf{f}_L - \mathbf{m}_L) \tag{3.12b}$$

deals with the prefect reconstruction condition with $\mathbf{B}_L$ and $\mathbf{m}_L$ defined in (3.10c) and (3.10b), respectively, and $\mathbf{f}_L = [\ f(0)\ f(1)\ \cdots\ f(N-1)\ ]^T$. The error component

$$E_{L2} = \int_0^{\omega_p} |F_0(e^{j\omega}) - e^{-jk_d\omega/2}|^2 d\omega + \int_{\omega_s}^{\pi} |F_0(e^{j\omega})|^2 d\omega \tag{3.12c}$$

deals with frequency-response requirements where $F_0(e^{j\omega}) = \mathbf{f}_L^T \mathbf{c}_L(\omega)$ and $\mathbf{c}_L(\omega) = [\ 1\ e^{-j\omega}\ \cdots\ e^{-j\omega(N-1)}\ ]^T$.

The iteration procedure starts by first designing a lowpass filter H_0 with a group delay $k_d/2$, where k_d is the desired system delay, and taking its impulse-response vector as the initial $\mathbf{h}_L$. Then error E_L in (3.12a) can be formulated as a quadratic function in $\mathbf{f}_L$, i.e.,

$$E_L = \mathbf{f}_L^T(\mathbf{B}_L^T\mathbf{B}_L + \alpha\mathbf{Q}_L)\ \mathbf{f}_L + (\alpha\mathbf{b}_L^T - 2\mathbf{m}_L^T\mathbf{B}_L)\ \mathbf{f}_L + \omega_p + 1 \tag{3.13}$$

where

$$\begin{aligned}\mathbf{Q}_L &= \mathrm{Re}\left[\int_0^{\omega_p} \mathbf{c}_L(\omega)\mathbf{c}_L^H(\omega)\ d\omega + \int_{\omega_s}^{\pi} \mathbf{c}_L(\omega)\mathbf{c}_L^H(\omega)\ d\omega\right] \\ &= \mathbf{U}_p + \mathbf{U}_s \end{aligned} \tag{3.14a}$$

with $\mathbf{U}_p$ and $\mathbf{U}_s$ being two Toeplitz matrices defined by

$$\mathbf{U}_p = \begin{bmatrix} \omega_p & \sin\omega_p & \cdots & \frac{1}{N-1}\sin(N-1)\omega_p \\ \sin\omega_p & \omega_p & \cdots & \frac{1}{N-2}\sin(N-2)\omega_p \\ \vdots & & \ddots & \vdots \\ \frac{1}{N-1}\sin(N-1)\omega_p & \cdots & \cdots & \omega_p \end{bmatrix}$$

$$\mathbf{U}_s = \begin{bmatrix} \pi - \omega_s & -\sin\omega_s & \cdots & -\frac{1}{N-1}\sin(N-1)\omega_s \\ -\sin\omega_s & \pi - \omega_s & \cdots & -\frac{1}{N-2}\sin(N-2)\omega_s \\ \vdots & & \ddots & \vdots \\ -\frac{1}{N-1}\sin(N-1)\omega_s & \cdots & \cdots & \pi - \omega_s \end{bmatrix}$$

and

$$\mathbf{b}_L = -2 \text{ Re } \left[\int_0^{\omega_p} \mathbf{c}(\omega) e^{jk_d\omega/2}\, d\omega\right]$$

$$= -2 \begin{bmatrix} \frac{2}{k_d} \sin\left(\frac{k_d\omega_p}{2}\right) \\ \frac{2}{k_d-2} \sin\left[\left(\frac{k_d}{2}-1\right)\omega_p\right] \\ \vdots \\ \frac{2}{k_d-2N+2} \sin\left[\left(\frac{k_d}{2}-N+1\right)\omega_p\right] \end{bmatrix} \tag{3.14b}$$

Since $\mathbf{B}_L^T\mathbf{B}_L + \alpha\mathbf{Q}_L$ is positive definite, the global minimum of E_L is achieved if

$$\mathbf{f}_L = -\tfrac{1}{2}(\mathbf{B}_L^T\mathbf{B}_L + \alpha\mathbf{Q}_L)^{-1}(\alpha\mathbf{b}_L - 2\mathbf{B}_L^T\mathbf{m}_L) \tag{3.15}$$

Having obtained $\mathbf{f}_L$, a linear formula is used to update $\mathbf{h}_L$

$$\mathbf{h}_L := (1-\tau)\mathbf{h}_L + \tau\mathbf{f}_L \tag{3.16}$$

and the above process is repeated until $\| \mathbf{h}_L - \mathbf{f}_L \|$ is less than a prescribed tolerance.

The design procedure can be summarized as follows:

Algorithm 3.2

Step 1 Use a least-squares approach mentioned in Chapter 2 to design a low-pass FIR filter of length N with a group delay $k_d/2$, and passband and stopband edges ω_p and ω_s, respectively; then use the coefficient vector of the filter obtained as the initial $\mathbf{h}_L$.

Step 2 Calculate $\mathbf{Q}_L$ and $\mathbf{b}_L$ using (3.14a) and (3.14b), respectively.

Step 3 Use (3.10c) and (3.10b) to form $\mathbf{B}_L$ and $\mathbf{m}_L$, and compute $\mathbf{f}_L$ in (3.15).

Step 4 If $\| \mathbf{h}_L - \mathbf{f}_L \| < \epsilon$, where ϵ is a prescribed tolerance, output $\mathbf{f}_L$ as the design result and stop; otherwise, update $\mathbf{h}_L$ using (3.16) with a τ close to 0.5 and repeat from Step 3.

As mentioned in Chapter 2, when a low reconstruction delay k_d is required, artifacts may occur in the transition band of the obtained analysis and synthesis filters. This problem can be eliminated by modifying the objective function to include an additional term $\alpha_1 E_3$, i.e.,

$$E_L = E_{L1} + \alpha E_{L2} + \alpha_1 E_{L3} \tag{3.17}$$

where

$$E_{L3} = \int_{\omega_{t1}}^{\omega_{t2}} |F_0(e^{j\omega}) - e^{-jk_d\omega/2}|^2 \, d\omega \tag{3.18}$$

and $[\omega_{t1},\ \omega_{t2}]$ is an interval in the transition band where the artifacts occur. It can be readily shown that with this additional error term, the proposed algorithm can still be used after modifying (3.13) as

$$E_L = \mathbf{f}_L^T(\mathbf{B}_L^T\mathbf{B}_L + \alpha\mathbf{Q}_L + \alpha_1\mathbf{Q}_t)\ \mathbf{f}_L + (\alpha\mathbf{b}_L^T + \alpha_1\mathbf{b}_t^T - 2\mathbf{m}_L^T\mathbf{B}_L)\ \mathbf{f}_L + K \tag{3.19}$$

where K is a constant,

$$\mathbf{Q}_t = \begin{bmatrix} \omega_{t2} - \omega_{t1} & \phi(\omega_{t2}, \omega_{t1}, 1) & \cdots & \phi(\omega_{t2}, \omega_{t1}, N-1) \\ \phi(\omega_{t2}, \omega_{t1}, 1) & \omega_{t2} - \omega_{t1} & & \\ \vdots & & & \\ \phi(\omega_{t2}, \omega_{t1}, N-1) & \cdots & \cdots & \omega_{t2} - \omega_{t1} \end{bmatrix}$$

$$\phi(\omega_{t2},\ \omega_{t1},\ k) = \frac{1}{k}\left[\sin k\omega_{t2} - \sin k\omega_{t1}\right]$$

and

$$\mathbf{b}_t = -2\ \mathrm{Re}\left[\int_{\omega_{t1}}^{\omega_{t2}} \mathbf{c}(\omega) e^{jk_d\omega/2}\, d\omega\right]$$

$$= -2 \begin{bmatrix} \phi(\omega_{t2}, \omega_{t1}, \frac{k_d}{2}) \\ \phi(\omega_{t2}, \omega_{t1}, \frac{k_d}{2} - 1) \\ \vdots \\ \phi(\omega_{t2}, \omega_{t1}, \frac{k_d}{2} - N + 1) \end{bmatrix}$$

The global minimum of E_L is now given by

$$\mathbf{f}_L = -\tfrac{1}{2}(\mathbf{B}_L^T \mathbf{B}_L + \alpha \mathbf{Q}_L + \alpha_1 \mathbf{Q}_t)^{-1}(\alpha \mathbf{b}_L + \alpha_1 \mathbf{b}_t - 2\mathbf{B}_L^T \mathbf{m}_L) \tag{3.20}$$

3.3.3 Design Examples

We now present a design example, which is referred to as Example 3.3, to illustrate the proposed iterative approach. The design parameters are $N = 32$, $k_d = 15$, $\alpha = 5 \times 10^{-3}$, $\alpha_1 = 3 \times 10^{-5}$, $\omega_p = 0.35\pi$, $\omega_s = 0.72\pi$, $\omega_{t1} = 0.35\pi$, $\omega_{t2} = 0.45\pi$, $\tau = 0.5$ and $\epsilon = 10^{-3}$. The design was achieved after 8 iterations.

For comparison purposes, we refer to Example 6.6.1 presented in [34], which is designed by a different time-domain approach. The comparisons are made in terms of the parameters defined in Sec. 2.2.3. The results are summarized in Table 3.2. The amplitude responses of the lowpass analysis filters designed by the proposed method and the method of [34] are depicted in Fig. 3.3 (a). The group delay characteristic of filter H_0 obtained by the proposed method is shown in Fig. 3.3 (b) from where it can be noticed that the filter has approximately linear phase in the passband.

As can be seen in Table 3.2, the proposed method has resulted in a large increase in the minimum stopband attenuation relative to the design approach in [34]. The number of floating-point operations needed for the design was only 1.26×10^6, which should be substantially lower than that required by the method of [34], which is not known.

Table 3.2: Comparisons between the proposed method and the method by Nayebi.

	Proposed	Method of [34]
MFLOPS	1.26	-
A_a (dB)	60.96	36.97
A_p (dB)	0.0532	0.0537
PRE (dB)	1.8×10^{-3}	1.2×10^{-3}
SNR_s (dB)	78.5	75.8
SNR_r (dB)	77.6	77.4

3.4 Conclusion

A new time-domain approach has been proposed in which the perfect reconstruction condition is formulated in the time-domain. Then an iterative method has been applied to minimize the objective function which reduces the computational complexity significantly compared with the iterative method proposed by Chen and Lee in which a discretized version of the objective function was formulated in the frequency-domain. The new time-domain approach has also been extended to the design of two-channel low-delay QMF banks. From the design examples, it can be observed that the proposed approaches for the design of two-channel QMF banks are very efficient.

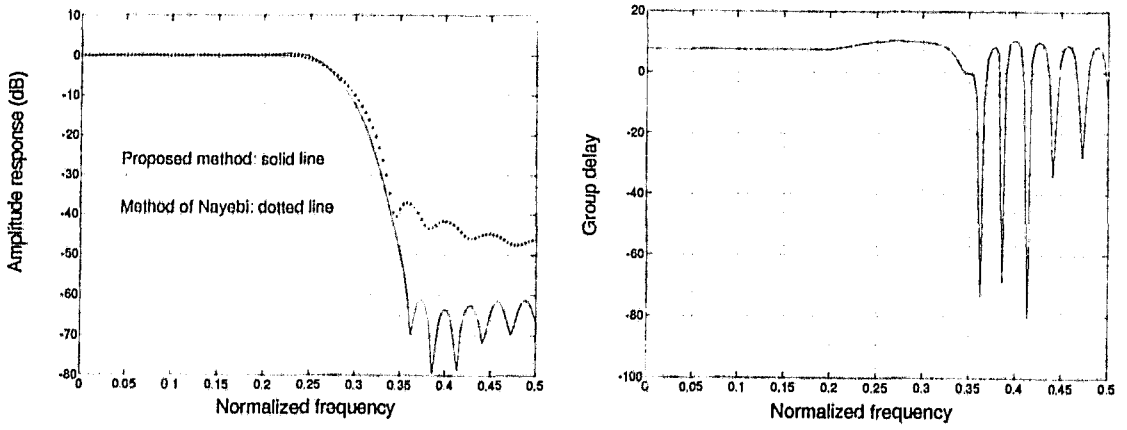

(a) (b)

Figure 3.3: Example 3.3 (a) Amplitude responses of analysis lowpass filters. (b) Group delay of H_0.

Chapter 4

Design of QMF Banks with Perfect Reconstruction

4.1 Introduction

The importance of QMF banks in subband coding has been widely recognized. Since the quadrature mirror structure leads to complete cancellation of interband aliasing due to the overlapping filter responses, the design is reduced to satisfying the perfect reconstruction condition while minimizing the intraband aliasing. Since the mid 70's several approaches have been proposed for the design of QMF banks. Some of the design methods lead to near-perfect reconstruction QMF banks [11] [12] while others lead to perfect reconstruction QMF banks [22][56].

In Chapters 2 and 3, we proposed several approaches for the design of two-channel QMF banks in which *near-perfect* reconstruction is achieved. In some applications filter banks with perfect reconstruction are desired. In this chapter, a new method for the design of linear phase *perfect reconstruction* QMF banks is proposed on the basis of a time-domain formulation. The analysis lowpass filter is first obtained by a conventional method and the synthesis lowpass filter is obtained by

a null-space projection approach. In Section 4.3, the proposed method is extended to the design of low-delay *perfect reconstruction* QMF banks which are useful in applications where long reconstruction delays are undesirable.

4.2 Design of Linear-Phase QMF Banks

4.2.1 Problem Formulation

Consider a two-channel filter bank whose output and input relation is given by

$$\begin{aligned}\hat{X}(z) = &\tfrac{1}{2}[H_0(z)G_0(z) + H_1(z)G_1(z)] \cdot X(z) \\ &+\tfrac{1}{2}[H_0(-z)G_0(z) + H_1(-z)G_1(z)] \cdot X(-z)\end{aligned} \tag{4.1}$$

where the second term on the right side represents the aliasing. By assuming that $G_1(z) = -H_0(-z), H_1(z) = G_0(-z)$, the aliasing term is cancelled and (4.1) becomes

$$\hat{X}(z) = \tfrac{1}{2}[H_0(z)G_0(z) - H_0(-z)G_0(-z)]X(z) \tag{4.2}$$

To reconstruct the output perfectly, it is required that

$$H_0(z)G_0(z) - H_0(-z)G_0(-z) = z^{-k_d} \tag{4.3}$$

where k_d is the system delay. If we assume that the coefficients of $H_0(z)$ and $G_0(z)$ are symmetrical and their lengths, N and M, are even, $M > N$, and $N + M$ is a multiple of 4, then it can be readily shown that k_d in (4.3) is equal to $(M+N)/2-1$.

In the time domain, (4.3) can be expressed as

$$\mathbf{Hg} = \mathbf{m} \tag{4.4}$$

where

$$\mathbf{H} = 2\ [\ \mathrm{b}_1 + \mathrm{b}_M\ \ \mathrm{b}_2 + \mathrm{b}_{M-1}\ \cdots\ \mathrm{b}_{\frac{M}{2}} + \mathrm{b}_{\frac{M}{2}+1}\ ]$$

$$\mathbf{B} = [\ \mathbf{b}_1\ \mathbf{b}_2\ \cdots\ \mathbf{b}_M\ ]$$

$$= \begin{bmatrix} h(1) & h(0) & 0 & \cdots & \cdots & 0 \\ h(3) & h(2) & h(1) & h(0) & \cdots & 0 \\ \vdots & & & & & \vdots \\ h(N-1) & h(N-2) & \cdots & & \cdots & 0 \\ 0 & 0 & h(N-1) & \cdots & & \\ \vdots & & \vdots & & & \vdots \end{bmatrix}$$

$$\mathbf{g} = [\ g(0)\ g(1)\ \cdots\ g(M/2-1)\ ]^T$$

$$\mathbf{m} = [\ 0\ \cdots\ 0\ 1\ ]^T \in \mathbf{R}^{\frac{M+N}{4}\times 1}$$

$\{h(n)$, for $n = 0, \ldots, N-1\}$ is the impulse response of filter H_0, and $\{g(n)$, for $n = 0, \cdots, M/2-1\}$ is the first half of the impulse response of filter G_0. In our approach, H_0 is first designed by a conventional FIR filter design method; then the entries of g are obtained by solving the linear system of equations in (4.4), where we have $(M+N)/4$ equations and $M/2$ unknowns. This leads to the number of degrees of freedom

$$f_d = \frac{M}{2} - \frac{M+N}{4} = \frac{M-N}{4} \tag{4.5}$$

4.2.2 Null-Space Projection Approach

As is well known, the general solution of (4.4) is given by

$$\mathbf{g} = \mathbf{H}^{\dagger}\mathbf{m} + (\mathbf{I} - \mathbf{H}^{\dagger}\mathbf{H})\phi \tag{4.6}$$

where $\mathbf{H}^{\dagger}$ is the Moore-Penrose pseudo-inverse of $\mathbf{H}$, and ϕ is an arbitrary column vector. Note that

$$\mathbf{H}(\mathbf{I} - \mathbf{H}^{\dagger}\mathbf{H})\phi = 0$$

i.e., the second term on the right side of (4.6) represents a vector in the null space of $\mathbf{H}$. In other words, $(\mathbf{I} - \mathbf{H}^{\dagger}\mathbf{H})\phi$ projects an arbitrary vector ϕ onto the null space of $\mathbf{H}$. Let

$$\mathbf{H} = \mathbf{U} \begin{bmatrix} \sigma_1 & & & 0 & \cdots & 0 \\ & \ddots & & \vdots & & \vdots \\ & & \sigma_{\frac{M+N}{4}} & 0 & \cdots & 0 \end{bmatrix} \mathbf{V}^T \tag{4.7}$$

be the singular value decomposition (SVD) of $\mathbf{H}$. It can be shown that $\mathbf{g}$ in (4.6) can be written as

$$\mathbf{g} = \mathbf{S}_c + \mathbf{V}^*\phi^* \tag{4.8}$$

where

$$\begin{aligned} \mathbf{S}_c &= \mathbf{H}^{\dagger}\mathbf{m} \\ &= \mathbf{V} \begin{bmatrix} \sigma_1^{-1} & & & \\ & \ddots & & \\ & & \sigma_{\frac{M+N}{4}}^{-1} & \\ 0 & \cdots & 0 & \\ \vdots & & \vdots & \\ 0 & \cdots & 0 & \end{bmatrix} \mathbf{U}^T\mathbf{m} \\ \mathbf{V}^* &= [\ \mathbf{v}_{\frac{M+N}{4}+1} \ \cdots \ \mathbf{v}_{\frac{M}{2}}\ ] \\ \phi^* &= [\ \phi_1^* \ \cdots \ \phi_{\frac{M-N}{4}}^*\ ]^T \end{aligned}$$

$\mathbf{v}_i$, for $i = (M+N)/4+1, \ldots, M/2$ is the ith column of matrix $\mathbf{V}$, and ϕ^* contains f_d free parameters. On comparing (4.8) with (4.6), it is observed that the last f_d column vectors of $\mathbf{V}^*$ constitute a basis of the null space of $\mathbf{H}$; hence the problem of designing G_0 amounts to finding an optimal ϕ^* such that the combination of the column vectors of $\mathbf{V}^*$, $\mathbf{V}^*\phi^*$, leads to the minimum of

$$E = \int_{\omega_s}^{\pi} M_0^2(\omega)\, d\omega$$

$$= (\mathbf{S}_c + \mathbf{V}^*\boldsymbol{\phi}^*)^T\mathbf{Q}(\mathbf{S}_c + \mathbf{V}^*\boldsymbol{\phi}^*) \tag{4.9}$$

where ω_s is the stopband edge of G_0,

$$\begin{aligned} M_g(\omega) &= 2\ \mathbf{g}^T\mathbf{c}(\omega) \\ \mathbf{c}(\omega) &= [\ \cos(\frac{M-1}{2}\omega)\ \cdots\ \cos(\frac{1}{2}\omega)\ ]^T \\ \mathbf{Q} &= 4\ \int_{\omega_s}^{\pi} \mathbf{c}(\omega)\mathbf{c}(\omega)^T\ d\omega \end{aligned}$$

and the $(i,\ j)th$ entry of $\mathbf{Q}$ is given by

$$q_{ij} = 2 \begin{cases} \pi - \omega_s - \frac{1}{a_1}\sin a_1\omega_s & i = j \\ -\frac{1}{a_1}\sin a_1\omega_s - \frac{1}{a_2}\sin a_2\omega_s & i \neq j \end{cases}$$

with $i,\ j = 1,\ \ldots,\ M/2$, $a_1 = i+j-N-1$, and $a_2 = i-j$. By imposing $\nabla_{\boldsymbol{\phi}^*} E = 0$, the minimum point can be obtained as

$$\boldsymbol{\phi}^*_{opt} = -(\mathbf{V}^{*\ T}\mathbf{Q}\mathbf{V}^*)^{-1}\mathbf{V}^{*\ T}\mathbf{Q}\mathbf{S}_c \tag{4.10}$$

and the coefficients of G_0 can be obtained as

$$\mathbf{g}^* = \mathbf{S}_c + \mathbf{V}^*\boldsymbol{\phi}^*_{opt} \tag{4.11}$$

The design procedure can now be summarized as follows:

Algorithm 4.1

Step 1 Use a conventional method to design a linear phase, lowpass, FIR filter H_0 whose length is N.

Step 2 Form matrices $\mathbf{H}$ and $\mathbf{m}$ in (4.4).

Step 3 Obtain the SVD of $\mathbf{H}$ as in (4.7), and calculate $\mathbf{S}_c$ and $\mathbf{Q}$ in (4.8) and (4.9), respectively.

Step 4 Obtain $\boldsymbol{\phi}^*_{opt}$ using (4.10) and $\mathbf{g}^*$ using (4.11).

4.2.3 Design Examples

We now present two design examples to illustrate the proposed algorithms. The related computer programs were written in MATLAB and run on a Sun SPARC station. The first example is referred as Example 4.1, and the design specifications are $N = 16, M = 24$. The analysis lowpass filter H_0 was first designed by the window method with passband and stopband edges 0.44π and 0.6π rad/s, respectively. The performance of the filter bank obtained is evaluated in terms of

$$\text{PRE} = \max_{\omega} |20 \log_{10} \left[|H_0(e^{j\omega})G_0(e^{j\omega}) - H_0(e^{j(\omega+\pi)})G_0(e^{j(\omega+\pi)})| \right]|$$

and SNR. The results obtained are listed in Table 4.1, and the amplitude responses of the analysis lowpass and highpass filters are depicted in Fig. 4.1 (a) and Fig. 4.1 (b) shows that of the obtained filter bank.

Table 4.1: Performance evaluations of filter banks for Examples 4.1 and 4.2.

	k_d	PRE (dB)	SNR_r (dB)
Example 4.1	19	3.02×10^{-13}	271.52
Example 4.2	25	1.28×10^{-14}	302.99

The second example is referred as Example 4.2 and the design specifications are $N = 20, M = 32$. The analysis lowpass filter H_0 was first designed by the window method with passband and stopband edges 0.44π and 0.61π rad/s, respectively. The results obtained are given in Table 4.1, and the amplitude responses of the analysis lowpass and highpass filters are depicted in Fig. 4.2 (a) and Fig. 4.2 (b) shows that of the filter bank.

The performance of the obtained filter banks can also be checked by observing

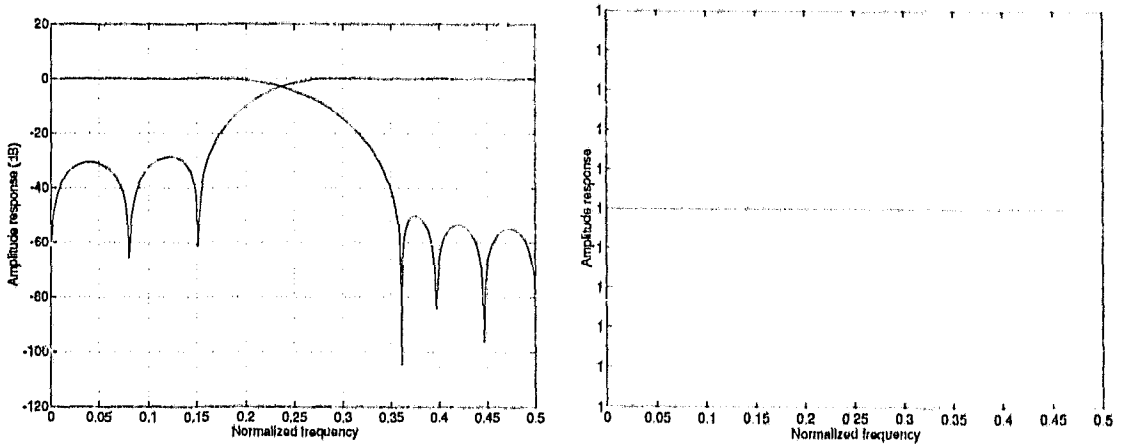

(a) (b)

Figure 4.1: Example 4.1 (a) Amplitude responses of analysis lowpass and highpass filters. (b) Amplitude response of the obtained filter bank.

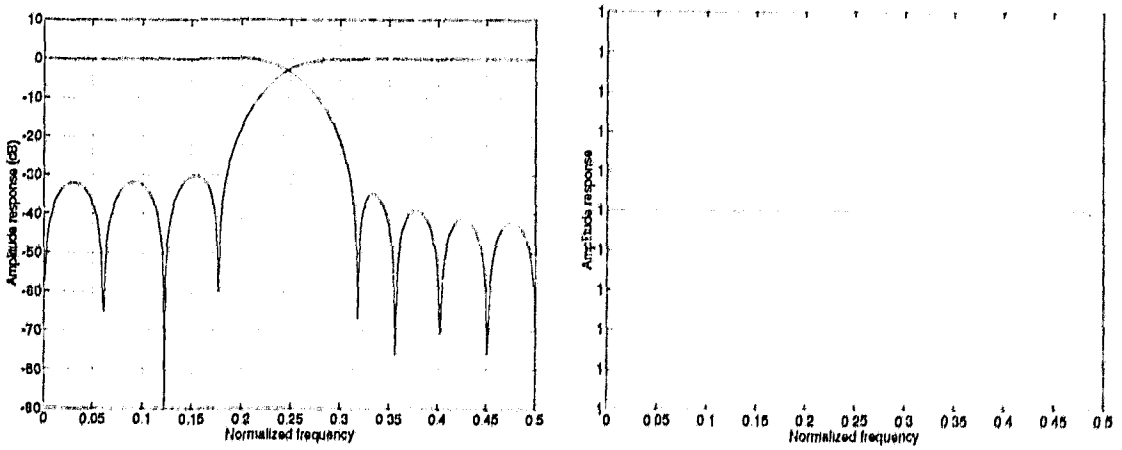

(a) (b)

Figure 4.2: Example 4.2 (a) Amplitude responses of analysis lowpass and highpass filters. (b) Amplitude response of the obtained filter bank.

Table 4.2: Outputs of the filter banks of Examples 4.1 and 4.2 with a ramp input.

n	$x(n)$	Example 4.1 $\hat{x}(n+19)$	Example 4.2 $\hat{x}(\ +25)$
0	1.0000000000000	1.0000000000000	1.0000000000000
1	2.0000000000000	2.0000000000000	2.0000000000000
2	3.0000000000000	3.0000000000000	3.0000000000000
3	4.0000000000000	4.0000000000000	4.0000000000000
4	5.0000000000000	5.0000000000000	5.0000000000000
5	6.0000000000000	6.0000000000000	6.0000000000000
6	7.0000000000000	7.0000000000001	7.0000000000000
7	8.0000000000000	8.0000000000001	8.0000000000000
8	9.0000000000000	9.0000000000001	9.0000000000000
9	10.0000000000000	10.0000000000001	10.0000000000000

the output when the input is a ramp signal. As shown in Table 4.2 where $x(n)$ and $\hat{x}(n)$ are input and output, respectively, for both examples the reconstructed signals were exactly the same as the input signal to within at least 12 significant digits after the decimal point.

4.3 Design of Low-Delay QMF Banks

4.3.1 Problem Formulation

The assumption of linear phase responses for H_0 and G_0 leads to fixed system delay $(M+N)/2-1$, which is sometimes undesirable in applications where the orders of the filters are high. If the assumption on symmetry of the coefficients in $H_0(z)$ and

$G_0(z)$ is removed, then it is possible to design a filter bank with low reconstruction delay. We assume that the desired reconstruction delay k_d is an odd integer. The perfect reconstruction condition expressed in (4.3) can be written in the time-domain as

$$\mathbf{H}_L \mathbf{g}_L = \mathbf{m}_L \tag{4.12}$$

where

$$\mathbf{H}_L = 2\begin{bmatrix} h(1) & h(0) & 0 & \cdots & \cdots & 0 \\ h(3) & h(2) & h(1) & h(0) & \cdots & 0 \\ \vdots & & & & & \vdots \\ h(N-1) & h(N-2) & \cdots & & \cdots & 0 \\ 0 & 0 & h(N-1) & \cdots & & \\ \vdots & & & & & \vdots \\ 0 & \cdots & & & h(N-1) & h(N-2) \end{bmatrix}$$

$$\mathbf{g}_L = [\, g(0)\ g(1)\ \cdots\ g(M-1)\,]^T$$

$$\mathbf{m}_L = [\, 0\ \cdots\ 0\ 1\ 0\ \cdots\ 0\,]^T \in \mathbf{R}^{\frac{M+N}{2}-1\times 1}$$

where the $[(k_d+1)/2]$th entry of $\mathbf{m}_L$ is unity. A lowpass FIR filter H_0 is first designed with group delay $k_{d1} < (N-1)/2$ and then $\mathbf{g}_L$ is obtained by solving (4.12). In (4.12) there are $(M+N)/2-1$ equations and M unknowns. Hence the number of degrees of freedom in the design is

$$f_d = M - \frac{M+N}{2} + 1 = \frac{M-N}{2} + 1 \tag{4.13}$$

4.3.2 Null-Space Projection Approach

As in the design of linear phase QMF banks described in the preceding section, the general solution of (4.12) is given by

$$\mathbf{g}_L = \mathbf{H}_L^{\dagger}\mathbf{m}_L + (\mathbf{I} - \mathbf{H}_L^{\dagger}\mathbf{H}_L)\boldsymbol{\phi}_L \tag{4.14}$$

By applying SVD on $\mathbf{H}$ as

$$\mathbf{H}_L = \mathbf{U}_L \begin{bmatrix} \sigma_1 & & & 0 & \cdots & 0 \\ & \ddots & & \vdots & & \vdots \\ & & \sigma_{\frac{M+N}{2}-1} & 0 & \cdots & 0 \end{bmatrix} \mathbf{V}_L^T \tag{4.15}$$

It can be shown that $\mathbf{g}_L$ in (4.14) can be written as

$$\mathbf{g}_L = \mathbf{S}_{cL} + \mathbf{V}_L^{*}\boldsymbol{\phi}_L^{*} \tag{4.16}$$

where

$$\begin{aligned} \mathbf{S}_{cL} &= \mathbf{H}_L^{\dagger}\mathbf{m}_L \\ &= \mathbf{V}_L \begin{bmatrix} \sigma_1^{-1} & & & \\ & \ddots & & \\ & & \sigma_{\frac{M+N}{2}-1}^{-1} & \\ 0 & \cdots & 0 & \\ \vdots & & \vdots & \\ 0 & \cdots & 0 & \end{bmatrix} \mathbf{U}_L^T\mathbf{m}_L \\ \mathbf{V}_L^{*} &= [\, \mathbf{v}_{\frac{M+N}{2}} \ \cdots \ \mathbf{v}_M \,] \\ \boldsymbol{\phi}_L^{*} &= [\, \phi_1^{*} \ \cdots \ \phi_{\frac{M-N}{2}+1}^{*} \,]^T \end{aligned}$$

$\mathbf{v}_i$, for $i = (M+N)/2, \ \ldots, \ M$, is the ith column of matrix $\mathbf{V}_L$, and $\boldsymbol{\phi}_L^{*}$ is an arbitrary vector of dimension $(M-N)/2+1$.

The coefficients of the transfer function constitute vector $\mathbf{g}_L$ given by (4.16) where parameter vector $\boldsymbol{\phi}_L^*$ is determined by minimizing the objective function

$$\begin{aligned} E_L &= \int_0^{\omega_p} |G_0(e^{j\omega}) - e^{-j\omega k_{d2}}|^2 \, d\omega + \int_{\omega_s}^{\pi} |G_0(e^{j\omega})|^2 \, d\omega \\ &= \boldsymbol{\phi}_L^{*\,T}(\mathbf{V}_L^{*\,T}\mathbf{Q}_L\mathbf{V}_L^*)\boldsymbol{\phi}_L^* + 2\boldsymbol{\phi}_L^{*\,T}(\mathbf{V}_L^{*\,T}\mathbf{Q}_L\mathbf{S}_{cL} - \mathbf{V}_L^{*\,T}\mathbf{d}_L) \\ &\quad + \omega_p + \mathbf{S}_{cL}^T\mathbf{Q}_L\mathbf{S}_{cL} \end{aligned} \tag{4.17}$$

where

$$\mathbf{Q}_L = \begin{bmatrix} \pi+\omega_p-\omega_s & \psi(\omega_p,\omega_s,1) & \cdots & \psi(\omega_p,\omega_s,N-1) \\ \psi(\omega_p,\omega_s,1) & \pi+\omega_p-\omega_s & & \\ \vdots & & \ddots & \vdots \\ \psi(\omega_p,\omega_s,N-1) & \cdots & \cdots & \pi+\omega_p-\omega_s \end{bmatrix}$$

$$\psi(\omega_p,\ \omega_s,\ k) = \frac{1}{k}\left(\sin k\omega_p - \sin k\omega_s\right)$$

$$\begin{aligned} \mathbf{d}_L &= \mathrm{Re}\int_0^{\omega_p} \mathbf{c}_L(\omega)e^{j\omega k_{d2}}\, d\omega \\ &= \begin{bmatrix} \frac{1}{k_{d2}}\sin k_{d2}\omega_p \\ \frac{1}{k_{d2}-1}\sin(k_{d2}-1)\omega_p \\ \vdots \\ \frac{1}{k_{d2}-N+1}\sin(k_{d2}-N+1)\omega_p \end{bmatrix} \end{aligned}$$

ω_p and ω_s are the passband and stopband edges of G_0, respectively, $k_{d2} = k_d - k_{d1}$ is the group delay of G_0. Obviously, the minimum point can be obtained as

$$\boldsymbol{\phi}_{L\ opt}^* = -(\mathbf{V}_L^{*\,T}\mathbf{Q}_L\mathbf{V}_L^*)^{-1}\cdot(\mathbf{V}_L^{*\,T}\mathbf{Q}_L\mathbf{S}_{cL} - \mathbf{V}_L^{*\,T}\mathbf{d}_L) \tag{4.18}$$

and the coefficients of G_0 are given by

$$\mathbf{g}_L^* = \mathbf{S}_{cL} + \mathbf{V}_L^*\boldsymbol{\phi}_{L\ opt}^* \tag{4.19}$$

The design procedure can now be summarized as follows:

Algorithm 4.2

Step 1 Use a least-squares approach to design a lowpass, FIR filter H_0 whose length is N and group delay is $k_{d1} < k_d$.

Step 2 Form matrices $\mathbf{H}_L$ and $\mathbf{m}_L$ in (4.12).

Step 3 Obtain the SVD of $\mathbf{H}_L$ as in (4.15), and calculate $\mathbf{S}_{cL}$ and $\mathbf{Q}_L$ in (4.16) and (4.17), respectively.

Step 4 Obtain $\boldsymbol{\phi}^*_{opt\,L}$ using (4.18) and $\mathbf{g}^*_L$ using (4.19).

4.3.3 Design Examples

The proposed algorithm is demonstrated by two design examples. The design specifications for Example 4.3 were $N = 20$, $M = 24$, $k_d = 9$, $k_{d1} = k_{d2} = 4.5$ and those for Example 4.4 were $N = 26$, $M = 34$, $k_d = 15$, $k_{d1} = k_{d2} = 7.5$. The performance of the filter banks obtained was evaluated in terms of the parameters defined in Sec. 4.2.3 and the results are listed in Table 4.3. For Example 4.3 the amplitude responses of the obtained analysis lowpass and highpass filters and the obtained filter bank are depicted in Fig. 4.3 (a) and (b), respectively; Fig. 4.3 (c) and (d) shows plots of the group delays characteristic of the obtained filters as well as filter bank. Fig. 4.4 depicts the results for Example 4.4. As can be observed from the plots, the obtained analysis lowpass and highpass filters have approximately linear phase responses in their respective passbands, while the obtained filter bank has exactly linear phase response and unity amplitude response in the entire baseband, which is due to the fact that the perfect reconstruction condition was exactly satisfied in the design.

The performance of the obtained filter banks can also be checked by observing the output when the input is a ramp signal. As shown in Table 4.4, for both examples

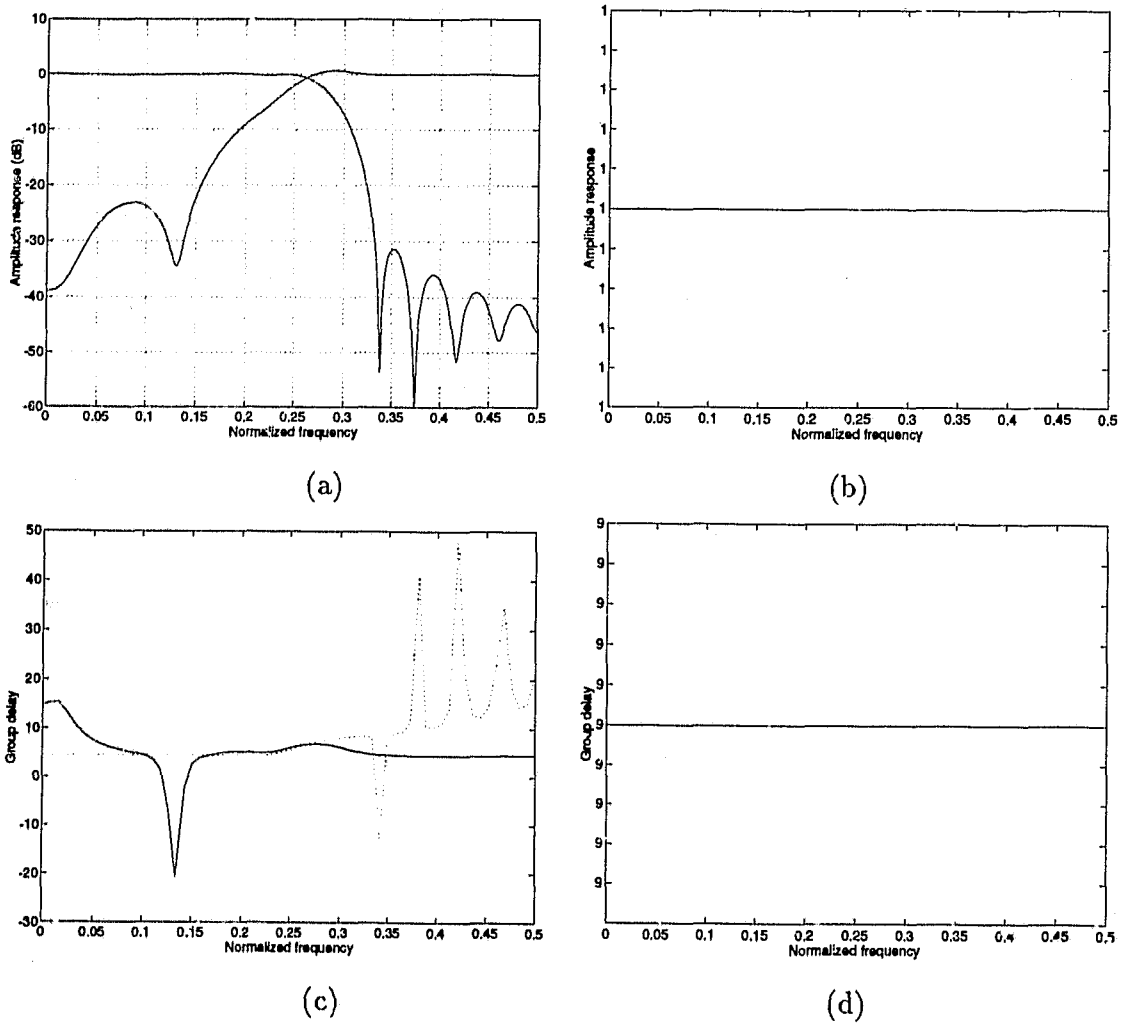

Figure 4.3: Example 4.3 (a) Amplitude responses of the analysis lowpass and highpass filters. (b) Amplitude response of the obtained filter bank. (c) Group delay of the analysis lowpass filter (dotted line) and highpass filter (solid line). (d) Group delay of the filter bank.

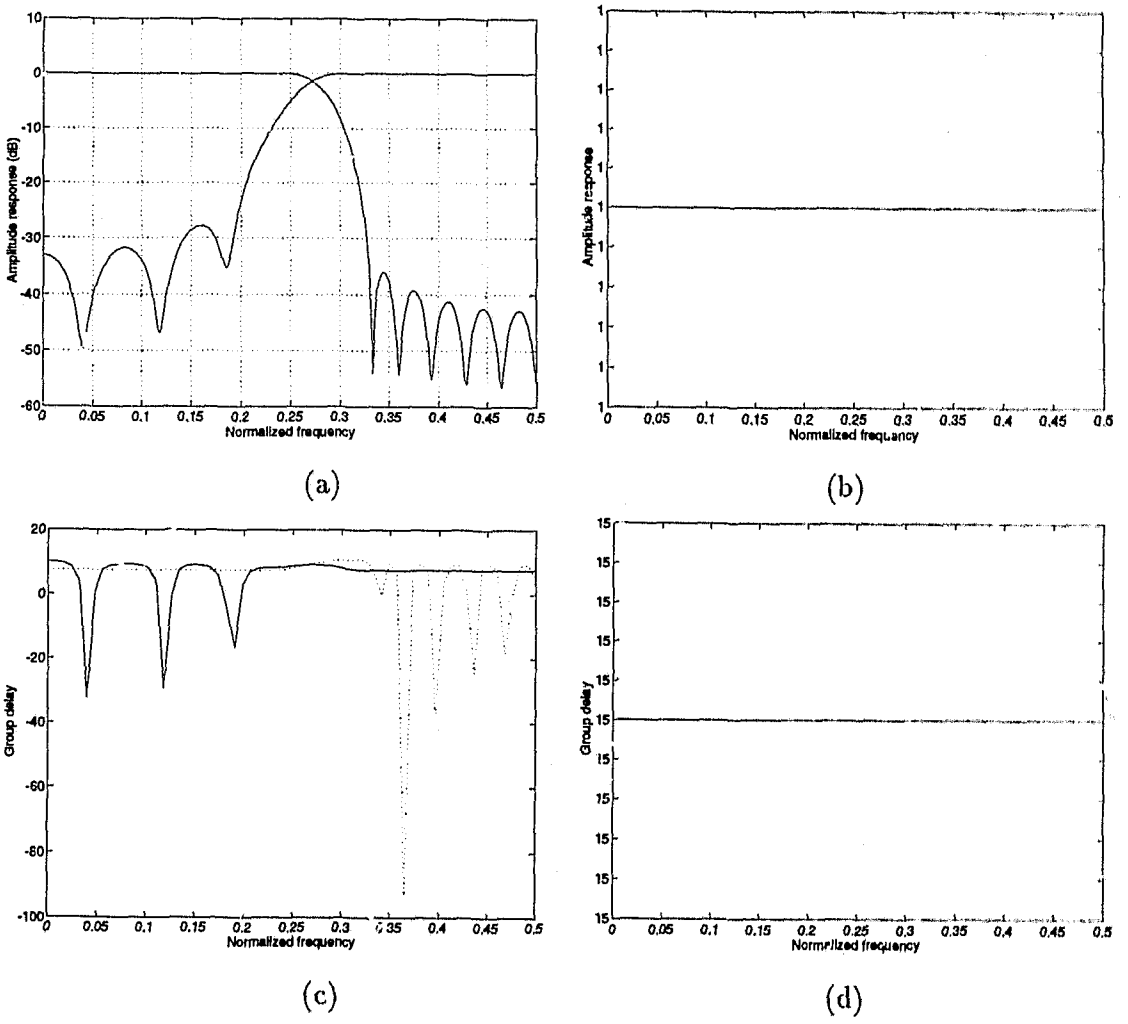

Figure 4.4: Example 4.4 (a) Amplitude responses of the analysis lowpass and highpass filters. (b) Amplitude response of the obtained filter bank. (c) Group delay of the analysis lowpass filter (dotted line) and highpass filter (solid line). (d) Group delay of the filter bank.

Table 4.3: Performance evaluations of filter banks for Examples 4.3 and 4.4.

	k_d	PRE (dB)	SNR_r (dB)
Example 4.3	9	7.81×10^{-14}	304.02
Example 4.4	15	1.56×10^{-13}	292.31

the reconstructed signals were exactly the same as the input signal to within 13 significant digits after the decimal point.

4.4 Conclusion

A null-space projection approach has been proposed for the design of two-channel linear phase perfect reconstruction QMF banks. In this approach the analysis lowpass filter is first designed by a conventional method and then the synthesis lowpass filter is obtained by solving a constrained optimization problem by the null-space project method. Later this approach has been extended to the design of low-delay perfect reconstruction QMF banks. From the design examples it can be seen that the proposed method leads to filter banks with perfect reconstruction in both the linear phase and the low-delay cases.

Table 4.4: Outputs of the filter banks of Examples 4.3 and 4.4 with a ramp input.

n	$x(n)$	Example 4.3 $\hat{x}(n+9)$	Example 4.4 $\hat{x}(n+15)$
0	1.0000000000000	1.0000000000000	1.0000000000000
1	2.0000000000000	2.0000000000000	2.0000000000000
2	3.0000000000000	3.0000000000000	3.0000000000000
3	4.0000000000000	4.0000000000000	4.0000000000000
4	5.0000000000000	5.0000000000000	5.0000000000000
5	6.0000000000000	6.0000000000000	6.0000000000000
6	7.0000000000000	7.0000000000000	7.0000000000000
7	8.0000000000000	8.0000000000000	8.0000000000000
8	9.0000000000000	9.0000000000000	9.0000000000000
9	10.0000000000000	10.0000000000000	10.0000000000000

Chapter 5

Design of Multi-Channel Cosine-Modulated QMF Banks

5.1 Introduction

Among the various multi-channel filter banks, the cosine-modulated QMF bank has two advantages:

1. The analysis and synthesis filters are all obtained from a prototype filter and, consequently, only the prototype filter needs to be designed. This results in high design efficiency.

2. There are polyphase structures which make the implementation of the filter bank very efficient.

Multi-channel cosine-modulated QMF banks can be categorized into two groups, near-perfect and perfect reconstruction banks.

To date, many approaches have been proposed for the design of multi-channel cosine-modulated QMF banks. In [26] [28] [29] [30] [33] [37], filter banks with near-perfect reconstruction are considered. In [31] [32], methods for the design of perfect reconstruction filter banks are proposed. With the exception of the method in [30],

these approaches use standard constrained or unconstrained optimization techniques to obtain the design, which are in general quite time consuming.

In this chapter, we propose a new optimization algorithm in which, instead of being minimized directly, the objective function is converted into a quadratic function of the filter coefficients whose minimum point can be obtained analytically. Then a linear formula is adopted to update the coefficient vector and the procedure is repeated until a termination criterion is met. The approach reduces the computational complexity significantly and leads to filter banks with high stopband attenuation and low aliasing and amplitude distortions.

Most cosine-modulated QMF banks investigated so far have reconstruction delays of $N-1$ where N is the filter length. When the filter length is high, which is very common in multi-channel filter bank designs, the reconstruction delay will be long, which is undesirable for real-time applications. In [37] some preliminary results have been given through a design example on low-delay cosine-modulated QMF banks. In [36], a class of cosine-modulated filter bank was proposed whose reconstruction delay can take several values. In this chapter, a general cosine-modulated QMF bank is considered in which no constraint is imposed on the filter length N and the reconstruction delay k_d. By letting $k_d < N-1$, a low-delay cosine-modulated QMF bank can be obtained. The iterative algorithm proposed is then applied for the design of low-delay filter banks with near-perfect reconstruction. Several design examples are included to demonstrate the proposed algorithms. In addition, performance comparisons with several other existing designs are provided.

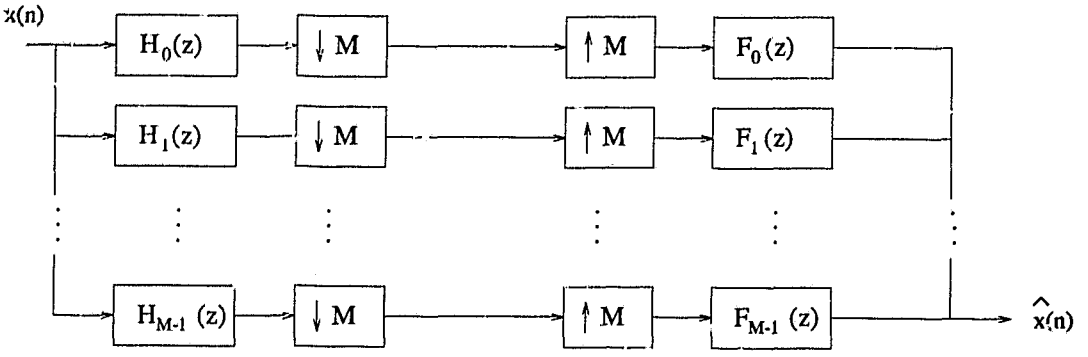

Figure 5.1: M-channel filter bank.

5.2 Conventional Cosine-Modulated QMF Bank

5.2.1 Review

In the M-channel filter bank shown in Fig. 5.1, the reconstructed signal is given by [29]

$$\begin{aligned}\hat{X}(z) &= \frac{1}{M}\sum_{k=0}^{M-1} F_k(z)\sum_{l=0}^{M-1} H_k(W_M^l z)X(W_M^l z)\\ &= \sum_{l=0}^{M-1} T_l(z)X(W_M^l z)\end{aligned} \tag{5.1}$$

where

$$\begin{aligned}W_M &= e^{-2\pi j/M}\\ T_l(z) &= \frac{1}{M}\sum_{k=0}^{M-1} F_k(z)H_k(W_M^l z)\end{aligned}$$

In order to cancel aliasing and achieve the perfect reconstruction, it is required that

$$T_l(z) = 0 \qquad \text{for } l = 1, 2, \ldots, M-1 \tag{5.2a}$$

$$T_0(z) = z^{-k_d} \qquad k_d \text{ is an integer} \tag{5.2b}$$

In a cosine-modulated QMF bank, the transfer functions of the analysis and synthesis filters, $H_k(z)$ and $F_k(z)$ for $k = 0, 1, \ldots, M-1$, respectively, are obtained by modulating the transfer function $P(z)$ of a prototype linear phase lowpass FIR filter P with bandwidth $\pi/(2M)$, i.e.,

$$H_k(z) = a_k c_k P(zW_{2M}^{(k+1/2)}) + a_k^* c_k^* P(zW_{2M}^{-(k+1/2)}) \tag{5.3a}$$

$$F_k(z) = a_k^* c_k P(zW_{2M}^{(k+1/2)}) + a_k c_k^* P(zW_{2M}^{-(k+1/2)}) \tag{5.3b}$$

for $0 \leq k \leq M-1$, where $a_k = e^{j\theta_k}$, $c_k = W_{2M}^{(k+\frac{1}{2})(\frac{N-1}{2})}$, $W_{2M} = e^{-j\pi/M}$ and N is the filter length of P. The superscript $*$ denotes the complex conjugate operation. It follows that the impulse responses of the analysis and synthesis filters H_k and F_k are given by

$$h_k(n) = 2p(n)\cos\left[(2k+1)\frac{\pi}{2M}\left(n - \frac{N-1}{2}\right) + \theta_k\right] \tag{5.4a}$$

$$f_k(n) = 2p(n)\cos\left[(2k+1)\frac{\pi}{2M}\left(n - \frac{N-1}{2}\right) - \theta_k\right] \tag{5.4b}$$

for $0 \leq n \leq N-1$ and $0 \leq k \leq M-1$, respectively, and $p(n)$ is the impulse response of the prototype filter P. From (5.3) and (5.4), the analysis and synthesis filters are related by

$$f_k(n) = h_k(N-1-n)$$

$$F_k(z) = z^{-(N-1)}\tilde{H}_k(z)$$

where $\tilde{H}_k(z) = H_k^*(z^{-1})$ for $k = 0, \ldots. M-1$. As shown in [29], θ_k can be chosen as

$$\theta_{k+1} = \theta_k \pm \frac{\pi}{2} \qquad \text{for } 0 \leq k < M-1 \tag{5.5}$$

in order to cancel significant aliasing terms. In order to assure a relatively flat overall

amplitude response, it is required that

$$\theta_0 = \pm\left(\frac{\pi}{4} + \frac{l\pi}{2}\right) \tag{5.6a}$$

$$\theta_{M-1} = \pm\left(\frac{\pi}{4} + \frac{m\pi}{2}\right) \tag{5.6b}$$

where l and m are integers. A good choice for θ_k that satisfies (5.5) and (5.6) is

$$\theta_k = (2k+1)\pi/4 \qquad \text{for } 0 \le k \le M-1 \tag{5.7}$$

Under these circumstance, the overall transfer function becomes

$$\begin{aligned} T_0(z) &= \frac{1}{M}\sum_{k=0}^{M-1} H_k(z)F_k(z) \\ &= \frac{z^{-(N-1)}}{M}\sum_{k=0}^{M-1} H_k(z)\tilde{H}_k(z) \end{aligned}$$

and hence

$$T_0(e^{j\omega}) = \frac{e^{-j\omega(N-1)}}{M}\sum_{k=0}^{M-1} |H_k(e^{j\omega})|^2 \tag{5.8}$$

Note that (5.8) is derived on the basis of the assumption in (5.2a) and hence it represents the overall frequency response of the filter bank exactly only if the aliasing components are exactly zero. From (5.8) it follows that the filter bank has a linear phase response, which leads to a reconstructed signal with no phase distortion. If the amplitude distortion introduced by the filter bank is eliminated as well, i.e.,

$$\sum_{k=0}^{M-1} |H_k(e^{j\omega})|^2 = 1 \tag{5.9}$$

for $0 \le \omega \le \pi$, then perfect reconstruction will be achieved and the reconstruction delay will be $N-1$ sampling periods.

5.2.2 New Iterative Method

It can be shown that $|T_0(e^{j\omega})|$ has a period of π/M and if the prototype filter P has a large stopband attenuation, (5.8) can be approximately expressed by

$$T_0(e^{j\omega}) \approx \frac{e^{-j\omega(N-1)}}{M}\left[|P(e^{j(\omega-\frac{k\pi}{M}-\frac{\pi}{2M})})|^2 + |P(e^{j(\omega-\frac{(k+1)\pi}{M}-\frac{\pi}{2M})})|^2\right] \tag{5.10}$$

for ω in the range of $(k+\frac{1}{2})\pi/M \leq \omega \leq (k+\frac{3}{2})\pi/M$ [29]. Note that the quantity in the square brackets of (5.10) is a frequency-shifted version of $|P(e^{j\omega})|^2 + |P(e^{j(\omega-\frac{\pi}{M})})|^2$ and, therefore, if this term can be made constant over $[0, \pi/M]$, $|T_0(e^{j\omega})|$ will be constant for all frequencies, that is, amplitude distortion is eliminated. Hence the design problem can be reduced to the problem of minimizing the objective function

$$E = E_1 + \alpha E_2 \tag{5.11a}$$

where

$$E_1 = \int_0^{\pi/M}\left[|P(e^{j\omega})|^2 + |P(e^{j(\omega-\frac{\pi}{M})})|^2 - 1\right]^2 d\omega \tag{5.11b}$$

deals with the amplitude distortion of the overall transfer function $T_0(z)$,

$$E_2 = \int_{\omega_s}^{\pi} |P(e^{j\omega})|^2 \, d\omega \tag{5.11c}$$

deals with the stopband attenuation of the prototype filter P, where $\omega_s = \pi/(2M) + \varepsilon$, and ε is a positive constant which depends on the required transition width. Parameter α is a positive weight. Since filter P is a linear phase lowpass filter with a symmetrical impulse response, when N is even, its frequency response can be expressed as [55]

$$P(e^{j\omega}) = M_p(\omega)e^{-j\omega(N-1)/2} \tag{5.12a}$$

$$M_p(\omega) = 2\ \mathbf{p}^T\mathbf{c}(\omega) \tag{5.12b}$$

where $\mathbf{c}(\omega) = [\ \cos(\frac{N-1}{2}\omega)\ \cdots\ \cos(\frac{1}{2}\omega)\ ]^T$, and $\mathbf{p} = [\ p(0)\ p(1)\ \cdots\ p(\frac{N}{2}-1)\ ]^T$. Therefore, E_1 and E_2 in (5.11) can be rewritten as

$$E_1 = \int_0^{\pi/M} \left[M_p^2(\omega) + M_p^2(\omega - \frac{\pi}{M}) - 1\right]^2 \, d\omega$$
$$E_2 = \int_{\omega_s}^{\pi} M_p^2(\omega)\, d\omega$$

Minimizing E in (5.11a) by using a standard optimization method tends to be time-consuming since the objective function is highly nonlinear. Instead of minimizing function E directly, we adopt an iterative procedure in which the objective function in (5.11a) is modified to

$$E' = E_1' + \alpha E_2' \tag{5.13a}$$

where

$$E_1' = \sum_{0\le\omega\le\pi/M} \left[M_p(\omega)\cdot M_q(\omega) + M_p\left(\omega - \frac{\pi}{M}\right)\cdot M_q\left(\omega - \frac{\pi}{M}\right) - 1\right]^2 \tag{5.13b}$$

$$\begin{aligned} E_2' &= \int_{\omega_s}^{\pi} M_q^2(\omega)\, d\omega \\ &= 4\mathbf{q}^T \left[\int_{\omega_s}^{\pi} \mathbf{c}(\omega)\mathbf{c}^T(\omega) d\omega\right] \mathbf{q} \\ &= \mathbf{q}^T \mathbf{U}_s \mathbf{q} \end{aligned} \tag{5.13c}$$

and

$$Q(e^{j\omega}) = M_q(\omega) e^{-j\omega(N-1)/2}$$
$$M_q(\omega) = 2\ \mathbf{q}^T \mathbf{c}(\omega)$$

where $\mathbf{q} = [\ q(0)\ q(1)\ \cdots\ q(\frac{N}{2}-1)\ ]^T$. $Q(e^{j\omega})$ is the frequency response of a lowpass linear phase FIR filter Q with a passband width $\pi/(2M)$.

At the beginning of the iterative procedure, filter P is first designed using one of the conventional methods such as the window method, Remez exchange algorithm

[55], etc. The summation in (5.13b) is carried out over a set of sampling points $\mathbf{\Omega}_p = \{\omega_{p1} = 0,\ \omega_{p2},\ \ldots,\ \omega_{pk} = \pi/M\ \}$. Then E' in (5.13a) can be formulated as a quadratic function of $\mathbf{q}$ given by

$$E' = (\mathbf{Uq} - \mathbf{d})^T(\mathbf{Uq} - \mathbf{d}) + \alpha(\mathbf{q}^T\mathbf{U}_s\mathbf{q}) \tag{5.14}$$

where $\mathbf{d}$ is a column vector with each entry being a 1, and

$$\mathbf{U} = \mathbf{H}(\mathbf{\Omega}_p)\mathbf{U}_t(\mathbf{\Omega}_p) + \mathbf{H}\left(\mathbf{\Omega}_p - \frac{\pi}{M}\right)\mathbf{U}_t\left(\mathbf{\Omega}_p - \frac{\pi}{M}\right) \tag{5.15a}$$

$$\mathbf{H}(\mathbf{\Omega}_p) = \mathrm{diag}[M_p(\omega_{p1}),\ M_p(\omega_{p2}),\ \ldots,\ M_p(\omega_{pk})] \tag{5.15b}$$

$$\mathbf{U}_t(\mathbf{\Omega}_p) = 2\begin{bmatrix} \cos(N-1)\omega_{p1}/2 & \cdots & \cos\omega_{p1}/2 \\ \cos(N-1)\omega_{p2}/2 & \cdots & \cos\omega_{p2}/2 \\ \vdots & & \vdots \\ \cos(N-1)\omega_{pk}/2 & \cdots & \cos\omega_{pk}/2 \end{bmatrix} \tag{5.15c}$$

The $(i,j)th$ entry of $\mathbf{U}_s$ is given by

$$\begin{aligned} u_{ij}^{(s)} &= 4\int_{\omega_s}^{\pi} \cos\left[\left(i - 1 - \frac{N-1}{2}\right)\omega\right]\cos\left[\left(j - 1 - \frac{N-1}{2}\right)\omega\right]\, d\omega \\ &= 4\cdot\begin{cases} \frac{\pi-\omega_s}{2} - \frac{\sin[(2i-N-1)\omega_s]}{2(2i-N-1)} & \text{for } i = j \\ \frac{\sin[(i-j)\omega_s]}{2(j-i)} - \frac{\sin[(i+j-N-1)\omega_s]}{2(i+j-N-1)} & \text{for } i \neq j \end{cases} \end{aligned} \tag{5.15d}$$

for $i, j = 1,\ 2,\ \ldots,\ N/2$.

Since $\mathbf{U}^T\mathbf{U} + \alpha\mathbf{U}_s$ is positive definite, E' has a global minimum point at

$$\mathbf{q} = (\mathbf{U}^T\mathbf{U} + \alpha\mathbf{U}_s)^{-1}\cdot(\mathbf{U}^T\mathbf{d}) \tag{5.16}$$

Having obtained $\mathbf{q}$, a linear formula is used to update $\mathbf{p}$ as

$$\mathbf{p} := (1-\tau)\mathbf{p} + \tau\mathbf{q} \tag{5.17}$$

where τ, $0 < \tau < 1$, is a smoothing parameter. The above process is repeated until $\| \mathbf{p} - \mathbf{q} \|_2$ is less than a specified tolerance.

The iterative algorithm can now be summarized in terms of the following steps:

Algorithm 5.1

Step 1 Use a conventional method to design a linear phase, lowpass, FIR filter of length N with a bandwidth of $\pi/(2M)$. Then use the coefficient vector of the filter obtained to initialize $\mathbf{p}$.

Step 2 Use (5.15d) to compute matrix $\mathbf{U}_s$.

Step 3 Form matrix $\mathbf{U}$ and vector $\mathbf{q}$ by using (5.15a) and (5.16), respectively.

Step 4 If $\| \mathbf{p} - \mathbf{q} \|_2 < \epsilon$, where ϵ is a prescribed tolerance, output $\mathbf{p}$ as the design result and stop; otherwise update $\mathbf{p}$ using (5.17) with τ in the range $0 < \tau < 1$, say $\tau = 0.5$, and repeat from Step 3.

In the above analysis, N is assumed to be even. If N is odd, the frequency response of P can still be expressed as in (5.12a) with

$$M_p(\omega) = \mathbf{p}^T \mathbf{c}(\omega)$$

where $\mathbf{c}(\omega) = [\ \cos(N-1)\omega/2\ \ \cos(N-3)\omega/2\ \cdots\ \cos\omega\ \ 1\ ]^T$, $\mathbf{p} = [\ 2p(0)\ 2p(1)\ \cdots\ 2p(\frac{N-3}{2})\ p(\frac{N-1}{2})\ ]^T$, and Algorithm 5.1 is valid if (5.15c) and (5.15d) are modified as

$$\mathbf{U}_t(\mathbf{\Omega}_p) = \begin{bmatrix} \cos(N-1)\omega_{p1}/2 & \cdots & \cos\omega_{p1} & 1 \\ \cos(N-1)\omega_{p2}/2 & \cdots & \cos\omega_{p2} & 1 \\ \vdots & & & \vdots \\ \cos(N-1)\omega_{pk}/2 & \cdots & \cos\omega_{pk} & 1 \end{bmatrix} \tag{5.18a}$$

$$u_{ij}^{(s)} = \begin{cases} \pi - \omega_s & \text{for } i = j = \frac{N+1}{2} \\ \frac{\pi-\omega_s}{2} - \frac{\sin[(2i-N-1)\omega_s]}{2(2i-N-1)} & \text{for } i = j < \frac{N+1}{2} \\ \frac{\sin[(i-j)\omega_s]}{2(j-i)} - \frac{\sin[(i+j-N-1)\omega_s]}{2(i+j-N-1)} & \text{for } i \neq j \end{cases} \tag{5.18b}$$

for $i, j = 1,\ 2,\ \ldots,\ (N+1)/2$, respectively.

Although a rigorous proof of the algorithm's convergence is not available at this time, the algorithm was found to always converge in a large set of designs when the initial point is obtained as in step 1. Moreover, the algorithm converges faster if τ is chosen to be in the vicinity of 0.5.

5.3 Low-Delay Cosine-Modulated QMF Bank

5.3.1 A General Cosine-Modulated QMF Bank

The reconstruction delay of the cosine-modulated QMF bank described in Sec. 5.2 (referred to as the conventional cosine-modulated QMF banks henceforth) is $N-1$ sampling periods, where N is the filter length. When the number of channels M increases in a filter bank, the bandwidth of each filter decreases and, as a result, high-order filters are required to achieve the narrow passband. Consequently, the filter banks designed have long reconstruction delays, which are highly undesirable in some applications. In this section we proposed a method for the design of low-delay cosine-modulated QMF banks.

Consider a prototype FIR lowpass filter P_L of length N with an *asymmetrical* impulse response, a bandwidth of $\pi/(2M)$, and a phase response which is approximately linear. Its frequency response can be expressed as

$$P_L(e^{j\omega}) \approx |P_L(e^{j\omega})|\, e^{-j\omega k_d/2} \tag{5.19}$$

and hence the group delay of the filter is $k_d/2$ where $k_d \leq N-1$. The transfer functions of the analysis and synthesis filters, $H_k(z)$ and $F_k(z)$, are related to the transfer function $P_L(z)$ of the prototype lowpass filter P_L as

$$H_k(z) = e^{j\phi_k} P_L(W_{2M}^{(k+1/2)} z) + e^{-j\phi_k} P_L(W_{2M}^{-(k+1/2)} z) \tag{5.20a}$$

$$F'_k(z) = e^{j\psi_k} P_L(W_{2M}^{(k+1/2)} z) + e^{-j\psi_k} P_L(W_{2M}^{-(k+1/2)} z) \tag{5.20b}$$

for $0 \leq k \leq M-1$, where

$$\phi_k = (M - k_d)(2k+1)\pi/(4M)$$
$$\psi_k = (-M - k_d)(2k+1)\pi/(4M)$$

From (5.1) and (5.20), the aliasing terms in the reconstructed signal can be written as

$$\begin{aligned} T_l(z) = \frac{1}{M} \sum_{k=0}^{M-1} & e^{j(\phi_k+\psi_k)} P_L(W_{2M}^{(2l+k+1/2)} z) P_L(W_{2M}^{(k+1/2)} z) \\ & + e^{j(\phi_k-\psi_k)} P_L(W_{2M}^{(2l+k+1/2)} z) P_L(W_{2M}^{-(k+1/2)} z) \\ & + e^{-j(\phi_k-\psi_k)} P_L(W_{2M}^{(2l-k-1/2)} z) P_L(W_{2M}^{(k+1/2)} z) \\ & + e^{-j(\phi_k+\psi_k)} P_L(W_{2M}^{(2l-k-1/2)} z) P_I(W_{2M}^{-(k+1/2)} z) \end{aligned} \tag{5.21}$$

for $1 \leq l \leq M-1$. If we assume that the stopband attenuation of filter P_L is high enough so that the overlap among non-adjacent channel filters can be neglected, the only none-zero terms in (5.21) occur when $k = M-l$, $k = M-l-1$ in the second term, and $k = l$, $k = l-1$ in the third term, and hence

$$\begin{aligned} T_l(z) = \frac{1}{M} \Big\{ & P_L(-W_{2M}^{(l+1/2)} z) P_L(-W_{2M}^{(l-1/2)} z) \left[e^{j(\phi_{M-l}-\psi_{M-l})} + e^{j(\phi_{M-l-1}-\psi_{M-l-1})} \right] \\ & + P_L(W_{2M}^{(l+1/2)} z) P_L(W_{2M}^{(l-1/2)} z) \left[e^{-j(\phi_l-\psi_l)} + e^{-j(\phi_{l-1}-\psi_{l-1})} \right] \Big\} \end{aligned} \tag{5.22}$$

Substituting ϕ_l and ψ_l into (5.22), it can be shown that

$$T_l(z) = 0 \qquad \text{for } 1 \leq l \leq M-1$$

which implies that the aliasing terms are cancelled.

Under the assumption that the aliasing components are completely cancelled, the overall frequency response now is expressed as

$$\begin{aligned} T_0(e^{j\omega}) &= \frac{1}{M}\sum_{k=0}^{M-1} H_k(e^{j\omega})F_k(e^{j\omega}) \\ &= \frac{1}{M}\sum_{k=0}^{M-1} e^{j(\phi_k+\psi_k)}P_L^2(W_{2M}^{(k+1/2)}e^{j\omega}) + e^{-j(\phi_k+\psi_k)}P_L^2(W_{2M}^{-(k+1/2)}e^{j\omega}) \end{aligned} \tag{5.23}$$

Substituting (5.19) into (5.23) and considering ω in the range of $[-\pi/(2M), \pi/(2M)]$, we have

$$T_0(e^{j\omega}) \approx \frac{e^{-jk_d\omega}}{M}\left[|P_L(e^{j(\omega-\frac{\pi}{2M})})|^2 + |P_L(e^{j(\omega+\frac{\pi}{2M})})|^2\right] \tag{5.24}$$

As in the design of conventional cosine-modulated QMF banks, if $|P_L(e^{j(\omega-\frac{\pi}{2M})})|^2 + |P_L(e^{j(\omega+\frac{\pi}{2M})})|^2$ is made sufficiently flat over $[-\pi/(2M), \pi/(2M)]$, $|T_0(e^{j\omega})|$ will be flat for all frequencies. The perfect-reconstruction condition can be approximated by minimizing the error component

$$\begin{aligned} E_{L1} &= \int_{-\pi/(2M)}^{\pi/(2M)} |MT_0(e^{j\omega}) - e^{-jk_d\omega}|^2 \, d\omega \\ &= \int_{-\pi/(2M)}^{\pi/(2M)} \left|e^{-jk_d\omega}\left[|P_L(e^{j(\omega-\frac{\pi}{2M})})|^2 + |P_L(e^{j(\omega+\frac{\pi}{2M})})|^2\right] - e^{-jk_d\omega}\right|^2 d\omega \\ &= \int_0^{\pi/M} \left|e^{-jk_d\omega}\left[|P_L(e^{j\omega})|^2 + |P_L(e^{j(\omega-\frac{\pi}{M})})|^2\right] - e^{-jk_d\omega}\right|^2 d\omega \\ &= \int_0^{\pi/M} \left||P_L(e^{j\omega})|^2 e^{-jk_d\omega} + e^{-k_d\pi/M}|P_L(e^{j(\omega-\frac{\pi}{M})})|^2 e^{-jk_d(\omega-\frac{\pi}{M})} - e^{-jk_d\omega}\right|^2 d\omega \\ &= \int_0^{\pi/M} \left|P_L^2(e^{j\omega}) + e^{-jk_d\pi/M}P_L^2(e^{j(\omega-\frac{\pi}{M})}) - e^{-jk_d\omega}\right|^2 d\omega \end{aligned} \tag{5.25a}$$

Since the phase response of P_L is only approximately linear, both the phase and amplitude responses must be optimized and hence the above objective function includes both phase and magnitude error components. By also considering the stopband attenuation of filter P_L, the error component

$$E_{L2} = \int_{\omega_s}^{\pi} |P_L(e^{j\omega})|^2 d\omega \tag{5.25b}$$

can be formed. A suitable objective function can now be constructed as

$$E_L = E_{L1} + \alpha E_{L2} \tag{5.26}$$

where α is a positive constant. To achieve the required design, the objective function in (5.26) is minimized with respect to the coefficients of P_L.

Having the coefficients of P_L, the impulse responses of the analysis filters H_k and the synthesis filters F_k can be obtained from (5.20) as

$$h_k(n) = 2p_L(n)\cos\left[(2k+1)\frac{\pi}{2M}\left(n-\frac{k_d}{2}\right)+\theta_k\right] \tag{5.27a}$$

$$f_k(n) = 2p_L(n)\cos\left[(2k+1)\frac{\pi}{2M}\left(n-\frac{k_d}{2}\right)-\theta_k\right] \tag{5.27b}$$

for $0 \leq n \leq N-1$ and $0 \leq k \leq M-1$, where $\theta_k = (2k+1)\pi/4$ and $p_L(n)$ is the impulse response of the prototype filter P_L.

On comparing (5.27) with (5.4), we observe that the design method proposed in Sec. 5.3 is a general version of the method of Sec. 5.2 which includes the latter design as the *particular* case when filter P_L has a symmetrical impulse response and $k_d = N-1$. It should also be emphasized that no constraint has been imposed on the filter length N and the reconstruction delay k_d of the cosine-modulated QMF bank in (5.27).

5.3.2 Design Method

Instead of minimizing the highly nonlinear objective function in (5.26) directly, an iterative procedure similar to that of Sec. 5.2.2 can be used in which the objective function is modified as

$$E'_L = E'_{L1} + \alpha E'_{L2} \tag{5.28a}$$

where

$$E'_{L1} = \sum_{0\le\omega\le\pi/M} \left| P_L(e^{j\omega})Q_L(e^{j\omega}) + e^{-jk_d\pi/M} P_L(e^{j(\omega-\frac{\pi}{M})})Q_L(e^{j(\omega-\frac{\pi}{M})}) - e^{-jk_d\omega} \right|^2 \tag{5.28b}$$

$$E'_{L2} = \int_{\omega_s}^{\pi} |Q_L(e^{j\omega})|^2 \, d\omega \tag{5.28c}$$

Q_L is a lowpass FIR filter with a bandwidth $\pi/(2M)$ and the frequency responses of P_L and Q_L can be expressed as

$$P_L(e^{j\omega}) = \mathbf{p}_L^T \mathbf{c}_L(\omega)$$

$$Q_L(e^{j\omega}) = \mathbf{q}_L^T \mathbf{c}_L(\omega)$$

where $\mathbf{c}_L(\omega) = [\ 1\ e^{-j\omega} \cdots\ e^{-j(N-1)\omega}\ ]^T$, $\mathbf{p}_L = [\ p(0)\ p(1)\ \cdots\ p(N-1)\ ]^T$ and $\mathbf{q}_L = [\ q(0)\ q(1)\ \cdots\ q(N-1)\ ]^T$ are the coefficient vectors of filters P_L and Q_L, respectively.

We begin the iterative procedure by designing a filter P_L with group delay $k_d/2 < (N-1)/2$ using a least-squares design approach similar to that in [82] and write E'_L in (5.28a) as

$$E'_L = (\mathbf{U}\mathbf{q}_L - \mathbf{d}_L)^H(\mathbf{U}\mathbf{q}_L - \mathbf{d}_L) + \alpha \mathbf{q}_L^H \mathbf{U}_s \mathbf{q}_L \tag{5.29}$$

where $\mathbf{d}_L = [e^{-j\omega_{p1}k_d}\ e^{-j\omega_{p2}k_d}\ \cdots\ e^{-j\omega_{pk}k_d}]^T$ and superscript H denotes complex conjugate transposition. In this case, we have

$$\mathbf{U} = \mathbf{H}(\mathbf{\Omega}_p)\mathbf{U}_t(\mathbf{\Omega}_p) + e^{-jk_d\pi/M}\mathbf{H}\left(\mathbf{\Omega}_p - \frac{\pi}{M}\right)\mathbf{U}_t\left(\mathbf{\Omega}_p - \frac{\pi}{M}\right) \tag{5.30a}$$

$$\mathbf{H}(\mathbf{\Omega}_p) = \mathrm{diag}[P_L(e^{j\omega_{p1}}),\ P_L(e^{j\omega_{p2}}),\ \ldots,\ P_L(e^{j\omega_{pk}})] \tag{5.30b}$$

$$\mathbf{U}_t(\Omega_p) = \begin{bmatrix} 1 & e^{-j\omega_{p1}} & \cdots & e^{-j\omega_{p1}(N-1)} \\ 1 & e^{-j\omega_{p2}} & \cdots & e^{-j\omega_{p2}(N-1)} \\ \vdots & \vdots & & \vdots \\ 1 & e^{-j\omega_{pk}} & \cdots & e^{-j\omega_{pk}(N-1)} \end{bmatrix} \tag{5.30c}$$

$$\mathbf{U}_s = \text{Re} \int_{\omega_s}^{\pi} \mathbf{c}_L(\omega)\mathbf{c}_L^H(\omega)\, d\omega$$

$$= \begin{bmatrix} \pi-\omega_s & -\sin\omega_s & -\frac{1}{2}\sin 2\omega_s & \cdots & -\frac{1}{N-1}\sin(N-1)\omega_s \\ -\sin\omega_s & \pi-\omega_s & -\sin\omega_s & \cdots & -\frac{1}{N-2}\sin(N-2)\omega_s \\ \vdots & \vdots & & & \vdots \\ -\frac{1}{N-1}\sin(N-1)\omega_s & \cdots & \cdots & \cdots & \pi-\omega_s \end{bmatrix} \tag{5.30d}$$

As E_L' in (5.29) is a quadratic function in $\mathbf{q}_L$ with $[\text{Re}\,(\mathbf{U}^H\mathbf{U}) + \alpha\mathbf{U}_s] > 0$, it has the unique global minimum point given by

$$\mathbf{q}_L = [\text{Re}\,(\mathbf{U}^H\mathbf{U}) + \alpha\mathbf{U}_s]^{-1} \cdot \text{Re}\,(\mathbf{U}^H\mathbf{d}_L) \tag{5.31}$$

where Re $[\cdot]$ is the real part of $[\cdot]$. Having obtained $\mathbf{q}_L$, a linear formula is used to update $\mathbf{p}_L$ as

$$\mathbf{p}_L := (1-\tau)\mathbf{p}_L + \tau\mathbf{q}_L \tag{5.32}$$

The procedure is repeated until $\| \mathbf{p}_L - \mathbf{q}_L \|_2$ is less than a prescribed tolerance. The iterative algorithm for the design of cosine-modulated QMF banks with low reconstruction delays can now be summarized in terms of the following simple steps:

Algorithm 5.2

Step 1 Use a least-squares approach to design a lowpass, FIR filter of length N with stopband edge ω_s and group delay $k_d/2$, and use the coefficient vector of the filter obtained to initialize $\mathbf{p}_L$.

Step 2 Use (5.30d) to compute matrix $\mathbf{U}_s$.

Step 3 Form matrix $\mathbf{U}$ and vector $\mathbf{q}_L$ by (5.30a) and (5.31), respectively.

Step 4 If $\| \mathbf{p}_L - \mathbf{q}_L \|_2 < \epsilon$, where ϵ is a prescribed tolerance, output $\mathbf{p}_L$ as the desired result and stop; otherwise, update $\mathbf{p}_L$ using (5.32) with τ in the range $0 < \tau < 1$, say $\tau = 0.5$, and repeat from Step 3.

In our experiments we noticed that some undesirable artifacts can sometimes occur in the amplitude responses of the analysis and synthesis filter when the reconstruction delay is low. Such artifacts have been observed by other researchers as well when designing low-delay two-channel filter banks [34][35] and multi-channel cosine-modulated filter banks [37][36]. In the multi-channel case, artifacts can occur in the transition band when the group delay is low if there is no constraint on the transition band of the prototype filter P_L. These artifacts then lead to artifacts in the amplitude responses of the analysis and synthesis filters. An effective treatment of this problem is to modify the objective function in (5.28a) to include an additional term $\alpha_1 E'_{L3}$, i.e.,

$$E'_L = E'_{L1} + \alpha E'_{L2} + \alpha_1 E'_{L3} \tag{5.33}$$

where

$$\alpha_1 E'_{L3} = \alpha_1 \int_{\omega_{t1}}^{\omega_{t2}} |Q_L(e^{j\omega}) - e^{-jk_d\omega/2}|^2 \, d\omega \tag{5.34}$$

and $[\omega_{t1},\ \omega_{t2}]$ is an interval in the transition region where the artifacts occur. It can be readily shown that the objective function in (5.33) can be written as

$$\begin{aligned} E'_L = {} & (\mathbf{U}\mathbf{q}_L - \mathbf{d}_L)^H(\mathbf{U}\mathbf{q}_L - \mathbf{d}_L) + \alpha \mathbf{q}_L^H \mathbf{U}_s \mathbf{q}_L \\ & + \alpha_1(\mathbf{q}_L^T \mathbf{U}_a \mathbf{q} - 2\mathbf{b}^T \mathbf{q}_L + \omega_{t2} - \omega_{t1}) \end{aligned} \tag{5.35}$$

where $\mathbf{U}$ and $\mathbf{U}_s$ are given by (5.30a) and (5.30d), respectively , and

$$\mathbf{U}_a = \begin{bmatrix} \omega_{t2} - \omega_{t1} & \phi(\omega_{t2},\ \omega_{t1},\ 1) & \cdots & \phi(\omega_{t2},\ \omega_{t1},\ N-1) \\ \phi(\omega_{t2},\ \omega_{t1},\ 1) & \omega_{t2} - \omega_{t1} & & \vdots \\ \vdots & \vdots & & \\ \phi(\omega_{t2},\ \omega_{t1},\ N-1) & \cdots & \cdots & \omega_{t2} - \omega_{t1} \end{bmatrix}$$

$$\phi(\omega_{t2},\ \omega_{t1},\ k) = \frac{1}{k}\left[\sin k\omega_{t2} - \sin k\omega_{t1}\right]$$

$$\mathbf{b} = \mathrm{Re} \int_{\omega_{t1}}^{\omega_{t2}} \mathbf{c}_L(\omega) e^{jk_d\omega/2}\, d\omega$$

$$= \begin{bmatrix} \frac{2}{k_d}\left[\sin\left(\frac{k_d\omega_{t2}}{2}\right) - \sin\left(\frac{k_d\omega_{t1}}{2}\right)\right] \\ \frac{2}{k_d-2}\left\{\sin\left[\left(\frac{k_d}{2}-1\right)\omega_{t2}\right] - \sin\left[\left(\frac{k_d}{2}-1\right)\omega_{t1}\right]\right\} \\ \vdots \\ \frac{2}{k_d-2N+2}\left\{\sin\left[\left(\frac{k_d}{2}-N+1\right)\omega_{t2}\right] - \sin\left[\left(\frac{k_d}{2}-N+1\right)\omega_{t1}\right]\right\} \end{bmatrix}$$

The global minimum point of E_L' in each step of the iterative algorithm can now be obtained as

$$\mathbf{q}_L = [\mathrm{Re}\,(\mathbf{U}^H\mathbf{U}) + \alpha\mathbf{U}_s + \alpha_1\mathbf{U}_a]^{-1} \cdot [\mathrm{Re}\,(\mathbf{U}^H\mathbf{d}_L) + \alpha_1\mathbf{b}] \tag{5.36}$$

The proposed low-delay cosine-modulated QMF bank can be implemented by the efficient polyphase implementation using discrete Fourier transform (DFT) as described in [37]. The numbers of multiplications and additions per output are comparable with those required by the cosine-modulated filter bank in [32], which is based on the extended lapped transformation.

5.4 Design Examples

In this section, we present results obtained by applying the iterative design algorithms described in Secs. 5.2 and 5.3 to several examples. All the designs were carried out by running MATLAB programs on a Sun SPARC workstation. The performance of the filter banks designed was evaluated in terms of computational efficiency, reconstruction error, and implementation considerations. The performance evaluation parameters are: NI, MFLOPS and SNR as defined in Sec. 2.2.3, and

- Maximum reconstruction error

$$E_r = \max_{\omega} \left| \left[|MT_0(e^{j\omega})| - 1 \right] \right|$$

- Aliasing error

$$E_a = \max_{\omega} E(\omega)$$

where

$$E(\omega) = \frac{1}{M} \left[\sum_{l=1}^{M-1} |T_l(e^{j\omega})|^2 \right]^{1/2}$$

$$T_l(e^{j\omega}) = \sum_{k=0}^{M-1} H_k(e^{j(\omega - \frac{2\pi l}{M})}) F_k(e^{j\omega})$$

- Number of multiplications per output in the implementation (MPU) [37]

$$\text{MPU} = 12 + 2N/M + 4\log_2(2M)$$

- Number of additions per output in the implementation (APU) [37]

$$\text{APU} = 4 + 2N/M + 4\log_2(2M)$$

5.4.1 Conventional Filter Banks

Algorithm 5.1 has been used to design two cosine-modulated QMF bank, as follows:

Example 5.1: In this example, a four-band cosine-modulated QMF bank satisfying the specifications

$$M = 4,\ N = 112,\ \alpha = 200,\ \omega_s = 0.2109\pi,\ \tau = 0.5,\ \epsilon = 10^{-4}$$

was designed. The initial point of $\mathbf{p}$ in Step 1 of Algorithm 5.1 was the coefficient

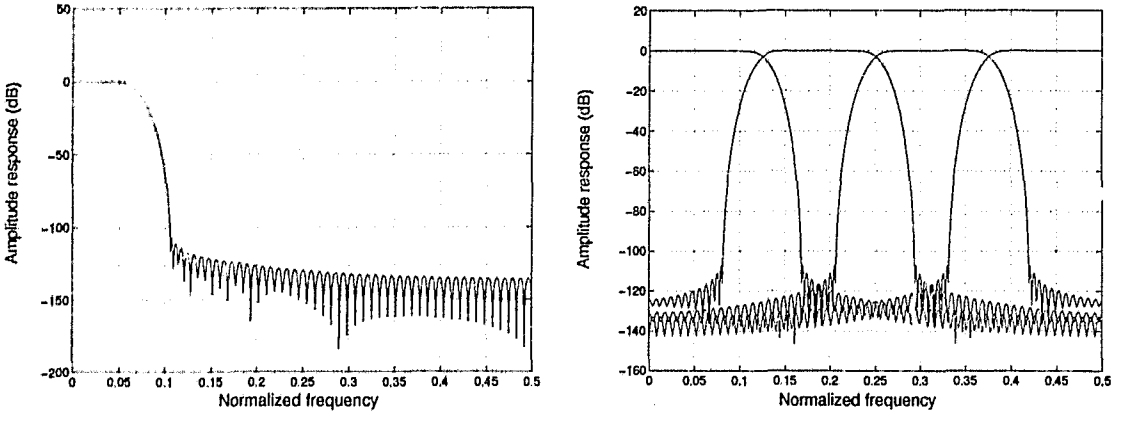

(a) (b)

Figure 5.2: Example 5.1 (a) Amplitude response of the prototype filter. (b) Amplitude responses of the analysis filters.

vector of a lowpass FIR filter designed by using the window method. The sampling grid contained 200 sampling points. The results obtained are summarized in Table 5.1. Fig. 5.2(a) and (b) shows the amplitude responses of the prototype filter and the analysis filters, respectively. To demonstrate the design efficiency of the iterative algorithm, the quasi-Newton method using the BFGS formula for updating the approximation of the inverse Hessian matrix of the objective function [57] was used to design the same filter bank with the same initial point and sampling points. The quasi-Newton method completed the design with about 502 MFLOPS which is almost 60 times that used by the iterative algorithm.

Example 5.2: A 16-channel cosine-modulated QMF bank was designed satisfying the specifications

$$M = 16,\ N = 386,\ \alpha = 100,\ \omega_s = 0.0567\pi,\ \tau = 0.5,\ \epsilon = 10^{-4}$$

The results obtained are listed in Table 5.1. Graphical displays for the filter bank

Table 5.1: Results for Examples 5.1 and 5.2.

	Example 5.1	Example 5.2
NI	12	14
MFLOPS	8.66	219
E_r	3.2594×10^{-6}	2.7563×10^{-6}
E_a	3.2178×10^{-7}	2.5814×10^{-7}
SNR_r (dB)	111.5	115.7
MPU	80	82
APU	72	74

in Example 5.2 are shown in Fig. 5.3(a) to (d). Fig. 5.3(a) illustrates the amplitude responses of the obtained analysis filters. Fig. 5.3(b) shows the overall amplitude response of the filter bank, i.e., $|MT_0(e^{j\omega})|$, and Fig. 5.3(c) shows the aliasing error $E(\omega)$. Fig. 5.3(d) depicts the spectrums of the input signal and the reconstruction error. From Table 1 and the figures it can be observed that the iterative algorithm leads to analysis and synthesis filters with a high stopband attenuation (≥ -120 dB) and low overall distortion and aliasing levels (≈ -100 dB). Such filter specifications were previously achieved with a constrained optimization method [33]. Using the algorithm in [33] the reconstruction error E_r is of the order of 10^{-13} while in our approach it is of the order of 10^{-6}. However, since the aliasing errors E_a achieved by both algorithms are of the order of 10^{-6} (-120 dB), in both cases the output signals $\hat{x}(n)$ approximate the input signals $x(n)$ with about -100 dB reconstruction error. This is evident from the gap between the spectrums of the input and the reconstructed error signals as depicted in Fig. 5.3(d).

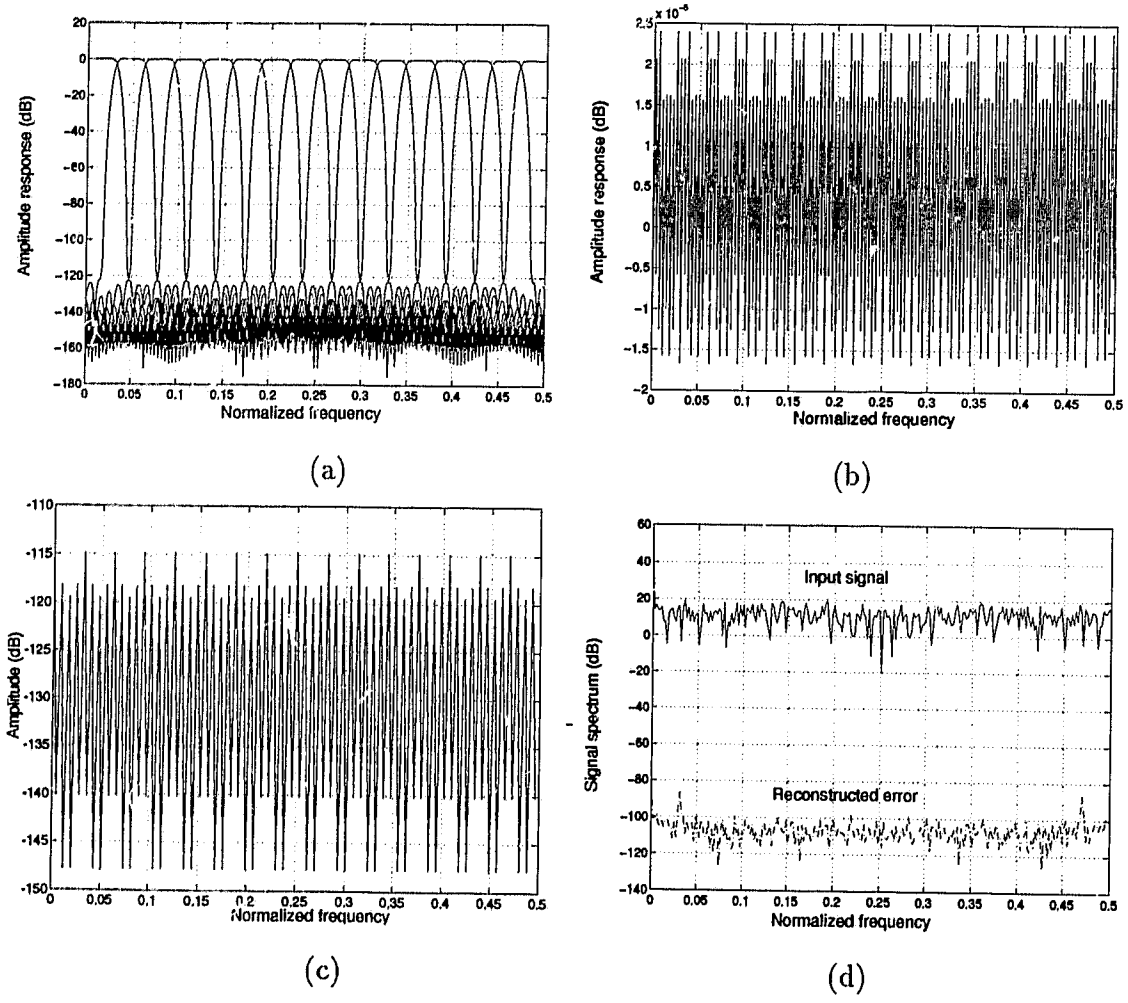

Figure 5.3: Example 5.2 (a) Amplitude responses of the analysis filters. (b) Amplitude response of the filter bank. (c) Plot of the aliasing error $E(\omega)$. (d) Spectrums of the input signal and the reconstruction error.

5.4.2 Filter Banks with Low Reconstruction Delays

Algorithm 5.2 has been used to design two low-delay cosine-modulated QMF banks.

Table 5.2: Results for Examples 5.3 and 5.4.

	Example 5.3	Example 5.4
k_d	55	65
NI	11	13
E_r	3.9808×10^{-5}	1.8041×10^{-4}
E_a	5.1584×10^{-6}	5.0333×10^{-5}
SNR_r (dB)	88.3	82.8
MPU	80	62
APU	72	54

Example 5.3: This example demonstrates that artifacts can occur when designing a low-delay cosine-modulated QMF bank and that it is possible to reduce them. First a four-channel filter bank was designed with $N = 112$, $k_d = 55$, and no constraint was applied to the transition band of the prototype filter. Fig. 5.4(a) and (b) shows the amplitude responses of the prototype filter P_L obtained and the analysis filters, respectively. It can be observed that there is a 'bump' in the transition band of P_L, which in turn leads to artifacts in the amplitude response of each analysis and synthesis filter. To reduce the artifacts the modified objective function in (5.33) was used to design a filter bank satisfying the specifications

$$M = 4,\ N = 112,\ k_d = 55,\ \alpha = 10,\ \alpha_1 = 10^{-3},\ \omega_s = 0.2078\pi$$

$$\tau = 0.5,\ \omega_{t1} = 0.1234\pi,\ \omega_{t2} = 0.1266\pi,\ \epsilon = 10^{-3}$$

The results obtained are summarized in Table 5.2. Fig. 5.4(c) and (d) shows the

amplitude responses of the prototype filter P_L and the analysis filters, respectively. Comparing them with Figs. 5.4(a) and (b), we note that the artifacts have been reduced significantly. On comparing the filter bank designed in this example with that in Example 5.1, we observe that the reconstruction delay in the present design is only about 50% of that in Example 5.1. However, this low delay is achieved at the cost of reduced stopband attenuation and SNR ratio. This was found to the case in a number of designs and in consequence, we believe that the designer can trade off stopband attenuation and reconstruction error for a lower reconstruction delay.

Example 5.4: In this example an 8-band low-delay cosine-modulated QMF bank satisfying the the specifications

$$M = 8,\ N = 132,\ k_d = 65,\ \alpha = 20,\ \alpha_1 = 10^{-3},\ \omega_s = 0.1357\pi$$

$$\tau = 0.5,\ \omega_{t1} = 0.0561\pi,\ \omega_{t2} = 0.0609\pi,\ \ \epsilon = 10^{-3}$$

was designed. The results are listed in Table 5.2. Fig. 5.5(a) shows the amplitude response of the prototype filter and Fig. 5.5(b) shows its group delay in the passband and transition band. Fig. 5.5(c) and (d) shows the amplitude response of the analysis filters obtained and the group delay of the filter bank. For comparison, Algorithm 5.1 was used to design a conventional cosine-modulated QMF bank with a filter length of 66 and a reconstruction delay of 65 sampling periods. The achieved SNR by this filter bank is 62 dB and the amplitude response of its prototype filter is also shown in Fig. 5.5(a). It is observed that with the same reconstruction delay, the low-delay cosine-modulated QMF bank shows improved performance over the conventional cosine-modulated QMF bank. From Fig. 5.5(b) it can be noticed that in the passband of the prototype filter linear phase response is well approximated and the phase distortion in its stopband can be neglected due to very small amplitude response. As mentioned in Sec. 5.3, in the low-delay QMF bank proposed both the

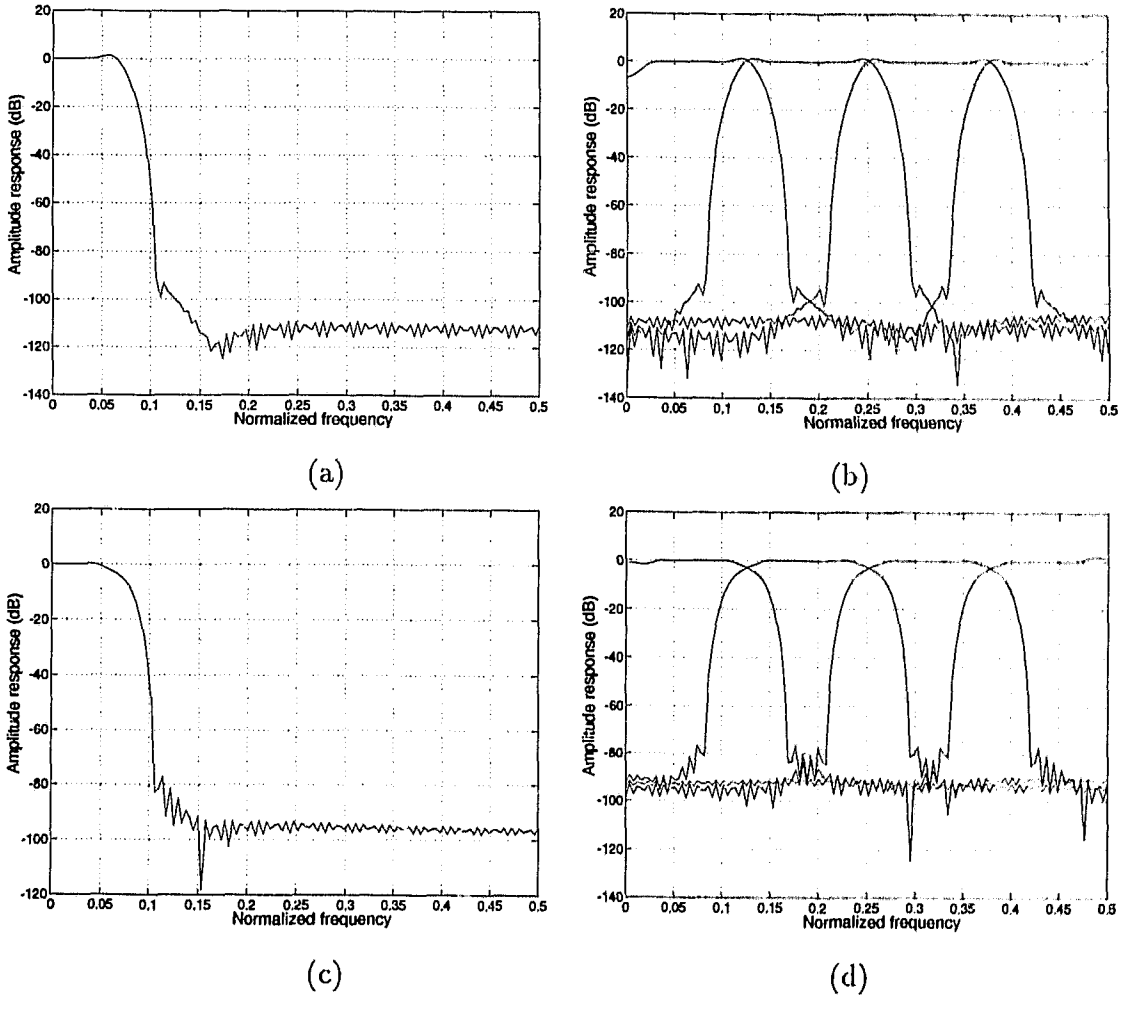

Figure 5.4: Example 5.3 (a) Prototype filter with artifacts. (b) Analysis filters with artifacts. (c) Prototype filter with reduced artifacts. (d) Analysis filters with reduced artifacts.

phase distortion and the amplitude distortion are minimized. Fig. 5.5(d) shows that the phase distortion of the obtained filter bank is small.

5.5 Conclusion

An iterative algorithm for the design of conventional cosine-modulated QMF banks has been proposed. The algorithm is very efficient and can design filter banks with high stopband attenuation and low aliasing and amplitude distortions. Although a rigorous proof on the convergence of the algorithm is not available at this time, the algorithm converged in all the design examples attempted. A general version of the algorithm has then been developed, which can be used to design low-delay cosine-modulated QMF banks. This algorithm is based on a weighted objective function that depends on the error between the actual frequency response and that of a linear phase ideal filter. Artifacts that can occur in the amplitude responses of the analysis and synthesis filters when designing low-delay filter banks can be reduced significantly by simply adding one more error component to the objective function. The two algorithms have been illustrated by designing several filter banks and the designs obtained have been compared with corresponding designs obtained by using some other known methods.

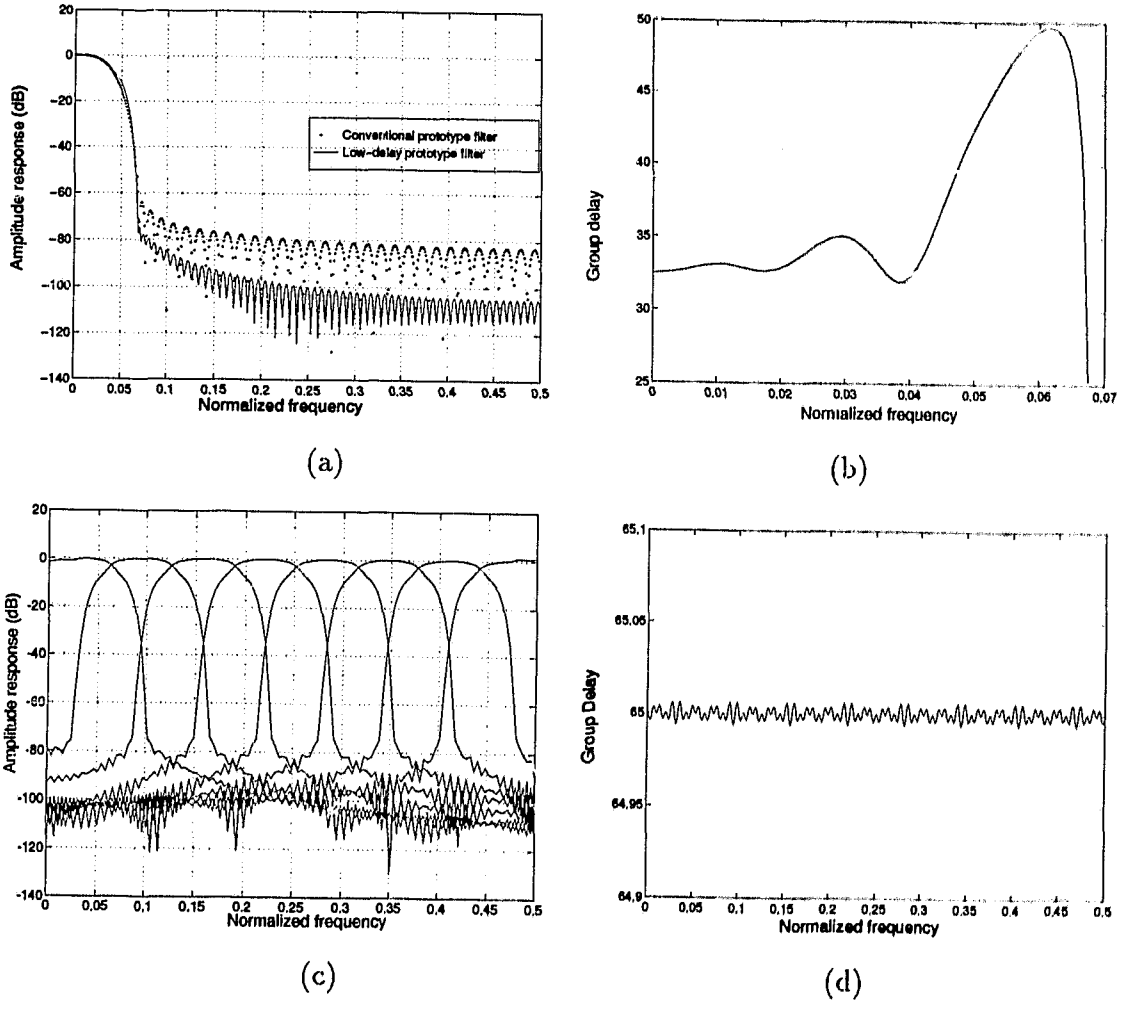

Figure 5.5: Example 5.4 (a) Prototype filters. (b) Group delay of the prototype filter (low-delay). (c) Analysis filters (low-delay). (d) Group delay of the filter bank (low-delay).

Chapter 6

Improved Designs of 2-D Nonseparable Filter Banks

6.1 Introduction

Most applications of QMF banks to 2-D signal processing, such as image subband coding, use separable filters, which can be designed by using 1-D techniques. In this scheme the frequency spectrum of the signal is split into central lowpass, horizontal highpass, vertical highpass, and diagonal highpass bands in which the diagonal highpass band contains a mixture of the two orientations. To avoid this problem, a nonseparable hexagonal QMF bank based on hexagonal sampling was proposed by Adelson and Simoncelli [43]. The analysis and synthesis filters in [43] have a similar structure to 1-D QMF banks and it was shown that aliasing in the system output is cancelled. The filters in [43] are designed by minimizing an objective function that deals with the perfect reconstruction condition as well as the intraband aliasing. In this chapter, we propose an improved method by taking the advantage of the symmetry properties exhibited by the hexagonal FIR filter, both in the time and frequency domains. This results in considerable computation reduction and the

filter banks designed exhibit improved performance. To further increase the design efficiency, an iterative method similar to that in chapters 2 and 3 is employed in the design.

One of the important classes of two-dimensional (2-D) filter banks is the class of nonseparable diamond-shaped filter banks in which significant horizontal and vertical frequency components are retained while less important diagonal frequency components are rejected. These filter banks have been applied to image and video compression in HDTV coding and the results obtained are satisfactory [44][45]. Existing methods for the design of 2-D nonseparable diamond-shaped filter banks are based on the application of transformations to one-dimensional (1-D) prototype filters [44][46][47] . In Sec. 6.3, an approach for the design of 2-D nonseparable diamond-shaped filter banks is proposed. To achieve perfect reconstruction and intraband aliasing minimization, we employ an objective function which is a weighted sum of two error components. This objective function turns out to be a fourth-order function of the filter coefficients and, consequently, its minimization by conventional optimization techniques would be computationally expensive. In our approach an iterative linearization technique is introduced which (a) modifies the objective function into a quadratic function so that its minimum can be obtained easily, and (b) the algorithm used to minimize the modified objective function converges rapidly, yielding a local solution of the design problem. The iterative method is first described in a discretized version and then in an improved version where all the integrals involved in the design are evaluated exactly. Compared with other existing methods, the proposed method is a direct 2-D design approach which does not require transformations. In addition, since a weighting factor is available which provides effective control on the tradeoff between the degree of perfect reconstruction and

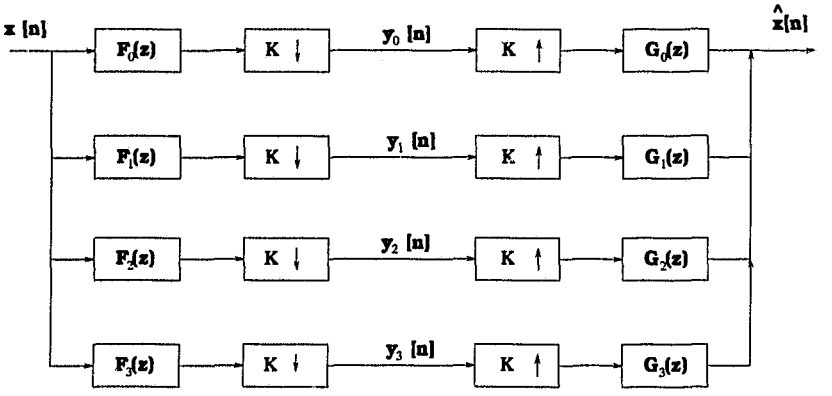

Figure 6.1: Diagram of a nonseparable hexagonal QMF filter bank.

the quality of the frequency responses of individual filters used, the design method is more flexible.

6.2 Design of Hexagonal QMF Banks

6.2.1 The Hexagonal QMF Banks

In [43], Adelson and Simoncelli proposed a nonseparable hexagonal quadrature mirror filter bank which is based on hexagonal sampling, and showed that the mixed orientation problem in separable QMF banks can be eliminated by using a nonseparable hexagonal QMF system.

A four-band, nonseparable, hexagonal analysis-synthesis filter bank in two dimensions is illustrated in Fig. 6.1. In this realization, $F_i(\boldsymbol{\omega})$, $i = 1, \ldots, 4$ and $G_i(\boldsymbol{\omega})$, $i = 1, \ldots, 4$ are the transfer functions of the analysis and synthesis filters, respectively. The input $x(\mathbf{n})$ with index $\mathbf{n} = [n_1\ n_2]^T$ is a 2-D digital signal sampled on a hexagonal sampling lattice, and the filtering and subsampling are accomplished in two dimensions, i.e., $\boldsymbol{\omega} = [\omega_1\ \omega_2]^T$ is a vector, and the subsampling is param-

eterized by a nonsingular two-by-two *subsampling matrix*, $\mathbf{K}$, with integer entries, which is chosen here as

$$\mathbf{K} = \begin{bmatrix} 2 & 0 \\ 0 & 2 \end{bmatrix} \tag{6.1}$$

Based on the scheme in Fig. 6.1, the relation between the input $x(\mathbf{n})$ and the overall filter bank output $\hat{x}(\mathbf{n})$ can be derived in the frequency domain as

$$\hat{X}(\omega) = \frac{1}{4}\sum_{l=0}^{3} X(\omega + \tilde{\mathbf{k}}_l)\left[\sum_{i=0}^{3} G_i(\omega)F_i(\omega + \tilde{\mathbf{k}}_l)\right] \tag{6.2}$$

where $\hat{X}(\omega)$ and $X(\omega)$ are the frequency spectra of $x(\mathbf{n})$ and $\hat{x}(\mathbf{n})$, respectively. Vectors $\tilde{\mathbf{k}}_l$, $l = 0, \ldots, 3$ are the four modulation vectors defined by

$$\tilde{\mathbf{k}}_0 = \begin{bmatrix} 0 \\ 0 \end{bmatrix}, \quad \tilde{\mathbf{k}}_1 = \begin{bmatrix} 2\pi/\sqrt{3} \\ 0 \end{bmatrix}$$

$$\tilde{\mathbf{k}}_2 = \begin{bmatrix} \pi/\sqrt{3} \\ \pi \end{bmatrix}, \quad \tilde{\mathbf{k}}_3 = \begin{bmatrix} -\pi/\sqrt{3} \\ \pi \end{bmatrix}$$

It can be observed from Eqn. (6.2) that the output of the filter bank system contains the input of the system, which corresponds to $\tilde{\mathbf{k}}_0$, and the aliasing terms, which correspond to $\tilde{\mathbf{k}}_l$, $l = 1, 2, 3$. If the analysis and synthesis filters are chosen as such that

$$\begin{aligned} F_0(\omega) &= G_0(-\omega) = H(\omega) = H(-\omega) \\ F_1(\omega) &= G_1(-\omega) = e^{j\omega\cdot\mathbf{s}_1}H(\omega + \tilde{\mathbf{k}}_1) \\ F_2(\omega) &= G_2(-\omega) = e^{j\omega\cdot\mathbf{s}_2}H(\omega + \tilde{\mathbf{k}}_2) \\ F_3(\omega) &= G_3(-\omega) = e^{j\omega\cdot\mathbf{s}_3}H(\omega + \tilde{\mathbf{k}}_3) \end{aligned} \tag{6.3}$$

where $H(\omega)$ is a function that is invariant under negation of its argument and the expressions $\omega \cdot \mathbf{s}_i$, $i = 1, 2, 3$, denote inner products of the two vectors, then the

analysis-synthesis system, is called a 2-D nonseparable *hexagonal* QMF bank. If $\mathbf{s}_i$, the shifting vectors, are assigned as

$$\mathbf{s}_1 = \begin{bmatrix} \sqrt{3}/2 \\ 1/2 \end{bmatrix}, \quad \mathbf{s}_2 = \begin{bmatrix} 0 \\ 1 \end{bmatrix}, \quad \mathbf{s}_3 = \begin{bmatrix} -\sqrt{3}/2 \\ 1/2 \end{bmatrix}$$

then it can be shown that the aliasing terms in Eqn. (6.2) will be cancelled regardless of the choice of $H(\boldsymbol{\omega})$, and the response in Eqn. (6.2) becomes

$$\hat{X}(\boldsymbol{\omega}) = \frac{1}{4} X(\boldsymbol{\omega}) \sum_{i=0}^{3} |H(\boldsymbol{\omega} + \tilde{\mathbf{k}}_i)|^2 \tag{6.4}$$

Now in order to achieve perfect reconstruction of the input from the output, the design problem is reduced to finding a filter with frequency response $H(\boldsymbol{\omega})$ that satisfies the constraint

$$\sum_{i=0}^{3} |H(\boldsymbol{\omega} + \tilde{\mathbf{k}}_i)|^2 = 4 \tag{6.5}$$

Usually, a hexagonal lowpass filter is adopted to produce a band-splitting system.

6.2.2 Improved Design Method

The design of 2-D nonseparable hexagonal QMFs is similar to the design of 1-D QMFs. It requires the design of only one filter represented by $H(\boldsymbol{\omega})$. The whole system then can be constructed from the relations in Eqn. (6.3). A "good" filter is one that satisfies constraint (6.5), which guarantees the perfect reconstruction. In addition, many applications require that the subband signals have minimal aliasing.

As the impulse response of an FIR hexagonal filter is defined on a hexagonal grid, the size of an FIR hexagonal filter kernel can be measured in terms of the number of hexagonal "rings" it contains. For example, a zero-ring filter contains only a single impulse located at the origin while a one-ring filter contains impulses at the origin

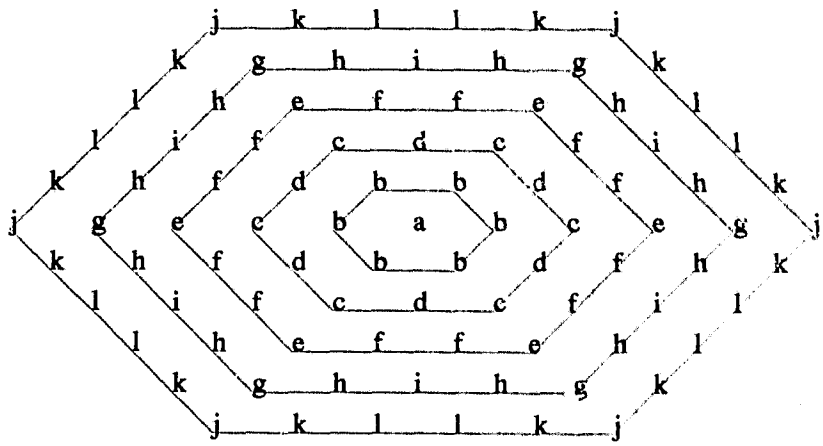

Figure 6.2: Coefficients of a hexagonal filter with symmetry.

and six more impulses around vertices of a hexagon centered at the origin. In general, the impulse response and frequency response of a hexagonal FIR system can have a 12-fold symmetry, i.e., they are symmetrical about the six vertices of a hexagon and across the bisectors of the six sides, as illustrated in Fig. 6.2. Therefore, the independent parameters that need to be determined are defined on a wedge-shaped region covering approximately one-twelfth of the whole kernel.

In order to satisfy Eqn. (6.5), an error function is defined as the p-norm of the approximation errors, i.e.,

$$E_1 = \left\{ \sum_{\omega} \left[\sum_{i=0}^{3} |H(\omega + \tilde{\mathbf{k}}_i)|^2 - 1 \right]^p \right\}^{1/p} \tag{6.6}$$

An FIR filter with hexagonal symmetry in its impulse response has hexagonal symmetry in its frequency response. Consequently, the sampling points ω can be chosen in a wedge-shaped region in the frequency domain, as shown by the shaded area in Fig. 6.3 (a).

In order to reduce the intraband aliasing, an error function, called intraband

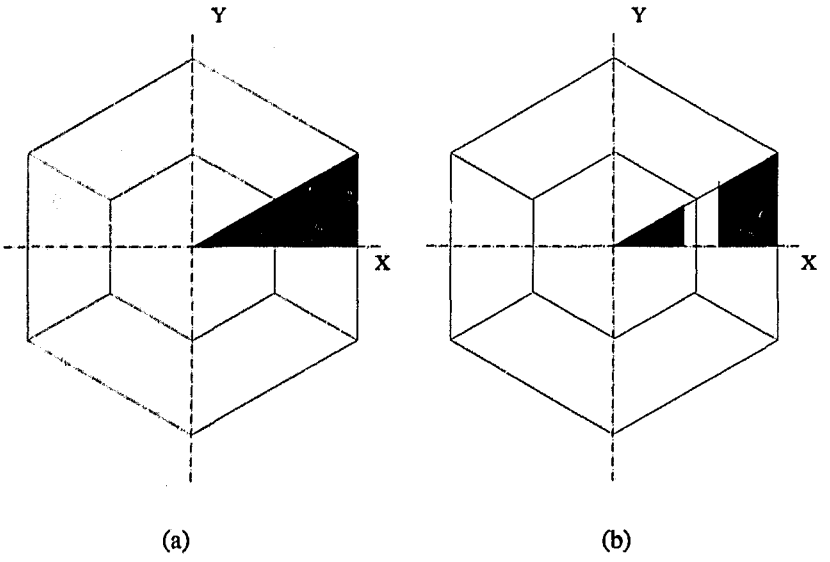

Figure 6.3: Sampling area in forming the objective function. (a) To form E_1. (b) To form E_2.

aliasing error function, is constructed as

$$E_2 = \left[\sum_{\omega}(|H(\omega)| - H_I(\omega))^p\right]^{1/p} \tag{6.7}$$

where $H_I(\omega)$ is the amplitude response of an ideal hexagonal lowpass filter. Again, the sampling points ω here are on a sampling grid in a wedge-shaped area, which is illustrate by shaded area in Fig. 6.3 (b). Note that there is no sampling point in the transition band. A method similar to the one used in [58] is utilized to construct the sampling grid, which gives more samples over the regions near the passband and stopband edges.

The design objective is to satisfy (6.5) while reducing the intraband aliasing . This can be achieved by defining an objective function that is the weighted sum of the above two error functions, i.e.,

$$E = \alpha E_1 + (1 - \alpha)E_2 \tag{6.8}$$

where $0 < \alpha < 1$. The weight α can be adjusted during the design.

A quasi-Newton optimization algorithm can be utilized to minimize the above objective function E with respect to the free parameters of the lowpass hexagonal filter represented by $H(\omega)$. The power p in Eqns. (6.6) and (6.7) should be chosen to be a large even number, e.g., $p = 128$, which would result in a nearly minimax design. A small weight α should be used at the beginning of the optimization to let error function E_2 be minimized first and then α should be increased to emphasize the error function E_1.

By using the proposed algorithm, several non-separable hexagonal filter banks have been designed. The coefficients of the hexagonal lowpass filters with 3, 4, and 5 rings, which are referred as Examples 6.1, 6.2 and 6.3, are listed in Table 6.1. The spatial positions of these coefficients in the 2-D space are illustrated in Fig. 6.2. The corresponding coefficients of the three highpass filters can be obtained by modulating and shifting the coefficients of the lowpass filters using Eqn. (6.3). For the 4-ring case, the 3-D plot of the amplitude response of the hexagonal lowpass filter is shown in Fig. 6.4 (a). For comparison purposes, a 3-D plot of the amplitude response of the 4-ring filter in [43] is shown in Fig. 6.4 (b). As can be seen the passbands of the two filters are almost the same but the stopband of the filter designed by the proposed method is better than that in [43]. In addition, as shown in Table 6.2 the filter banks designed in general satisfies the perfect reconstruction more accurately in terms of having smaller PRE where

$$\text{PRE} = \max_{\omega} \left| 20 \log_{10} \frac{1}{4} \left[\sum_{i=0}^{3} H(\omega + \tilde{\mathbf{k}}_i)^2 \right] \right|$$

The design method in [43] also involves optimizing an objective function containing two terms to deal with the perfect reconstruction condition and the intraband

Table 6.1: The impulse responses of Examples 6.1, 6.2 and 6.3.

Coef.	3-ring filter	4-ring filter	5-ring filter
a	0.668372	0.639332	0.593442
b	0.297021	0.305619	0.321198
c	−0.062023	−0.043298	−0.039581
d	−0.001132	0.009974	−0.004391
e	−0.006730	−0.015317	−0.006768
f	−0.006650	−0.033678	−0.036109
g		0.000359	−0.004358
h		0.008229	0.010173
i		0.020284	0.018715
j			0.001359
k			−0.003973
l			0.003823

Table 6.2: PRE of Examples 6.1, 6.2 and 6.3 and those of Simoncelli.

	3-ring filter	4-ring filter	5-ring filter
Proposed method	0.0080	0.0262	0.0165
Method in [43]	0.0026	0.1165	0.4548

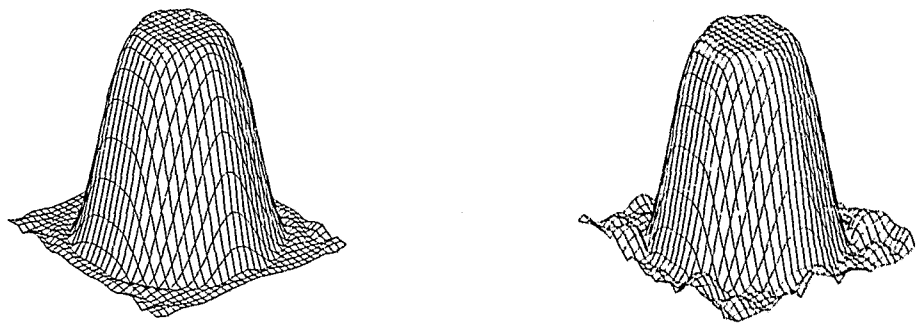

(a) (b)

Figure 6.4: (a) Amplitude response of the 4-ring filter by proposed method. (b) Amplitude response of the 4-ring filter by Simoncelli.

aliasing. However, the objective function is evaluated on a grid of sample points over the whole baseband. Our method makes use of the symmetry property of the filter and takes into consideration only the samples in a wedge-shaped area, which is one-twelfth of the total area. This leads to a significant improvement in the efficiency of the optimization involved. In [43], the error function dealing with the intraband aliasing is in the form of a product of the frequency response of the hexagonal lowpass filter with its nonzero modulation version, which is not very sensitive to the characteristics of the filter in the passband and the stopband. Our method, on the other hand, uses a p-norm approximation error as the intraband aliasing error function associated with a nonuniform sampling grid which is quite sensitive to the filter characteristics in the passband and stopband, including band edges. This is believed to be the reason why the designed filters have better frequency responses, especially in the stopband.

6.2.3 Iterative Method

Directly minimizing the objective function in (6.8) is a standard unconstrained optimization problem. In this section, an iterative method is proposed which avoids direct minimization thereby reducing the computational complexity. The objective function to be minimized is written as

$$E = E_1 + \alpha E_2 \tag{6.9a}$$

$$E_1 = \sum_{\mathbf{\Omega}} \left[\sum_{i=0}^{3} H(\omega + \tilde{\mathbf{k}}_i)^2 - 1 \right]^2 \tag{6.9b}$$

$$E_2 = \sum_{\mathbf{\Omega}_s} H(\omega)^2 \tag{6.9c}$$

where $\alpha > 0$, is a weighting constant. Error component E_1[1] is used to approximate the perfect reconstruction condition where $H(\omega)$ is the transfer function of a hexagonal lowpass filter, and $\mathbf{\Omega} = \{\omega_1, \omega_2, \cdots, \omega_s, \ldots, \omega_m\}$ are sampling points as shown in Fig. 6.3 (a). Intra-band aliasing is reduced by minimizing E_2 where $\mathbf{\Omega}_s = \{\omega_s, \ldots, \omega_m\}$ are the sampling points which correspond to the stopband area in Fig. 6.3 (b).

With 12-fold symmetry in its impulse response, a hexagonal FIR filter will have zero-phase frequency response. Then $H(\omega)$ can be written as

$$H(\omega) = \mathbf{b}(\omega)^T \mathbf{u}$$

where $\mathbf{u} = [h_a \; h_b \; h_c \; \cdots \;]^T$ is a column vector containing N independent filter coefficients and $\mathbf{b}(\omega) = [T_0(\omega) \; T_1(\omega) \; \cdots \; T_{N-1}(\omega)]^T$ is a column vector with entries being real functions of ω.

To use the iterative method, the objective function in (6.9) is modified into

$$E' = E_1' + \alpha E_2' \tag{6.10a}$$

[1] E_1 differs from that in Sec. 6.2.2 by a constant multiplier of 4

$$E_1' = \sum_{\Omega} \left[\sum_{i=0}^{3} H(\omega + \tilde{\mathbf{k}}_i) G(\omega + \tilde{\mathbf{k}}_i) - 1 \right]^2 \tag{6.10b}$$

$$E_2' = \sum_{\Omega_s} G(\omega)^2 \tag{6.10c}$$

Like $H(\omega)$, $G(\omega)$ is the transfer function of a lowpass hexagonal filter of the same length with 12-fold symmetry in its impusle response and

$$G(\omega) = \mathbf{b}(\omega)^T \mathbf{v}$$

where $\mathbf{v} = [g_a \; g_b \; g_c \; \cdots \;]^T$ is a column coefficient vector. It is assumed that at the start of the optimization, the coefficients in $\mathbf{u}$ are known and so $H(\omega)$ is known. By defining

$$\mathbf{U_t}(\Omega) = \begin{bmatrix} T_0(\omega_1) & T_1(\omega_1) & \cdots & T_{N-1}(\omega_1) \\ \vdots & & & \vdots \\ T_0(\omega_s) & T_1(\omega_s) & \cdots & T_{N-1}(\omega_s) \\ \vdots & & & \vdots \\ T_0(\omega_m) & T_1(\omega_m) & \cdots & T_{N-1}(\omega_m) \end{bmatrix} \tag{6.11a}$$

$$\mathbf{U_s} = \begin{bmatrix} T_0(\omega_s) & T_1(\omega_s) & \cdots & T_{N-1}(\omega_s) \\ \vdots & & & \vdots \\ T_0(\omega_m) & T_1(\omega_m) & \cdots & T_{N-1}(\omega_m) \end{bmatrix} \tag{6.11b}$$

$$\mathbf{H}(\Omega) = \mathrm{diag}[H(\omega_1), \ldots, H(\omega_s), \ldots, H(\omega_m)] \tag{6.11c}$$

$$\mathbf{U} = \sum_{i=0}^{3} \mathbf{H}(\Omega + \tilde{\mathbf{k}}_i) \mathbf{U_t}(\Omega + \tilde{\mathbf{k}}_i) \tag{6.11d}$$

E' in (6.10a) can be expressed as

$$E' = (\mathbf{Uv} - \mathbf{I})^T (\mathbf{Uv} - \mathbf{I}) + \alpha (\mathbf{U_s v})^T (\mathbf{U_s v}) \tag{6.12}$$

where $\mathbf{I}$ is a column vector with each entry being a 1. E' in (6.12) is a quadratic function of the coefficients in $\mathbf{v}$ and its minimum point can be obtained by an

analytic solution as

$$\mathbf{v} = (\mathbf{U}^T\mathbf{U} + \alpha\mathbf{U_s}^T\mathbf{U_s})^{-1} \cdot (\mathbf{U}^T\mathbf{I}) \tag{6.13}$$

After obtaining $\mathbf{v}$, a linear formula is adopted to update $\mathbf{u}$ as

$$\mathbf{u} := (1-\tau)\mathbf{u} + \tau\mathbf{v} \tag{6.14}$$

and the above process is repeated until $|| \mathbf{u}-\mathbf{v} ||$ is less than a prescribed tolerance..

A step-by-step procedure based on the above analysis is as follows:

Algorithm 6.1

Step 1 Use a conventional method, e.g., optimization method, to design a hexagonal lowpass filter and to form the initial $\mathbf{u}$ using its coefficients.

Step 2 Calculate the matrices $\mathbf{U}_s$ in (6.11b).

Step 3 Obtain $\mathbf{U}$ and $\mathbf{v}$ using (6.11d) and (6.13), respectively.

Step 4 If $|| \mathbf{u}-\mathbf{v} || < \epsilon$, where ϵ is a prescribed tolerance, terminate the process; Otherwise, update coefficient vector $\mathbf{u}$ using (6.14) and go to step 3.

The proposed iterative method has been used to design 2-D nonseparable hexagonal QMF filter banks. Three examples, referred as Examples 6.4, 6.5 and 6.6, are to design 2-D hexagonal QMF banks with 3, 4, and 5 rings, respectively. The obtained coefficients are listed in Table 6.3. The experimental results are summarized in Table 6.4 in terms of

$$\text{PRE} = \max_{\omega} |20\log_{10}\left[\sum_{i=0}^{3} H(\omega + \tilde{\mathbf{k}}_i)^2\right]|$$

and NI. Fig. 6.5(a), (b) and (c) shows the 3-D plot of the amplitude responses of the lowpass hexagonal filter in three examples. The designs by the iterative method are in general superior to those in [13] in terms of having better performance, and needing less computational effort, since no computationally demanding standard optimization method is involved.

Table 6.3: The impulse responses of Examples 6.4, 6.5 and 6.6.

Coef.	3-ring filter	4-ring filter	5-ring filter
a	0.676408	0.653134	0.650778
b	0.295155	0.302232	0.303184
c	−0.056309	−0.041640	−0.045457
d	−0.006377	0.006792	0.006826
e	−0.005789	−0.019342	−0.016672
f	−0.005626	−0.028962	−0.027096
g		0.002091	0.001845
h		0.008020	0.006875
i		0.016321	0.014618
j			0.000405
k			−0.000431
l			0.000769

Table 6.4: Results for Examples 6.4, 6.5 and 6.6.

	3-ring filter	4-ring filter	5-ring filter
PRE (dB)	0.0070	0.0283	0.0182
NI	9	6	9

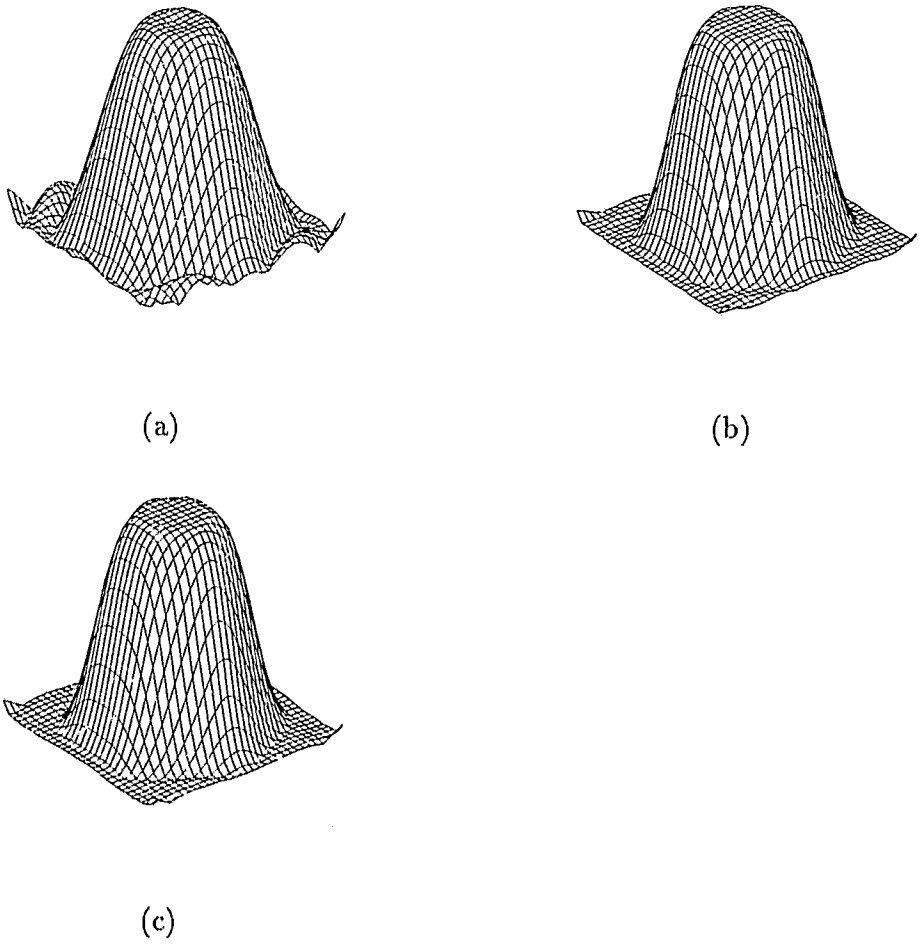

Figure 6.5: Amplitude response of obtained hexagonal filters. (a) 3-ring. (b) 4-ring. (c) 5-ring.

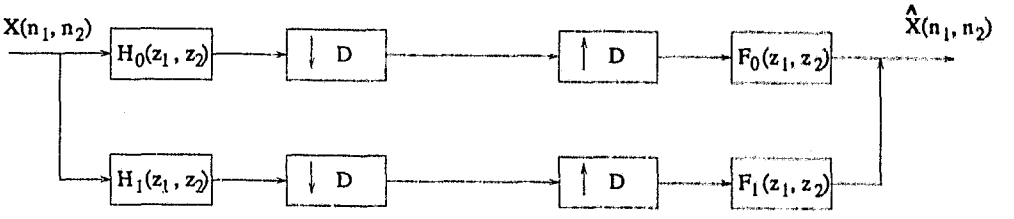

Figure 6.6: Diagram of a 2-D nonseparable diamond-shaped filter bank.

6.3 Design of Diamond-Shaped QMF Banks

6.3.1 Formulation of the Objective Function

A 2-D nonseparable diamond-shaped filter bank can be designed as shown in Fig. 6.6. The ideal frequency response of the analysis lowpass filter H_0 is illustrated in Fig. 6.7 (a). After analysis filtering, the signals are quincunx downsampled as shown in Fig. 6.7 (b), where effectively half of the samples are discarded. At the reconstruction end, upsampling will replace the discarded samples with zero values. The input and output relationship of the filter bank can be expressed as

$$\begin{aligned}\hat{X}(z_1,z_2) = {} & \tfrac{1}{2}[H_0(z_1,z_2)F_0(z_1,z_2) + H_1(z_1,z_2)F_1(z_1,z_2)] \\ & \cdot X(z_1,z_2) + \tfrac{1}{2}[H_0(-z_1,-z_2)F_0(z_1,z_2) \\ & + H_1(-z_1,-z_2)F_1(z_1,z_2)] \cdot X(-z_1,-z_2) \end{aligned} \tag{6.15}$$

where the first term represents the input signal component and the second term represents the aliasing component.

By assuming that

$$H_1(z_1,z_2) = z_1^{-1}H_0(-z_1,-z_2) \tag{6.16a}$$

$$F_0(z_1,z_2) = H_0(z_1,z_2) \tag{6.16b}$$

$$F_1(z_1,z_2) = z_1H_0(-z_1,-z_2) \tag{6.16c}$$

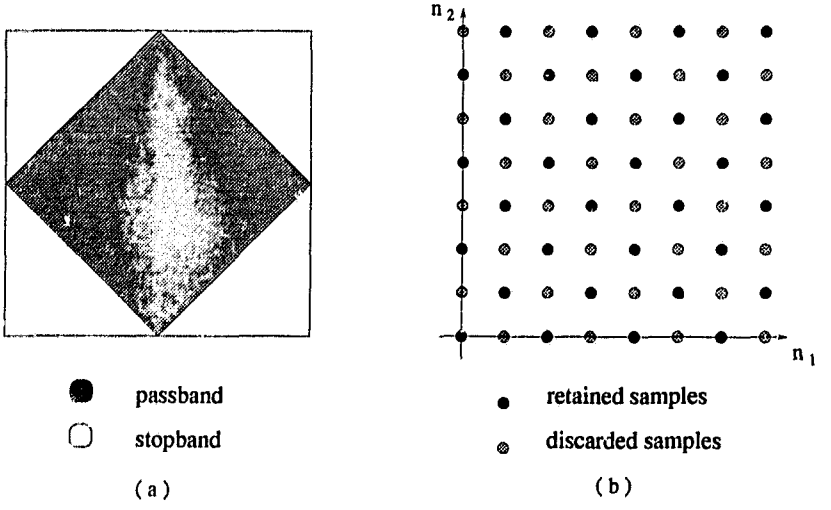

Figure 6.7: (a) Band Characteristics. (b) Quincunx sampling.

the aliasing term in Eqn. (6.15) is cancelled and (6.15) becomes

$$\hat{X}(z_1, z_2) = \tfrac{1}{2}[H_0^2(z_1, z_2) + H_0^2(-z_1, -z_2)] \cdot X(z_1, z_2) \tag{6.17}$$

So if the condition

$$H_0^2(\omega_1, \omega_2) + H_0^2(\omega_1 + \pi, \omega_2 + \pi) = 1 \tag{6.18}$$

is satisfied for $-\pi \leq \omega_1 \leq \pi, -\pi \leq \omega_2 \leq \pi$, the output will be a replica of the input.

In our design the region of support of filter H_0 is assumed to be an $N \times N$ square centered at the origin where N is an odd number. If the impulse response of H_0, $h(n_1, n_2)$, for $-N \leq n_1 \leq N, -N \leq n_2 \leq N$, has octagonal symmetry, then the frequency response has zero phase and can be written as [59]

$$\begin{aligned} H_0(\omega_1, \omega_2) = & \sum_{n_2=0}^{(N-3)/2} \sum_{n_1=n_2+1}^{(N-1)/2} a(n_1, n_2) \\ & \cdot[\cos(n_1\omega_1)\cos(n_2\omega_2) + \cos(n_2\omega_1)\cos(n_1\omega_2)] \\ & + \sum_{n=0}^{(N-1)/2} a(n, n)\cos(n\omega_1)\cos(n\omega_2) \end{aligned} \tag{6.19}$$

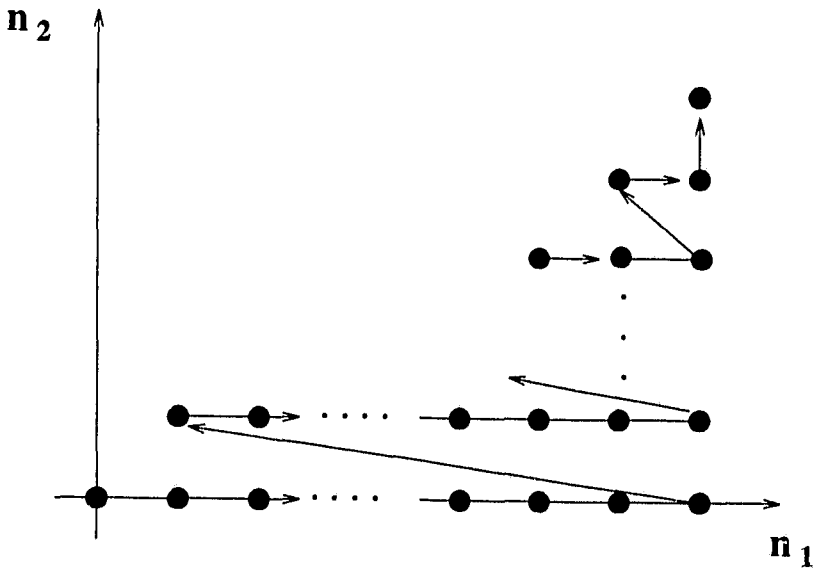

Figure 6.8: The order of the $a(n_1, n_2)$ in forming vector $\mathbf{y}$.

where

$$\begin{aligned} a(0,0) &= h(0,0) \\ a(n_1,0) &= 2h(n_1,0) \qquad \text{for } 1 \le n_1 \le (N-1)/2 \\ a(n_1,n_2) &= 4h(n_1,n_2) \quad \text{for } 1 \le n_2 \le (N-1)/2, \\ &\qquad\qquad\qquad\quad \text{and } n_2 \le n_1 \le (N-1)/2 \end{aligned}$$

For convenience, we write the frequency response in a matrix form as

$$H_0(\boldsymbol{\omega}) = \mathbf{c}(\boldsymbol{\omega})^T \mathbf{y}$$

where $\boldsymbol{\omega} = (\omega_1, \omega_2)$, $\mathbf{y}$ is a column vector formed by $a(n_1, n_2)$ in the order shown in Fig. 6.8, and $\mathbf{c}(\boldsymbol{\omega})$ denoted as $[T_0(\boldsymbol{\omega})\ T_1(\boldsymbol{\omega})\ \cdots\ T_{K-1}(\boldsymbol{\omega})]^T$ with $K = (N+3)(N+1)/8$ is a column vector with $T_i(\boldsymbol{\omega})$ being the corresponding multiplier of $a(n_1, n_2)$ in (6.19).

The design can be accomplished by minimizing the objective function given by

$$E = E_1 + \alpha E_2 \tag{6.20}$$

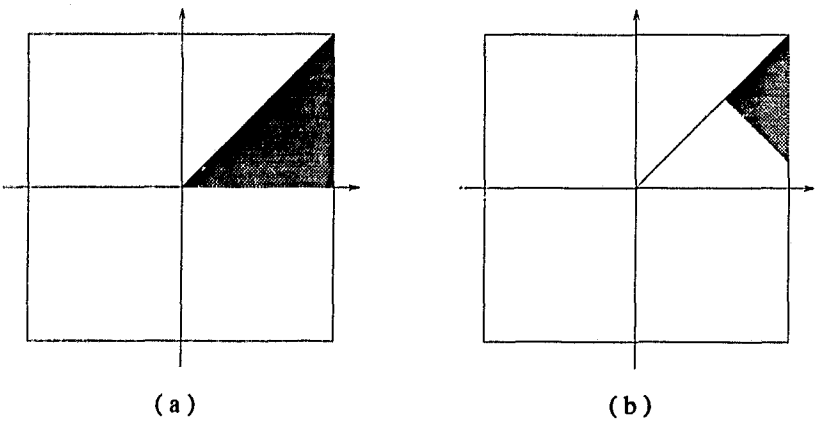

Figure 6.9: Sampling areas (a) whole band. (b) stopband.

where α is a positive weight,

$$E_1 = \sum_{\Omega} \left[H_0^2(\omega) + H_0^2(\omega + \pi) - 1 \right]^2$$

where $\Omega = [\omega_1, \omega_2, \ldots, \omega_p]$ are chosen from the shaded area shown in Fig. 6.9 (a), and

$$E_2 = \sum_{\Omega_s} H_0^2(\omega)$$

where $\Omega_s = [\omega_{s1}, \omega_{s2}, \ldots, \omega_{sm}]$ are chosen from the shaded area in Fig. 6.9 (b). On comparing (6.20) with (6.18), we see that term E_1 in (6.20) deals with the reconstruction requirement whereas E_2 is used to reduce the intraband aliasing effects.

6.3.2 Iterative Approach

The objective function E in (6.20) is a fourth-order function with respect to the coefficients in $\mathbf{y}$. Instead of minimizing the objective function directly, which is a nonlinear optimization problem, an iterative method is adopted in which the error

function in (6.20) is modified into

$$E' = E'_1 + \alpha E'_2 \tag{6.21}$$

where

$$E'_1 = \sum_{\mathbf{\Omega}} [H_0(\omega)G_0(\omega) + H_0(\omega+\pi)G_0(\omega+\pi) - 1]^2$$
$$E'_2 = \sum_{\mathbf{\Omega}_s} G_0^2(\omega)$$

Like H_0, G_0 is an $N \times N$ lowpass FIR filter with octagonal symmetrical impulse response, and $G_0(\omega)$ can be expressed as

$$G_0(\omega) = \mathbf{c}(\omega)^T \mathbf{x}$$

where $\mathbf{x}$ is a column vector formed by the coefficients of G_0. To start the iteration, we first design a diamond-shaped lowpass filter H_0, and write term E' in (6.21) as

$$E' = (\mathbf{U}\mathbf{x} - \mathbf{I})^T(\mathbf{U}\mathbf{x} - \mathbf{I}) + \alpha(\mathbf{U}_s\mathbf{x})^T(\mathbf{U}_s\mathbf{x}) \tag{6.22}$$

where

$$\mathbf{U}_t(\mathbf{\Omega}) = \begin{bmatrix} T_0(\omega_1) & T_1(\omega_1) & \cdots & T_{K-1}(\omega_1) \\ T_0(\omega_2) & T_1(\omega_2) & \cdots & T_{K-1}(\omega_2) \\ \vdots & & & \vdots \\ T_0(\omega_p) & T_1(\omega_p) & \cdots & T_{K-1}(\omega_p) \end{bmatrix} \tag{6.23a}$$

$$\mathbf{U}_s = \begin{bmatrix} T_0(\omega_{s1}) & T_1(\omega_{s1}) & \cdots & T_{K-1}(\omega_{s1}) \\ T_0(\omega_{s2}) & T_1(\omega_{s2}) & \cdots & T_{K-1}(\omega_{s2}) \\ \vdots & & & \vdots \\ T_0(\omega_{sm}) & T_1(\omega_{sm}) & \cdots & T_{K-1}(\omega_{sm}) \end{bmatrix} \tag{6.23b}$$

$$\mathbf{H}(\mathbf{\Omega}) = \mathrm{diag}[H_0(\omega_1), \ldots, H_0(\omega_s), \ldots, H_0(\omega_p)] \tag{6.23c}$$

$$\mathbf{U} = \mathbf{H}(\mathbf{\Omega})\mathbf{U}_t(\mathbf{\Omega}) + \mathbf{H}(\mathbf{\Omega}+\pi)\mathbf{U}_t(\mathbf{\Omega}+\pi) \tag{6.23d}$$

$$\mathbf{I} = [\,1\;1\;\cdots\;\cdots\;1\,]^T \in \mathbf{R}^{p\times 1} \tag{6.23e}$$

Since $\mathbf{U}^T\mathbf{U} + \alpha\mathbf{U}_s^T\mathbf{U}_s$ is positive definite, E' has a global minimum point given by

$$\mathbf{x} = (\mathbf{U}^T\mathbf{U} + \alpha\mathbf{U}_s{}^T\mathbf{U}_s)^{-1} \cdot (\mathbf{U}^T\mathbf{I}) \tag{6.24}$$

After obtaining $\mathbf{x}$, $\mathbf{y}$ is updated using

$$\mathbf{y} := (1-\tau)\mathbf{y} + \tau\mathbf{x} \tag{6.25}$$

where $0 < \tau < 1$ is a smoothing parameter. The above process is repeated until $\| \mathbf{y} - \mathbf{x} \|$ is less than a prescribed tolerance.

A step-by-step description of this design method is as follows:

Algorithm 6.2

Step 1 Use a conventional method (e.g., SVD method) to design a 2-D $N \times N$ diamond-shaped FIR filter and use its coefficients to form the initial $\mathbf{y}$.

Step 2 Calculate $\mathbf{U}_i(\Omega)$, $\mathbf{U}_s$ and $\mathbf{I}$ using (6.23a), (6.23b), and (6.23c), respectively.

Step 3 Use (6.23c) and (6.23d) to form $\mathbf{H}(\Omega)$ and $\mathbf{U}$, and compute $\mathbf{x}$ in (6.24).

Step 4 If $\| \mathbf{y} - \mathbf{x} \| < \epsilon$, where ϵ is a prescribed tolerance, output $\mathbf{x}$ as the design result and stop. Otherwise, update $\mathbf{y}$ using (6.25) and repeat from Step 3.

By applying the proposed iterative algorithm, a set of 2-D nonseparable diamond-shaped filter banks were designed. The parameters used are $\alpha = 10^{-5}$, $\tau = 0.7$, $\epsilon = 10^{-3}$ in three design examples where $N = 7$, 9, 11, referred to as Example 6.7, 6.8 and 6.9, respectively. The impulse responses of the obtained H_0 are listed in Table 6.5. They are in the order indicated in Fig. 6.8. The 3-D plots of the amplitude responses of H_0 and corresponding analysis highpass filter H_1 with $N = 9$ are shown in Fig. 6.10 (a) and (b) respectively. To evaluate the reconstruction

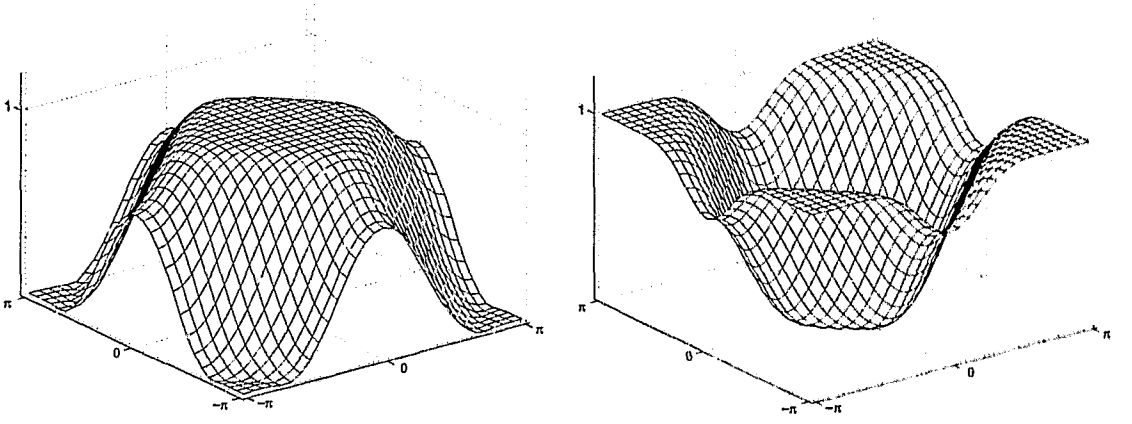

(a) (b)

Figure 6.10: Example 6.8 (a) Amplitude response of H_0. (b) Amplitude response of H_1.

performance of the filter bank

$$\text{PRE} = \max_{\omega} \left\{ \left| 20 \log_{10} \left[H_0^2(\omega) + H_0^2(\omega + \pi) \right] \right| \right\}$$

was calculated where ω varies over the entire frequency domain. The PRE and NI for each design are listed in Table 6.6. From Table 6.6 and the plots, it is obvious that good designs can be achieved after a small number of iterations.

6.3.3 Improved Iterative Approach

In the above section, the objective function is evaluated on discrete sampling points and, therefore, if the density of the sampling points is not high enough, the performance of the obtained filter bank will be degraded. In this section, an improved iterative method is proposed in which the objective function is evaluated in an explicit closed form.

Table 6.5: The impulse responses of Examples 6.7, 6.8 and 6.9.

Coef. No.	N=7	N=9	N=11
1	6.303933e-01	6.133241e-01	5.988531e-01
2	1.550647e-01	1.682721e-01	1.778429e-01
3	−1.414847e-02	−1.245620e-02	−1.010828e-02
4	−7.125124e-04	1.426121e-03	1.940527e-03
5	−3.333147e-02	−1.104196e-03	−1.265525e-03
6	−1.279112e-02	−3.472240e-02	−2.571798e-04
7	2.544806e-03	−2.329296e-02	−3.521509e-02
8	5.145418e-03	4.409431e-03	−3.190801e-02
9	3.895804e-04	2.493733e-04	6.252349e-03
10	−7.061552e-05	1.102501e-02	−3.512157e-04
11	-	1.911315e-03	3.730406e-04
12	-	−5.020628e-04	1.576852e-02
13	-	−1.062799e-03	4.451412e-03
14	-	−1.620485e-04	−1.196672e-03
15	-	2.189800e-05	−9.916944e-05
16	-	-	−3.143924e-03
17	-	-	−3.937832e-04
18	-	-	6.164737e-05
19	-	-	1.429489e-04
20	-	-	9.356728e-05
21	-	-	−1.059957e-05

Table 6.6: Results for Examples 6.7, 6.8 and 6.9.

	N=7	N=9	N=11
PRE (dB)	0.0135	0.0067	0.0090
NI	7	8	7

Assuming that the region of support of $H_0(z_1, z_2)$ is a $(2N_1 - 1) \times (2N_2 - 1)$ rectangle centered at the origin and its impulse responses $h(n_1, n_2)$, for $n_1 = -(N_1 - 1), \ldots, N_1 - 1$ and $n_2 = -(N_2 - 1), \ldots, N_2 - 1$, is of quadrantal symmetry, then the frequency response of filter H_0 can be expressed as [59]

$$\begin{aligned} H_0(\omega_1, \omega_2) &= \sum_{n_1=0}^{N_1-1} \sum_{n_2=0}^{N_2-1} a(n_1, n_2) \cos(n_1\omega_1) \cos(n_2\omega_2) \\ &= \mathbf{h}^T \mathbf{c}(\omega_1, \omega_2) \end{aligned} \tag{6.26}$$

where

$$\begin{aligned} &a(0, 0) = h(0, 0) \\ &a(n_1, 0) = 2h(n_1, 0) \qquad \text{for } 1 \le n_1 \le N_1 - 1 \\ &a(0, n_2) = 2h(0, n_2) \qquad \text{for } 1 \le n_2 \le N_2 - 1 \\ &a(n_1, n_2) = 4h(n_1, n_2) \quad \text{for } 1 \le n_1 \le (N_1 - 1),\ 1 \le n_2 \le (N_2 - 1) \end{aligned}$$

and

$$\mathbf{h} = [\, a(0, 0)\ a(1, 0) \cdots a(N_1-1, 0)\ a(0, 1) \ \ldots\ a(N_1-1, 1) \ \ldots a(N_1-1, N_2-1)]^T$$

is a column vector formed by reordering $a(n_1, n_2)$ as shown in Fig 6.11; on the other hand, $\mathbf{c}(\omega_1, \omega_2)$ is a column vector whose ith entry can be expressed as

$$\begin{aligned} c(i) &= \cos p(i)\omega_2 \cdot \cos q(i)\omega_1 \\ p(i) &= \text{int}\left[\frac{i-1}{N_1}\right] \\ q(i) &= i - 1 - \text{int}\left[\frac{i-1}{N_1}\right] \cdot N_1 \end{aligned}$$

for $1 \le i \le N_1 \times N_2$.

The error function E in the iterative method is given by

$$E' = E'_1 + \alpha E'_2 \tag{6.27}$$

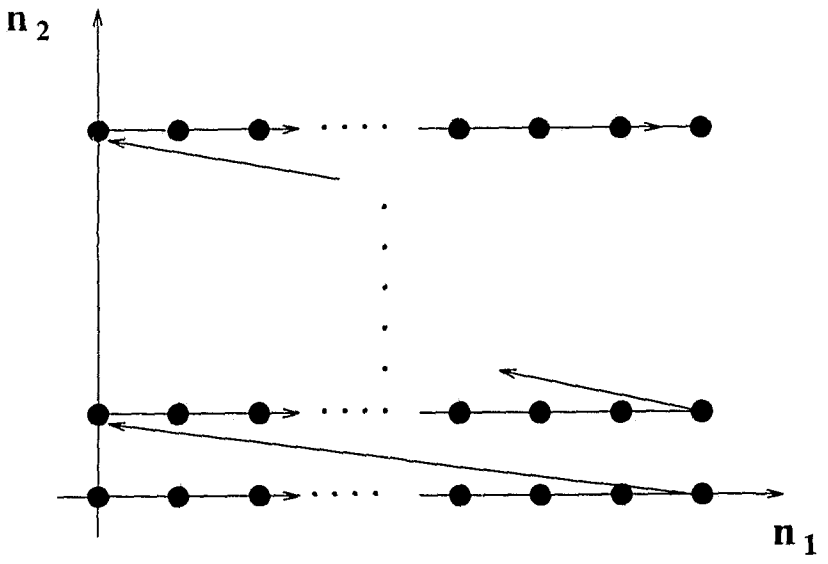

Figure 6.11: Reordering of the impulse responses of H_0.

where

$$E_1' = \int_0^{\pi}\int_0^{\pi} [H_0(\omega_1,\omega_2)G_0(\omega_1,\omega_2)+H_0(\omega_1+\pi,\omega_2+\pi)G_0(\omega_1+\pi,\omega_2+\pi)-1]^2\, d\omega_1 d\omega_2$$

and

$$E_2' = \int\int_{\Omega_s} G_0^2(\boldsymbol{\omega})\, d\omega_1 d\omega_2$$

where the integration region Ω_s is the shaded area in Fig. 6.12. Like H_0, G_0 is a low-pass FIR filter of the same order with quadrantally symmetrical impusle response, and frequency response

$$G_0(\omega_1,\omega_2) = \mathbf{g}^T\mathbf{c}(\omega_1,\omega_2)$$

where $\mathbf{g}$ is a column vector whose elements are the impulse responses of G_0. To start the iteration, we design a 2-D diamond-shaped lowpass filter by a conventional 2-D FIR filter design method [59], and use its coefficients to form the initial $\mathbf{h}$.

After extensive manipulations, it can be shown that E' in (6.27) can be written

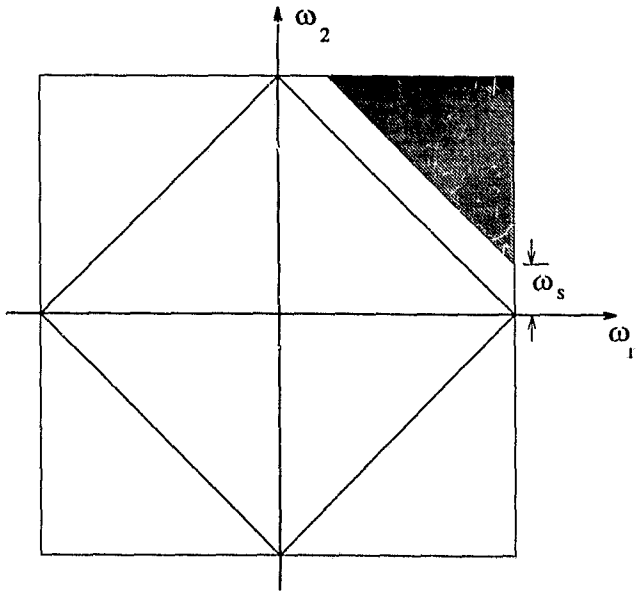

Figure 6.12: Sampling area in the stopband of H_0.

in terms of a quadratic form of $\mathbf{g}$ as

$$E' = \mathbf{g}^T(\mathbf{U} + \alpha\mathbf{U}_s)\mathbf{g} - 2\mathbf{h}^T\mathbf{B}\mathbf{g} + \pi^2 \tag{6.28}$$

where

$$\mathbf{B} = \int_0^\pi \int_0^\pi \left[\mathbf{c}(\omega_1,\omega_2)\mathbf{c}^T(\omega_1,\omega_2) + \mathbf{c}(\omega_1+\pi,\omega_2+\pi)\mathbf{c}^T(\omega_1+\pi,\omega_2+\pi)\right]\, d\omega_1 d\omega_2$$

with the $(i,\, j)th$ entry given by

$$b_{ij} = \frac{\pi^2}{2}\{\delta[p(i)+p(j)] + \delta[p(i)-p(j)]\} \cdot \{\delta[q(i)+q(j)] + \delta[q(i)-q(j)]\} \tag{6.29a}$$

for $1 \le i,\, j \le N_1N_2$, where

$$\delta(k) = \begin{cases} 1\,, & k = 0 \\ 0\,, & \text{otherwise} \end{cases}$$

and

$$\mathbf{U} = \int_0^{\pi}\int_0^{\pi} [H_0(\omega_1, \omega_2)\mathbf{c}(\omega_1, \omega_2) + H_0(\omega_1+\pi, \omega_2+\pi)\mathbf{c}(\omega_1+\pi, \omega_2+\pi)] \cdot [H_0(\omega_1, \omega_2)\mathbf{c}(\omega_1, \omega_2) + H_0(\omega_1+\pi, \omega_2+\pi)\mathbf{c}(\omega_1+\pi, \omega_2+\pi)]^T \, d\omega_1 d\omega_2$$

with the $(i, j)th$ entry being

$$u_{ij} = 2\sum_{n_1=0}^{N_1-1}\sum_{n_2=0}^{N_2-1}\sum_{m_1=0}^{N_1-1}\sum_{n_2=0}^{N_2-1} h(n_1, n_2)h(m_1, m_2)\left[1+(-1)^{m_1+m_2+p(j)+q(j)}\right] \cdot I(n_1, m_1, q(i), q(j))\, I(n_2, m_2, p(i), p(j)) \tag{6.29b}$$

for $1 \le i, j \le N_1N_2$, where

$$I(n_1, n_2, n_3, n_4) = \int_0^{\pi} \cos n_1\omega \cos n_2\omega \cos n_3\omega \cos n_4\omega \; d\omega \tag{6.29c}$$

Note that the integrations in (6.29c) can be easily obtained.

To evaluate $\mathbf{U}_s$, we note from Fig. 6.12 that

$$\begin{aligned} E_2' &= \int_{\omega_s}^{\pi} d\omega_2 \int_{\pi-(\omega_2-\omega_s)}^{\pi} G_0^2(\omega_1, \omega_2)\, d\omega_1 \\ &= \mathbf{g}^T \left[\int_{\omega_s}^{\pi} d\omega_2 \int_{\pi-(\omega_2-\omega_s)}^{\pi} \mathbf{c}(\omega_1, \omega_2)\mathbf{c}^T(\omega_1, \omega_2)\, d\omega_1\right]\mathbf{g} \end{aligned}$$

where ω_s is the stopband edge and hence

$$\mathbf{U}_s = \int_{\omega_s}^{\pi} d\omega_2 \int_{\pi-(\omega_2-\omega_s)}^{\pi} \mathbf{c}(\omega_1, \omega_2)\mathbf{c}^T(\omega_1, \omega_2)\, d\omega_1$$

with the $(i, j)th$ entry being

$$\begin{aligned} u_{ij}^{(s)} &= \int_{\omega_s}^{\pi} d\omega_2 \int_{\pi-(\omega_2-\omega_s)}^{\pi} \cos p(i)\omega_2 \cos q(i)\omega_1 \cos p(j)\omega_2 \cos q(j)\omega_1 \, d\omega_1 \\ &= \tfrac{1}{4}\left\{\int_{\omega_s}^{\pi}[\cos(p(i)+p(j))\omega_2 + \cos(p(i)-p(j))\omega_2]\, d\omega_2 \right. \\ &\quad \left. \cdot \int_{\pi-(\omega_2-\omega_s)}^{\pi}[\cos(q(i)+q(j))\omega_1 + \cos(q(i)-q(j))\omega_1]\, d\omega_1\right\} \end{aligned} \tag{6.29d}$$

for $1 \leq i, j \leq N_1 N_2$. The integration in (6.29d) can be evaluated by integrating first with respect to ω_1 and then with respect to ω_2.

Since that $\mathbf{U}^T\mathbf{U} + \alpha\mathbf{U}_s^T\mathbf{U}_s$ is positive, E' has a global minimum point given by

$$\mathbf{g} = (\mathbf{U} + \alpha\mathbf{U}_s)^{-1} \cdot (\mathbf{B}^T\mathbf{h}) \tag{6.30}$$

Having obtained $\mathbf{g}$, a linear formula can be used to update $\mathbf{h}$ as

$$\mathbf{h} := (1 - \tau)\mathbf{h} + \tau\mathbf{g} \tag{6.31}$$

and the above process is repeated until $\| \mathbf{h} - \mathbf{g} \|$ is less than a prescribed tolerance.

The design procedure can now be summarized in terms of the following algorithm:

Algorithm 6.3

Step 1 Use a conventional method (e.g., SVD method) to design a 2-D, $(2N_1 - 1) \times (2N_2 - 1)$ diamond-shaped FIR filter and use its impulse response to form the initial $\mathbf{h}$.

Step 2 Calculate $\mathbf{B}$, $\mathbf{U}_s$ using (6.29a) and (6.29d), respectively.

Step 3 Use (6.29b) to form $\mathbf{U}$, and compute $\mathbf{g}$ in (6.30).

Step 4 If $\| \mathbf{h} - \mathbf{g} \| < \epsilon$, where ϵ is a prescribed tolerance, output $\mathbf{g}$ as the design result and stop. Otherwise, update $\mathbf{h}$ using (6.31) and repeat from Step 3.

Note that matrices $\mathbf{B}$ and $\mathbf{U}_s$ in Step 2 of Algorithm 6.3 can be pre-calculated as soon as N_1, N_2, and ω_s are determined; this would make the design algorithm computationally more efficient. In addition, the integrations involved in determining the entries of $\mathbf{U}$ can also be pre-calculated and stored in a table, which can be loaded for use when the iteration starts. Note that $\mathbf{B}, \mathbf{U}_s$ and $\mathbf{U}$ are all symmetric matrices

and, therefore, only about half of their entries need to be computed.

Three design examples are presented to illustrate the proposed algorithm, which were obtained using MATLAB on Sun SPARC stations. The design specifications were $N_1 = N_2 = 4$, $\alpha = 0.005$, $\tau = 0.5$, $\omega_s = 2$, $\epsilon = 10^{-3}$ for Example 6.10; $N_1 = N_2 = 4$, $\alpha = 0.5$, $\tau = 0.5$, $\omega_s = 2$, $\epsilon = 10^{-3}$ for Example 6.11 and $N_1 = N_2 = 5$, $\alpha = 0.05$, $\tau = 0.5$, $\omega_s = 1.5$, $\epsilon = 10^{-3}$ for Example 6.12. The perfect reconstruction performance of the filter banks obtained was evaluated in terms of PRE defined in Sec. 6.3.2. Stopband attenuation of the individual filter was evaluated in terms of the minima of stopband attenuation defined as

$$\text{MSA} = \min_{\omega_1,\omega_2 \in \Omega_s} [-20 \log_{10} |H_0(\omega_1, \omega_2)|]$$

The results and NI used for each design are listed in Table 6.7. The 3-D plot of the amplitude responses of the obtained analysis lowpass and highpass filters of Example 6.10 are shown in Fig. 6.13 (a) and (b), respectively. Fig. 6.14 (a) and (b) shows those for Example 6.12. From the results of Examples 6.10 and 6.11, we observe that as α is increased from 0.005 to 0.5, the MSA is increased from 27.79 to 34.36 dB but the PRE is also increased from 1.26×10^{-2} to 3.05×10^{-2}. In effect, the weight α provides effective control of the tradeoff between the quality of the reconstruction and the quality of the individual filters whereby low values of α lead to reduced PRE and large values lead to increased MSA in the individual filters.

6.4 Conclusion

In this chapter, we have proposed two methods for the design of 2-D nonseparable hexagonal QMF Banks. The new approaches are computational efficient and superior to the existing method in [43]. Moreover, we have proposed an iterative

Table 6.7: Results for Examples 6.10, 6.11 and 6.12.

	Example 6.10	Example 6.11	Example 6.12
NI	4	5	6
PRE (dB)	1.26×10^{-2}	3.05×10^{-2}	3.25×10^{-2}
MSA (dB)	27.79	34.36	38.90

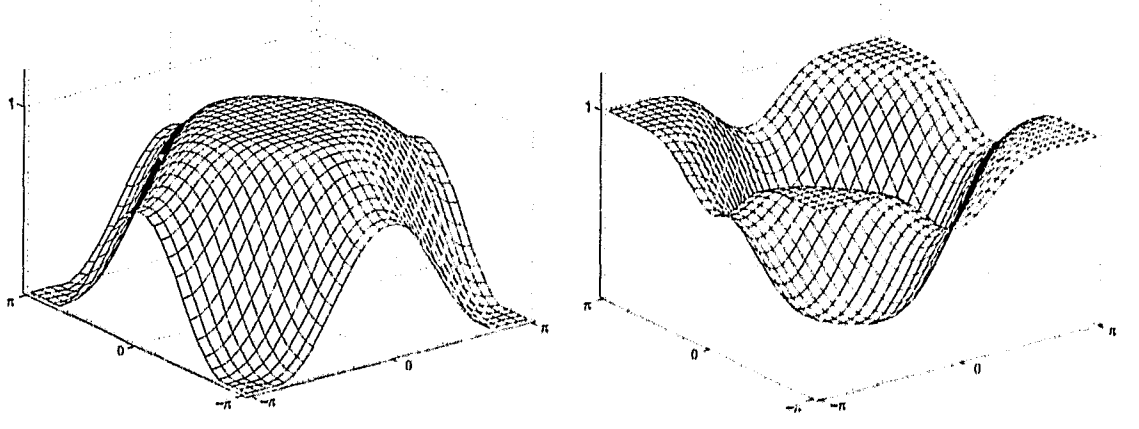

(a) (b)

Figure 6.13: Example 6.10 (a) Amplitude response of H_0. (b) Amplitude response of H_1.

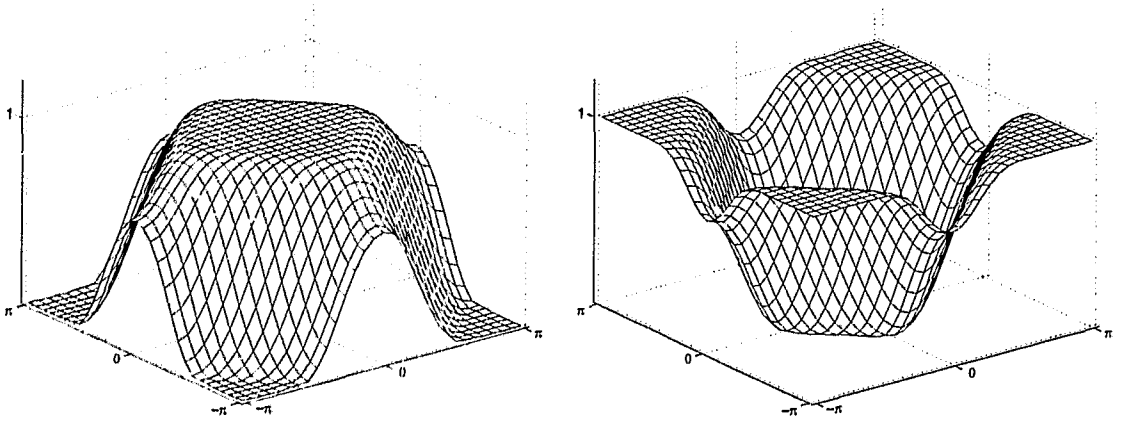

(a) (b)

Figure 6.14: Example 6.12 (a) Amplitude response of H_0. (b) Amplitude response of H_1.

method for the design of 2-D nonseparable diamond-shaped QMF banks in which no transformation from 1-D to 2-D is required and the design efficiency is achieved by using a linearization technique in the optimization. The availability of parameter α renders the approach more flexible and enables the designer to choose between low PRE in the filter bank and high MSA in the individual filters.

Chapter 7

Filter Banks for the MPEG Audio Codec

7.1 Introduction

Digital coding of high quality audio signals is becoming an important issue in the field of acoustics and signal processing. Here the term "high quality audio" is referred to signals with fidelity similar to that generated by compact discs (CDs). Since 1986, applications which require high quality audio at low bit-rates have emerged in:

- Professional studio sound recording, playback, editing, and postprocessing.
- Digital compact cassette (DCC), which can record a stereophonic sound on a mini cassette in digital sound compressed mode.
- Primary distribution links from studio to transmitter stations.
- Radio sound programme emission. Digital audio broadcasting (DAB) based on coded orthogonal frequency division multiplexing (COFDM).

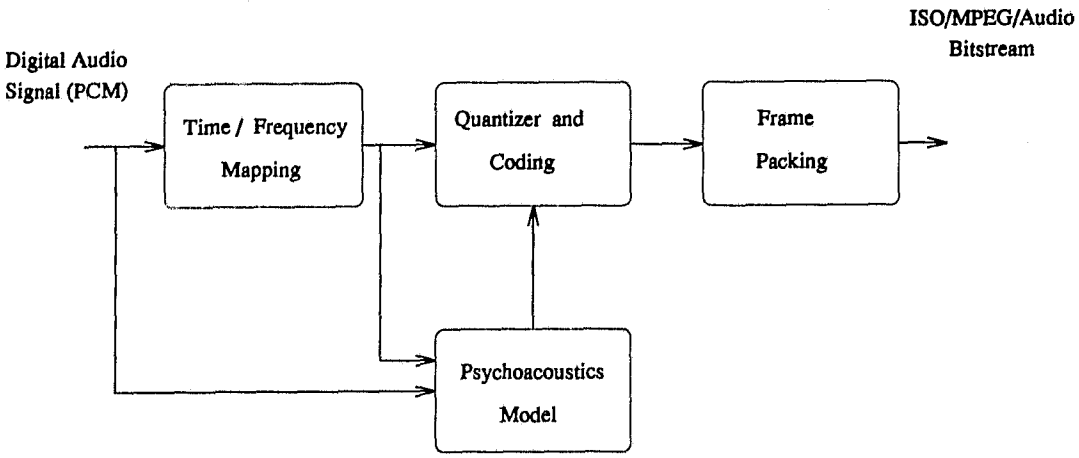

Figure 7.1: Sketch of the basic structure of the ISO/MPEG/AUDIO encoder.

- Stereophonic transmission via narrowband ISDN for reporting links and video-conferencing.

- Multimedia and hypermedia applications.

The international interest in audio coding algorithms is centered around the recently completed MPEG audio standardization under International Standard Organization (ISO) [27]. The ISO/MPEG audio coding standard consists of three layers (codecs) of increasing complexity and improving subjective performance. It supports coding of PCM audio signals with sampling rates of 32, 44.1, and 48 kHz at bit rates in a range of 32 and 192 kbit/s per mono or 64 to 384 kbit/s per stereo audio channel. As shown in Fig. 7.1, the MPEG audio coding system does the following:

- A time/frequency mapping (i.e., a filter bank) is used to decompose the input signal into subsampled spectral components.

- The output of this filter bank is used to obtain an estimate of actual masking threshold using rules known from psychoacoustics.
- The subband samples are quantized and coded to ensure that the noise introduced by quantization is lower than the masking threshold.
- A frame packing is used to assemble the bit stream.

See [60] and [61] for more technical details on MPEG.

In layer I and II of the MPEG, a 32 band equal-spaced cosine-modulated FIR filter bank with 512 taps is employed. This filter bank exhibits satisfactory frequency response with at least 96 dB stopband attenuation and allows an efficient polyphase implementation. In this chapter, we first use the iterative method developed in Chapter 5 to design a cosine-modulated filter bank for MPEG audio coding and then compare it with the filter bank currently used in MPEG. To reduce the reconstruction delay caused by the MPEG audio coding process, we use the method proposed in Chapter 5 to design a low-delay cosine-modulated filter bank with a 50% reduction of the reconstruction delay needed by the current MPEG filter bank. A polyphase implementation of this low-delay 32-band filter bank will also be derived.

7.2 Design of the MPEG Filter Bank

Although the prototype filter in the current MPEG filter bank is of 512 tap, the impulse response of the filter is of odd symmetrical. Therefore, the actual filter length should be 513 with the last coefficient dropped for the sake of implementation convenience. The design in this case is specified by the following parameters:

$$M = 32,\ N = 513,\ \alpha = 100,\ \omega_s = 0.0315\pi,\ \tau = 0.5,\ \epsilon = 10^{-4}$$

Table 7.1: SNR of the current MPEG filter bank and the filter bank designed.

	MPEG filter bank	filter bank designed
SNR_r (dB)	84.97	97.37

The Algorithm 5.1 converges after 11 iterations. Table 7.1 lists the SNR of the current MPEG filter bank and the filter bank designed. The amplitude responses of the analysis filters of the current MPEG filter bank and the filter bank designed are depicted in Fig 7.2 (a) and (b), respectively. Fig 7.3 (a) and (b) shows the amplitude responses of the first three analysis filters in both cases. From Table 7.1 it is observed that the filter bank designed achieves a SNR of 97 dB while the current MPEG filter bank could only achieve a SNR of 84 dB. In addition, Fig. 7.3 shows the filters designed have improved stopband attenuation over those in the current MPEG filter bank. Therefore, the filter bank designed is superior to the current MPEG filter bank.

7.3 Low-Delay Filter Bank for MPEG Audio Codec

7.3.1 Low-Delay Filter Bank

For some applications, low reconstruction delays are desired for the MPEG audio coding and decoding process. Obviously, the reconstruction delay of the filter bank contributes to the total delay of a MPEG audio codec. In the current MPEG audio codec, the filter bank has a reconstruction delay of 512 T where T is the sampling period. From Chapter 5, we know that one can design a general M-channel cosine-modulated filter bank in which the impulse responses of the analysis filters H_k and

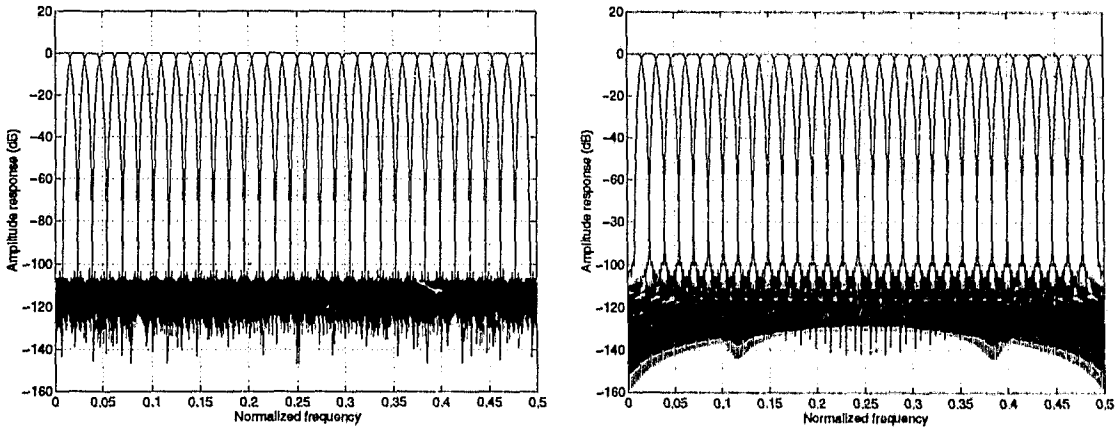

(a) (b)

Figure 7.2: Amplitude responses of the analysis filters in (a) the current MPEG filter bank, (b) the filter bank designed.

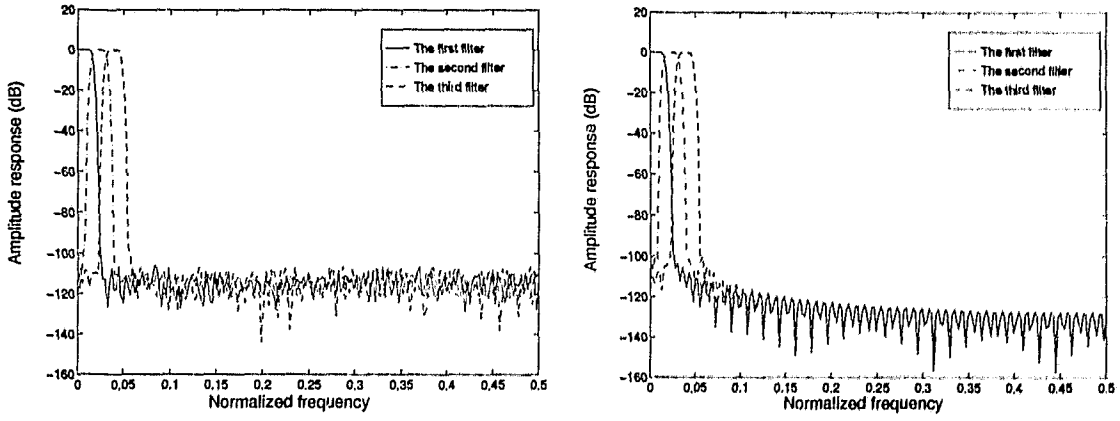

(a) (b)

Figure 7.3: Amplitude responses of the first three analysis filters in (a) the current MPEG filter bank, (b) the filter bank designed.

the synthesis filters F_k are given by

$$h_k(n) = 2p_L(n)\cos\left[(2k+1)\frac{\pi}{2M}\left(n-\frac{k_d}{2}\right)-(2k+1)\frac{\pi}{4}\right] \tag{7.1a}$$

$$f_k(n) = 2p_L(n)\cos\left[(2k+1)\frac{\pi}{2M}\left(n-\frac{k_d}{2}\right)+(2k+1)\frac{\pi}{4}\right] \tag{7.1b}$$

for $0 \leq n \leq N-1$ and $0 \leq k \leq M-1$, where $p_L(n)$ is the *asymmetrical* impulse response of the prototype filter P_L. The reconstruction delay of this filter bank is k_d with $k_d \leq N-1$.

We applied Algorithm 5.2 in Chapter 5 to design a low-delay filter bank with $M = 32$, $N = 513$ and $k_d = 255$ for use in a MPEG audio codec. The performance of the filter bank obtained is evaluated in terms of the same parameters as in Sec. 5.4. For comparison, the performance of the current MPEG filter bank is also evaluated using the same criteria, and the results are listed in Table 7.2. The amplitude response of the analysis filters of the low-delay QMF bank are illustrated in Fig. 7.4. From the design specification it can be observed that the low-delay filter bank designed has a reconstruction delay about half of the current MPEG filter bank.

Table 7.2: Comparisons of the low-delay filter bank and current MPEG filter bank.

	k_d	E_r	E_a	SNR_r (dB)
Low-delay filter bank	255	7.1657×10^{-5}	4.6497×10^{-6}	88.14
MPEG filter bank	512	8.6296×10^{-5}	2.7128×10^{-6}	84.34

7.3.2 Polyphase Implementation

The current MPEG filter bank can be implemented by the efficient polyphase structure. In this section we show that a polyphase implementation also exists for the

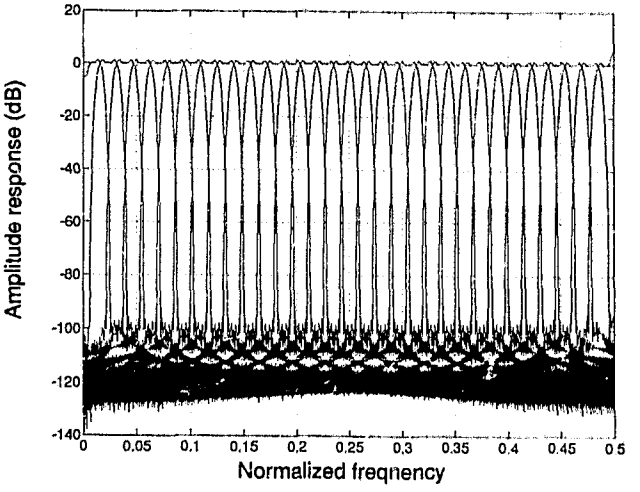

Figure 7.4: Amplitude responses of the analysis filters in the low-delay filter bank.

low-delay filter bank designed.

A. Analysis Subband Filtering

For implementation convenience, coefficient $p_L(512)$ is dropped as in the MPEG. At the l-th instant, the subsampled signal in the kth channel $x_k(l)$ is given by

$$x_k(l) = \sum_{n=0}^{N-1} h_k(n)x(lM - n)$$

for $k = 0, 1, \ldots, M-1$ with $N = 512$, $M = 32$, and $x(n)$ represents the input audio signal. Let $n = 2\gamma M + \rho$, for $\gamma = 0, 1, \ldots, 7$, $\rho = 0, 1, \ldots, 63$ and by substituting n in the above equation, we obtain

$$\begin{aligned} x_k(l) &= \sum_{\rho=0}^{63}\sum_{\gamma=0}^{7} h_k(2\gamma M + \rho)x(lM - 2\gamma M - \rho) \\ &= \sum_{\rho=0}^{63}\sum_{\gamma=0}^{7} 2\cos\left[(2k+1)\frac{\pi}{2M}\left(2\gamma M + \rho - \frac{k_d}{2}\right) - (2k+1)\frac{\pi}{4}\right] \\ &\quad \cdot p_L(2\gamma M + \rho)x(lM - 2\gamma M - \rho) \\ &= \sum_{\rho=0}^{63}\cos\left[(2k+1)\frac{\pi}{2M}(\rho - 16 - \frac{k_d}{2})\right]\sum_{\gamma=0}^{7} 2(-1)^{\gamma}p_L(64\gamma + \rho)x(32l - 64\gamma - \rho) \end{aligned} \tag{7.2}$$

where $k = 0, \ldots, 31$. It follows that the analysis subband filtering can be performed by the following steps:

- Input 32 audio samples.
- Construct an input sample vector $\mathbf{x}$ of 512 entries. Shift in 32 samples of the audio signals at positions 0 to 31 with the most recent one at position 0 and shift out the 32 oldest signal samples.
- Compute $\mathbf{z}_i = 2 \cdot (-1)^{int[i/64]} \mathbf{x}_i \cdot p_L(i)$, for $i = 0, 1, \ldots, 511$.
- Compute $\mathbf{y}_i = \sum_{j=0}^{7} \mathbf{z}_{i+64j}$, for $i = 0, 1, \ldots, 63$.
- Compute $\mathbf{s}_i = \sum_{k=0}^{63} \mathbf{M}_{ik} \cdot \mathbf{y}_k$, for $i = 0, \ldots, 31$, where

$$\mathbf{M}_{ik} = \cos\left[(2i+1)(k - 16 - k_d/2)\pi/64\right] \tag{7.3}$$

  for $i = 0$ to 31 and $k = 0$ to 63.
- Output $\mathbf{s}_i$ for $i = 0, \ldots, 31$ as the subband samples.

B. Synthesis Subband Filtering

The upsampled signal $\tilde{x}_k(n)$ and the subsampled signal $x_k(n)$ in the kth channel is related by

$$\tilde{x}_k(n) = \begin{cases} x_k(n) & n = lM, \quad \text{for integer } l \\ 0 & \text{otherwise} \end{cases}$$

for $k = 0, 1, \ldots, M-1$. Hence the reconstructed signal can be expressed as

$$\begin{aligned} \hat{x}(n) &= \sum_{k=0}^{M-1} \tilde{x}_k(n) * f_k(n) \\ &= \sum_{k=0}^{M-1} \sum_{i=0}^{N-1} f_k(i) \tilde{x}_k(n-i) \end{aligned}$$

If we let $y(n,i) = \sum_{k=0}^{M-1} f_k(i)\tilde{x}_k(n-i)$, then

$$\hat{x}(n) = \sum_{i=0}^{N-1} y(n,i)$$

By assuming

$$\mathbf{Q} = \begin{bmatrix} f_0(0) & f_0(1) & \cdots & f_0(N-2) & f_0(N-1) \\ f_1(0) & f_1(1) & \cdots & f_1(N-2) & f_1(N-1) \\ \vdots & & & & \vdots \\ f_{M-1}(0) & f_{M-1}(1) & \cdots & f_{M-1}(N-2) & f_{M-1}(N-1) \end{bmatrix}$$
$$= [\, p_L(0)\mathbf{q}_0 \;\; p_L(1)\mathbf{q}_1 \;\; \cdots \;\; p_L(N-1)\mathbf{q}_{N-1} \,]$$

where $\mathbf{q}_i$ for $i = 0, 1, \ldots, N-1$ are column vectors and

$$q_i(k) = \cos\left[(2k+1)\frac{\pi}{2M}\left(i - \frac{k_d}{2}\right) + (2k+1)\frac{\pi}{4}\right] = \cos\left[\left(16 + i - \frac{k_d}{2}\right)(2k+1)\frac{\pi}{64}\right]$$

for $k = 0, \ldots, M-1$, we obtain $y(n,i) = < p_L(i)\mathbf{q}_i, \mathbf{w}_{n-i} >$ where $\mathbf{w}_n = [\, \tilde{x}_0(n)\; \tilde{x}_1(n) \cdots \tilde{x}_{M-1}(n) \,]^T$ and $<\ ,\ >$ denotes the inner product. Hence $\hat{x}(n)$ can be expressed as

$$\hat{x}(n) = \sum_{i=0}^{N-1} < p_L(i)\mathbf{q}_i, \mathbf{w}_{n-i} > \tag{7.4}$$

Now consider a reconstructed signal vector $\hat{\mathbf{x}}_{lM}$ formed by the reconstructed signals at the lM-th, $(lM+1)$-th, ..., $(lM+31)$-th instants, by (7.4) and noting that only $\mathbf{w}_{lM} \neq 0$ for integer l, we can write

$$\hat{\mathbf{x}}_{lM} = \begin{bmatrix} \hat{x}(lM) \\ \hat{x}(lM+1) \\ \vdots \\ \hat{x}(lM+31) \end{bmatrix} = \begin{bmatrix} \sum_{i=l}^{l-15} < p_L((l-i)M)\mathbf{q}_{(l-i)M}, \mathbf{w}_{iM} > \\ \sum_{i=l}^{l-15} < p_L((l-i)M+1)\mathbf{q}_{(l-i)M+1}, \mathbf{w}_{iM} > \\ \vdots \\ \sum_{i=l}^{l-15} < p_L((l-i)M+31)\mathbf{q}_{(l-i)M+31}, \mathbf{w}_{iM} > \end{bmatrix}$$
$$= \mathbf{A}\mathbf{D}_{lM} \tag{7.5}$$

where $\mathbf{A} = [\ \mathbf{A}_0\ \mathbf{A}_1\ \ldots\ \mathbf{A}_{15}\ ]$ and $\mathbf{A}_i = \text{diag}[\ p_L(iM)\ \cdots\ p_L((i+1)M-1)\ ]$ for $i = 0,\ 1,\ \ldots,\ 15$, and

$$\mathbf{D}_{lM} = \begin{bmatrix} \mathbf{d}_1 \\ \mathbf{d}_2 \\ \mathbf{d}_3 \\ \vdots \\ \mathbf{d}_{15} \end{bmatrix} = \begin{bmatrix} [\mathbf{q}_0\ \mathbf{q}_1\ \cdots\ \mathbf{q}_{31}]^T \mathbf{w}_{lM} \\ [\mathbf{q}_{32}\ \mathbf{q}_{33}\ \cdots\ \mathbf{q}_{63}]^T \mathbf{w}_{(l-1)M} \\ [\mathbf{q}_{64}\ \mathbf{q}_{65}\ \cdots\ \mathbf{q}_{95}]^T \mathbf{w}_{(l-2)M} \\ \vdots \\ [\mathbf{q}_{480}\ \mathbf{q}_{481}\ \cdots\ \mathbf{q}_{511}]^T \mathbf{w}_{(l-15)M} \end{bmatrix}$$

Note that for an integer m

$$\begin{aligned} q_{64m+i}(k) &= \cos[(16 + 64m + i - k_d/2)(2k+1)\pi/64] \\ &= (-1)^m \cos[(16 + i - k_d/2)(2k+1)\pi/64] = (-1)^m q_i(k) \end{aligned}$$

for $i = 0, \ldots, 63$, then $\mathbf{q}_{64m+i} = (-1)^m \mathbf{q}_i$. Therefore, to form $\mathbf{D}_{lM}$, only $\mathbf{q}_0\ \mathbf{q}_1\ \cdots\ \mathbf{q}_{63}$ need to be calculated.

In summary, the synthesis subband filtering can be carried out by the following steps:

- Input 32 new subband samples $\mathbf{s}_i$, for $i = 0, \ldots, 31$ and initialize vector $\mathbf{v}$ of length 1024.
- Set $\mathbf{v}_i = \mathbf{v}_{i-64}$, for $i = 1023$ to 64.
- Compute $\mathbf{v}_i = \sum_{k=0}^{31} \mathbf{N}_{ik} \cdot \mathbf{s}_k$, for $i = 0, \ldots, 63$, where

$$\mathbf{N}_{ik} = \cos\left[(16 + i - k_d/2)(2k+1)\pi/64\right] \tag{7.6}$$

  for $0 \le i \le 63,\ 0 \le k \le 31$.

- Construct vector $\mathbf{u}$ as follows

  for $i = 0$ to 7,

for $j = 0$ to 31,

$\{ \quad \mathbf{u}_{64i+j} = \mathbf{v}_{128i+j}$

$\mathbf{u}_{64i+j+32} = \mathbf{v}_{128i+96+j} \quad \}$

- Compute $\mathbf{w}_i = 2 \cdot (-1)^{int[i/64]} \mathbf{u}_i \cdot p_L(i)$, for $i = 0, \ldots, 511$.
- Compute 32 samples $\hat{\mathbf{x}}_j = 32 \sum_{i=0}^{15} \mathbf{w}_{j+32i}$, for $j = 0, \ldots, 31$, and output $\hat{\mathbf{x}}_j$ as the reconstructed PCM samples.

7.3.3 Comparisons

The polyphase implementation described in Sec. 7.3.2 is a modified version of that in the MPEG standard [27] in that the prototype filter with symmetrical impulse response in [27] is replaced by a filter with asymmetrical impulse response, and entries $\mathbf{M}_{ik}$ and $\mathbf{N}_{ik}$ are now calculated using (7.3) and (7.6), respectively.

To show the efficiency of the polyphase implementation, the numbers of multiplications (multi) and additions (add) per input and per output for the polyphase implementation, and those for a direct implementation [29] where each channel is implemented individually in a polyphase form, are listed in Table 7.3. It is observed that the operations required in a polyphase implementation are much less than those in the direct implementation.

To verify the polyphase implementation, we used two sound signals "Hallelujah" and "Chinese Gong" supplied by MATLAB as test signals. For comparison the current MPEG filter bank was also implemented by the polyphase structure as described in [27]. Fig. 7.5 (a), (b) and (c) shows the original, the MPEG filter bank reconstructed, and the low-delay filter bank reconstructed, "Hallelujah", respectively. Fig. 7.6 (a), (b) and (c) shows the original, the MPEG filter bank reconstructed,

Table 7.3: Operations in polyphase and direct implementations

	per input		per output	
	multi.	add.	multi.	add.
Polyphase	80	77	80	77
Direct	512	511	512	511

and the low-delay filter bank reconstructed, "Chinese Gong", respectively. It can be observed that in agreement with the design specification the low-delay QMF bank has reduced the reconstruction delay to about half of that produced by the current MPEG QMF bank.

7.4 Conclusion

In this chapter, we have designed a conventional cosine-modulated QMF filter bank for MPEG audio codec by using the iterative method proposed in Chapter 5. It is observed that the overall performance of the filter bank designed is superior to the current MPEG filter bank. To reduce the reconstruction delay of the MPEG audio codec, a low-delay filter bank has been designed by using the method described in Chapter 5. Moreover, an efficient polyphase implementation of this low-delay filter bank has been derived.

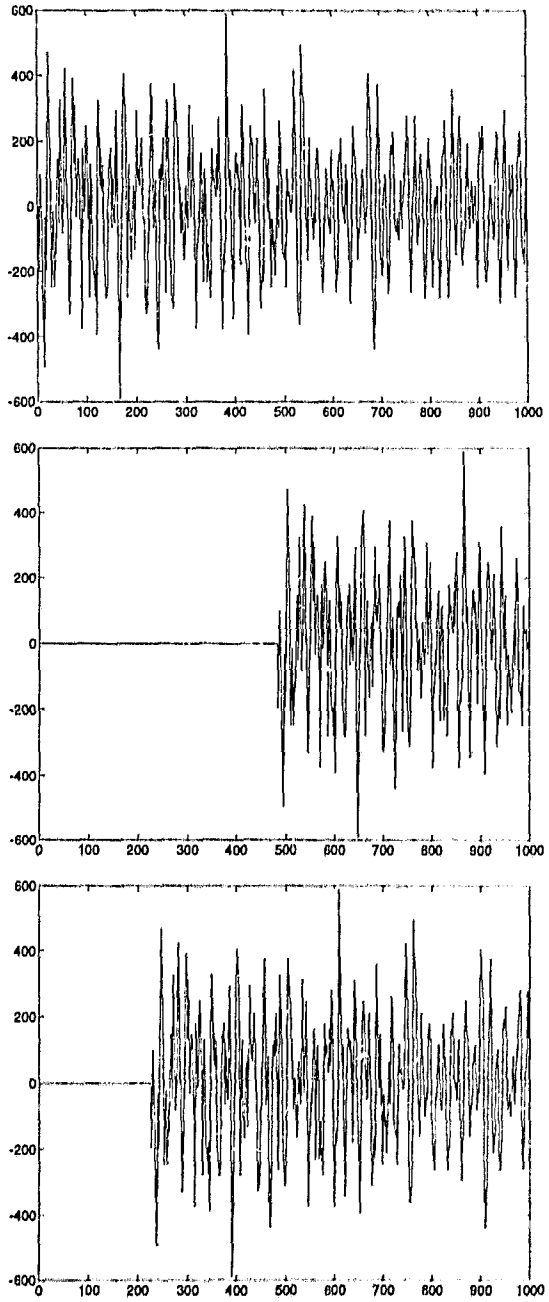

Figure 7.5: From top to bottom: Original "Hallelujah", reconstructed from MPEG filter bank, reconstructed from the low-delay filter bank.

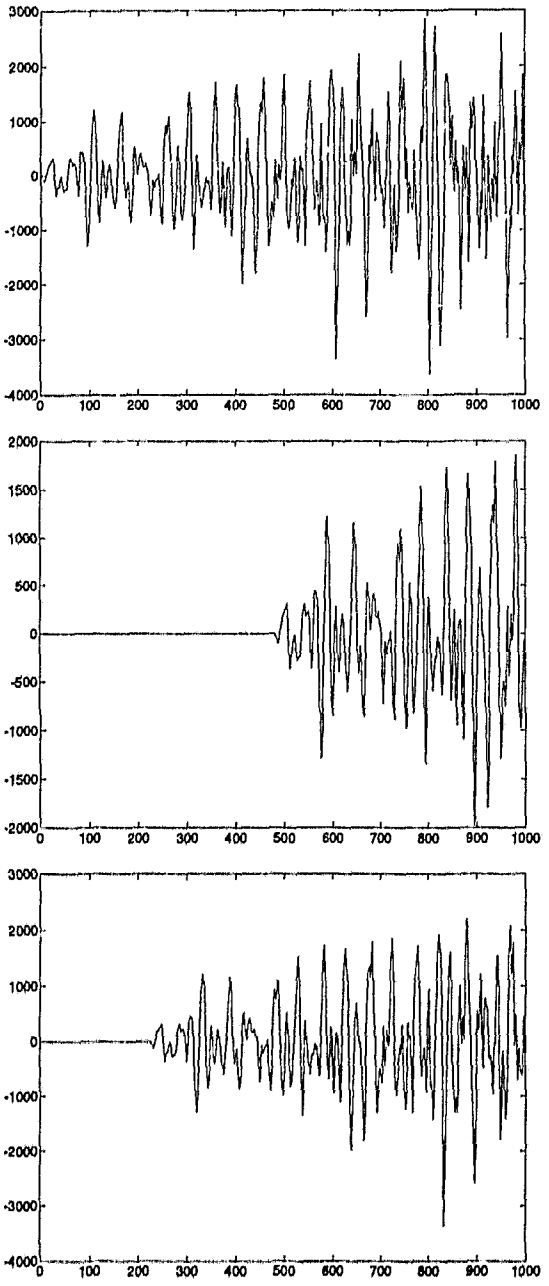

Figure 7.6: From top to bottom: Original "Chinese Gong", reconstructed from MPEG filter bank, reconstructed from the low-delay filter bank.

Chapter 8

Subband Coding of Images

8.1 Introduction

The concept of subband coding and its application to image signals goes back to as early as 1959 [62]. The practical implication of this concept was not recognized until the introduction of the quadrature mirror filtering (QMF) technique which was proposed by Esteban and Galand [8] for subband coding of speech signals. More recently, the concept of QMF has been extended to the 2-D case [38] and its application to image coding has emerged [39] [63].

The idea of subband coding of images is based on the observation that for a typical natural scene, the signal energy is non-uniformly distributed in the frequency domain and the signal components from the different regions of the spectrum have different tolerance to quantization errors from a perceptual point of view. One can thus take advantage of it by partitioning the signal into subband components and suitably allocating bits according to their perceptual significance. As illustrated in Fig. 8.1, an input image is decomposed into several subimages using a bank of filters called the analysis filter bank. The lowest frequency component is a lower resolution version of the original scene, and the high frequency bands carry the

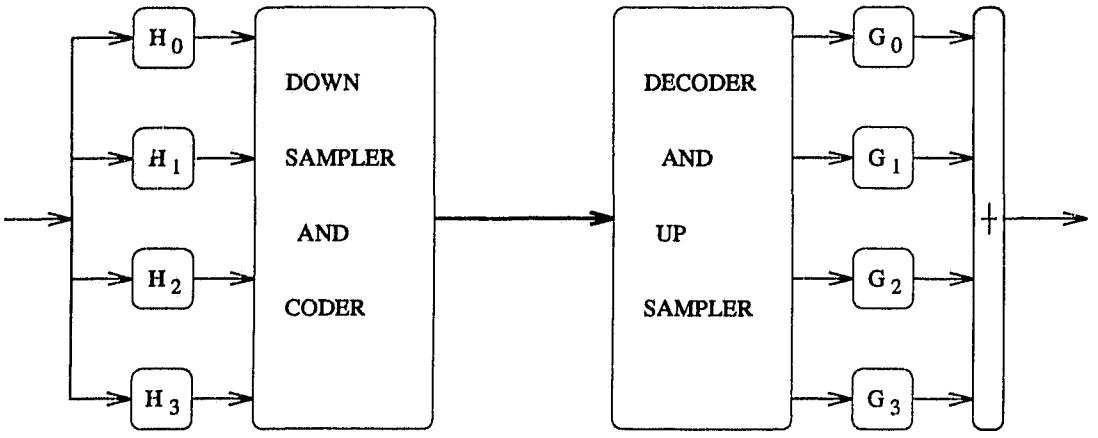

Figure 8.1: Subband coding procedure.

information about the contours, edges and other finer details of the image. These filtered signals are then downsampled to yield the subband signals, which are coded using procedures appropriate to the information content. With a prescribed bit rate, one has to apportion the bits among the different subband signals. A judicious allocation of a given budget of bits/pixel can be made by choosing the quantizer to produce an overall good reconstruction. With roughly equal bandwidth for the different analysis filters, the lowest frequency subband signal usually ends up with the largest slice of the budgeted bits. At the receiver the bit stream of encoded signals are decoded, upsampled and merged by the synthesis filter bank to yield a close approximation to the input scene.

In this regard the wavelet transform has emerged as a powerful tool for non-stationary signal analysis. Mallat [64][65] developed a framework which unified the wavelet theory and subband decomposition based multiresolution signal representation methods. By using Mallat's framework, a two-dimensional (2-D) wavelet transform can be performed separably by applying 1-D wavelet transforms to rows

and columns of a image to successively decompose it into uncorrelated subimages.

In this chapter we first construct a nonseparable quincunx subband coding scheme for image compression. Then we use a 2-D separable wavelet transform with Daubechies wavelet coefficients to decompose images into subbands and encode the subband signals accordingly. Comparisons will be made with the current JPEG encoder.

8.2 Quincunx Subband Coding of Images

As shown in Fig. 8.2 (a), a quincunx subband image coding scheme consists of two stages. The first stage is a diamond-shaped prefilter, followed by a 2:1 line quincunx downsampling pattern. The second stage uses a nonseparable diamond-shaped filter bank to decompose the signal into two bands, and a quincunx downsampling in each band. The downsampled signals are then encoded by different coders. Fig. 8.2 (b) illustrates the subband partition in a quincunx subband coding scheme. After the first stage, the frequency bands marked by "H" are deleted, while the diamond-shaped frequency band is preserved. In the second stage, the diamond-shaped frequency band is further decomposed into two frequency bands denoted by "LL" and "LH" and downsampled. The "LL" band signal is then encoded by a JPEG encoder and the "LH" band signal is encoded by a Huffman encoder after being quantized by a dead-band uniform quantizer. The decoding process is the dual process of the encoding process, in which the bit stream is first decoded and then quincunx upsampled before going through two synthesis diamond-shaped filters. The filtered signals are summed up and quincunx upsampled again before going through a diamond-shaped post-filter to form the reconstructed image.

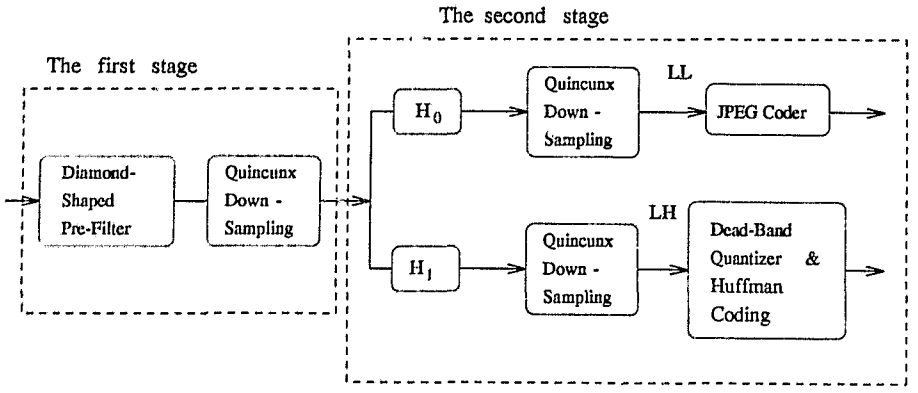

(a)

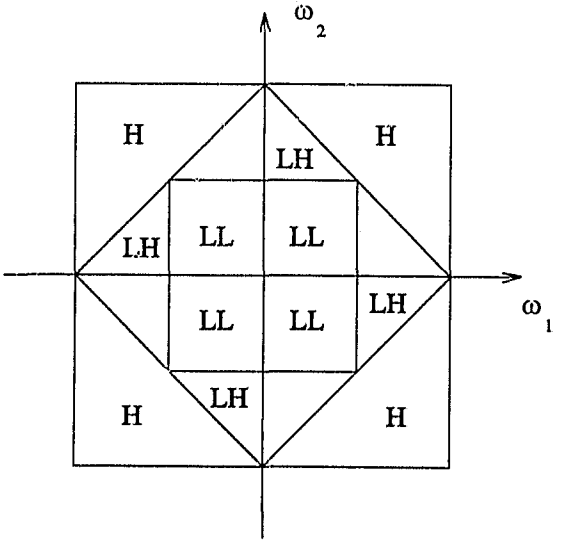

(b)

Figure 8.2: (a) Diagram of a quincunx subband coding scheme. (b) Subband partition.

8.2.1 First Stage

The ideal frequency response of a diamond-shaped prefilter is shown in Fig. 8.3 (a). The reason why a diamond-shaped prefilter is used here is that the frequency content of an image in most cases is largely confined to a diamond-shaped frequency band. Therefore, by preserving the information in this frequency band while deleting the content in the corner high frequency bands will not cause much distortion in the reconstructed image. The prefiltering is followed by a non-rectangular sampling, which is often referred to as a line quincunx sampling pattern shown in Fig. 8.3 (b), to reduce the signal amount to half of that in the original image.

8.2.2 Second Stage

In the second stage, the prefiltered and downsampled signal is further decomposed by a nonseparable diamond-shaped filter bank consisting of filters H_0 and H_1. The frequency responses of these filters are illustrated in Fig. 8.4. They are designed by using the methods described in Chapter 6. After the filtering, signals are quincunx downsampled again to obtain signals corresponding to the "LL" and "LH" bands shown in Fig. 8.2(b).

A. Encoding of the LL Band Signal

As will be seen from the examples described in Sec. 8.2.3, the "LL" band signal is a low resolution version of the original image and is encoded by a JPEG coder. A block diagram of the JPEG coder is shown in Fig. 8.5.

In a JPEG encoder, the inpu nage is first divided into small disjoint blocks of

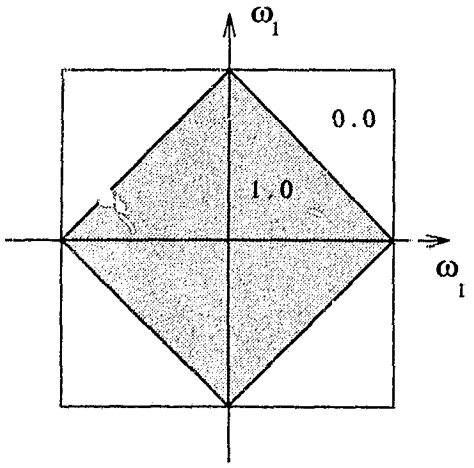

(a)

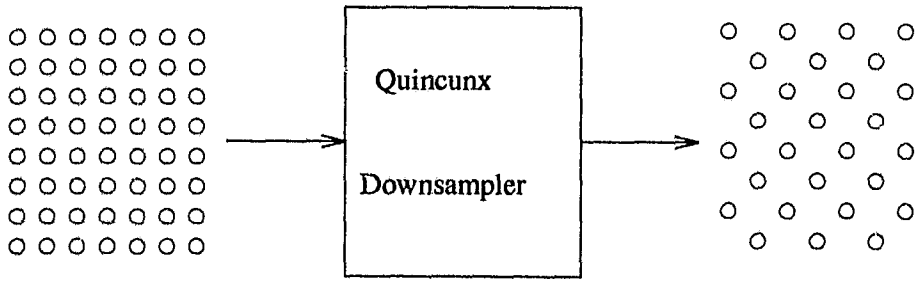

(b)

Figure 8.3: (a) Diamond-shaped prefilter frequency response. (b) Quincunx sampling grid.

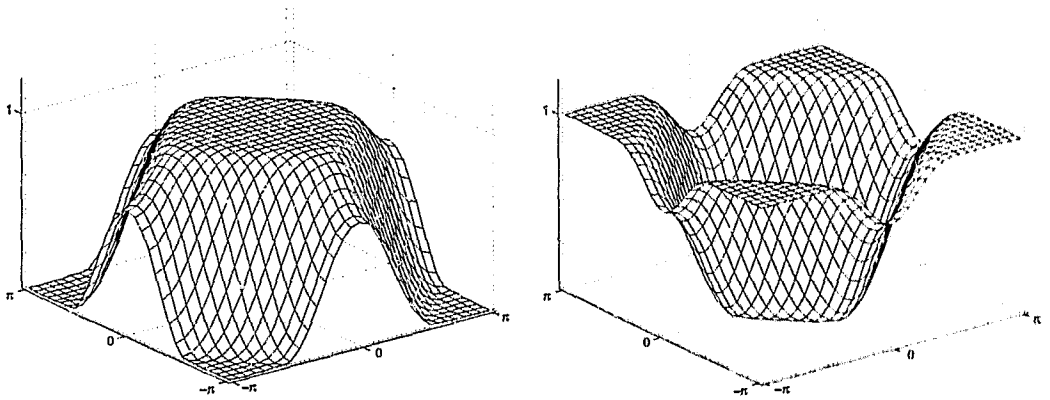

Figure 8.4: (a) Amplitude response of filter H_0. (b) Amplitude response of filter H_1.

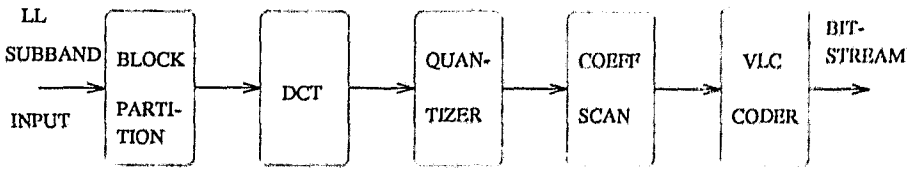

Figure 8.5: JPEG encoder diagram.

size $N_1 \times N_2$, say $N_1 = N_2 = 8$. Then DCT is applied to each block to obtain

$$X(k_1, k_2) = \frac{4}{N_1 N_2} c(k_1) c(k_2) \sum_{n_1=0}^{N_1-1} \sum_{n_2=0}^{N_2=1} x(n_1, n_2) \cos \frac{(2n_1+1)k_1\pi}{2N_1} \cos \frac{(2n_2+1)k_2\pi}{2N_2} \tag{8.1}$$

for $k_1 = 0, 1, \ldots, N_i - 1$, $i = 1, 2$, where $x(n_1, n_2)$ is the image pixel and $X(k_1, k_2)$ is the DCT coefficient. The function c(·) in (8.1) is given by

$$c(k) = \begin{cases} \frac{1}{\sqrt{2}} & \text{for } k = 0 \\ 1 & \text{otherwise} \end{cases} \tag{8.2}$$

The DCT coefficients $X(k_1, k_2)$ obtained are then quantized and re-arranged to form a 1-D sequence by a zigzag scanning. Finally, the nonzero amplitudes and run-length of zeros are entropy coded.

B. Encoding of the LH Band Signal

The "LH" band signal contains more information about edges and contours and is not suitable for transform coding. Instead these signals are directly quantized in the spatial domain. Since most signal values in this band are close to zero, the quantizer used is a dead-band uniform quantizer shown in Fig. 8.6, which has a dead-zone centered at zero and uniformly spaced outer quantization intervals. After the quantization, the nonzero amplitudes and run-length of zeros are entropy coded by a Huffman encoder.

8.2.3 Examples

The programs that implement the encoder and decoder described above are written in C. The JPEG encoder for coding the "LL" band signals was obtained from a public ftp site. Several test images are encoded and decoded and hereby we describe two examples. The first image is "Lenna" and the second image is "plane", both of a

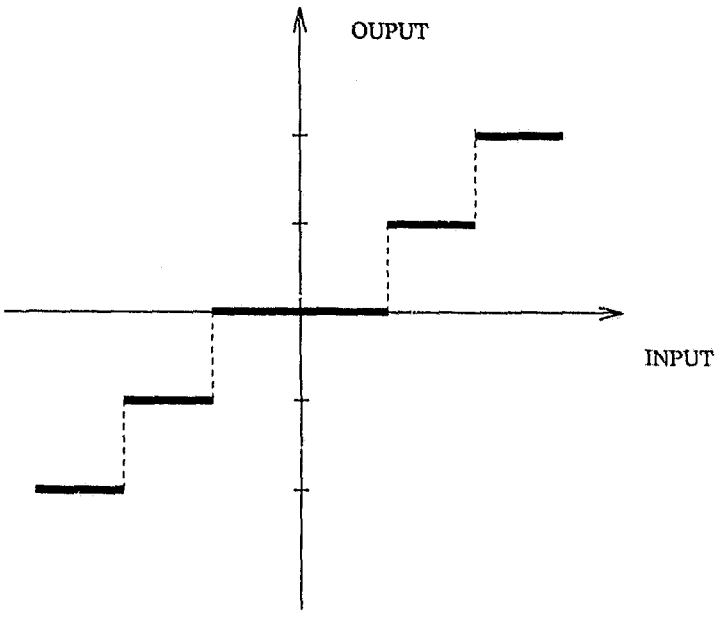

Figure 8.6: A dead-band uniform quantizer.

size of 256×256. Fig. 8.7 (a) and (b) show the subband images of "Lenna" after the prefiltering and quincunx downsampling, the image in (a) is further decomposed into (c) and (d), which correspond to the "LL" and "LH" band, respectively. Fig. 8.8 (a), (b), and (c) show the original "Lenna", the reconstructed "Lenna" from subband coding, and the difference image, respectively. Similar results for the "plane" are shown in Figs. 8.9 and 8.10, respectively.

The SNR is used to measure the difference between the original image and the reconstructed image. It is defined by

$$\text{SNR} = 10 \log_{10} \sum_{n_1=0}^{M_1-1} \sum_{n_2=0}^{M_2-1} \frac{x^2(n_1, n_2)}{[x(n_1, n_2) - \hat{x}(n_1, n_2)]^2} \tag{8.3}$$

where $x(n_1, n_2)$ is the pixel of the original image, $\hat{x}(n_1, n_2)$ is that of the reconstructed image, and M_1 and M_2 are the sizes of image. In our examples, $M_1 = M_2 = 256$. The SNR values for two examples are listed in Table 8.1. The bit allo-

Table 8.1: Bit allocation and SNR values for the examples.

image	bpp			SNR (dB)
	LL	LH	Total	
Lenna	3	0.2	0.8	21.10
plane	2	0.4	0.6	23.48

cation for each band of the signals as well as the total bit rate denoted by bits per pixel (bpp) are also listed in Table 8.1, where bpp is defined as

$$\text{bpp} = \frac{\text{total bits}}{\text{pixel number}}$$

8.3 Image Compression Using Discrete Wavelet Transform

8.3.1 Wavelet Transform

From the Fourier transform of a function $f(x)$, irregularities (high frequencies) of the signal can be observed. However, this information is not spatially localized. The reason is that the basis functions of the Fourier transform, i.e., the cosine and sine functions are supported by the entire spatial domain, leading to the difficulty of identifying the positions where the irregularities occur. In order to localize the information contained in the signal, the window Fourier transform which incorporates a spatial window $g(x)$ into the Fourier integral may be employed. This window is translated along the spatial axis to cover the entire spatial domain. At a position u and for a frequency ω, the window Fourier transform of a function $f(x) \in \mathbf{L}^2(\mathbf{R})$ is

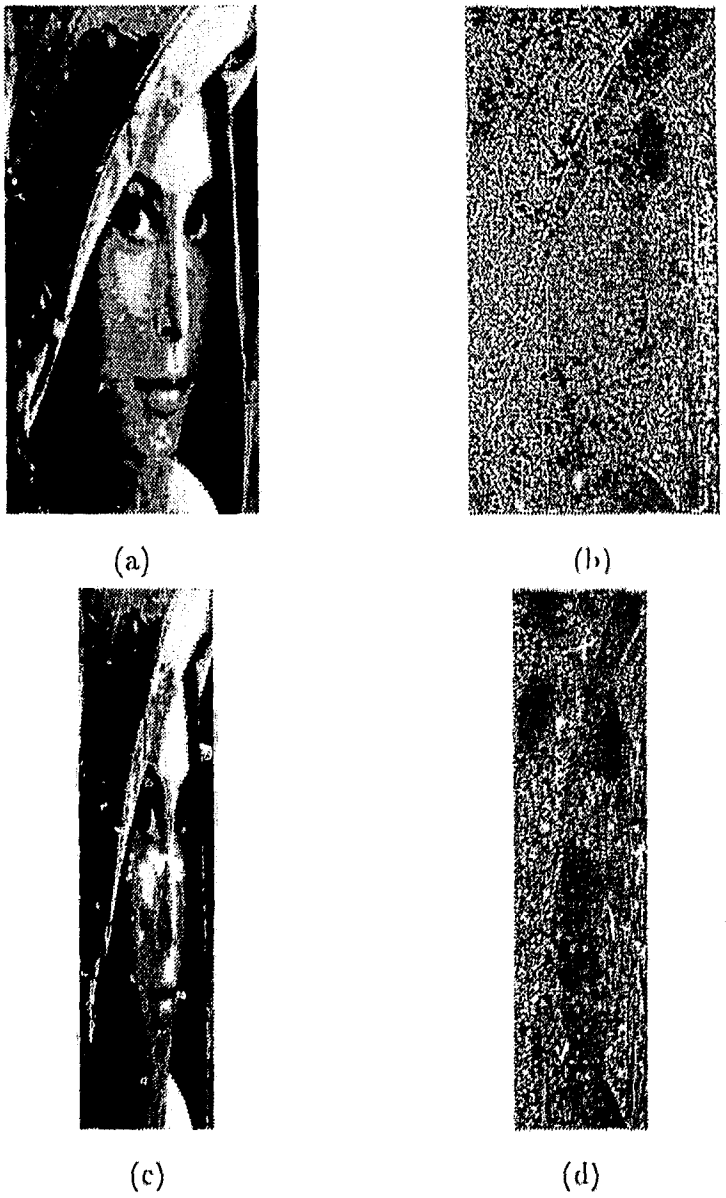

(a) (b)

(c) (d)

Figure 8.7: Decomposition stages for "Lenna": First-stage (a) Lowpass filtered image (L), (b) Highpass filtered image (H). Second-stage (c) Lowpass filtered image (LL), (d) Highpass filtered image (LH).

(a)

(b)

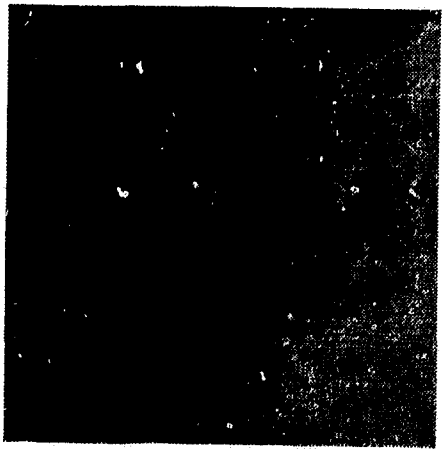

(c)

Figure 8.8: (a) Original "Lenna". (b) Reconstructed "Lenna". (c) Difference image.

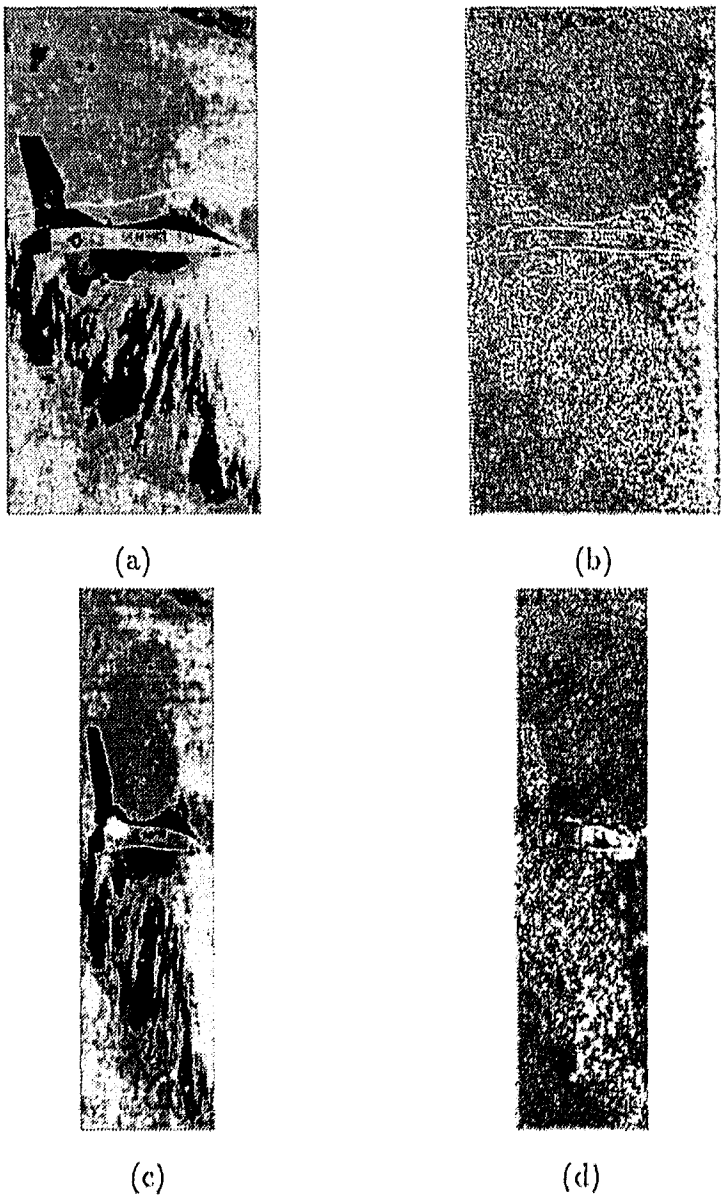

(a) (b)

(c) (d)

Figure 8.9: Decomposition stage for "plane". First-stage (a) Lowpass filtered image (L). (b) Highpass filtered image (H). Second-stage (c) Lowpass filtered image (LL). (d) Highpass filtered image (LH).

(a)

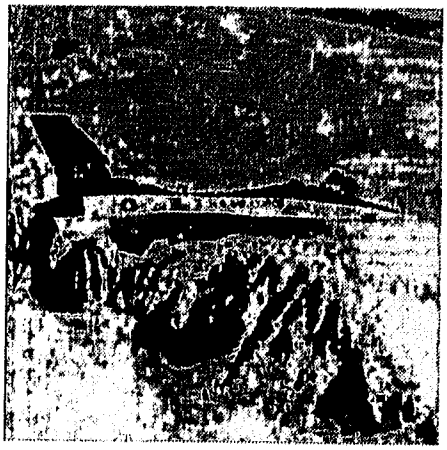

(b)

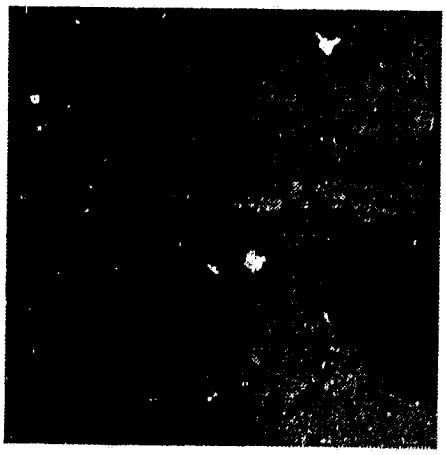

(c)

Figure 8.10: (a) Original "plane". (b) Reconstructed "plane". (c) Difference image.

defined by

$$Gf(\omega, u) = \int_{-\infty}^{+\infty} e^{-i\omega x} g(x-u) f(x)\, dx \tag{8.4}$$

It provides the local frequency behaviour of the signal around the point u.

It can be shown that the spatial and frequency resolutions of a window Fourier transform are constant, which for some applications is not adequate.

The wavelet transform decomposes the signal into a family of functions which are the translations and dilations of a unique function $\psi(x)$. The function is called a wavelet and the corresponding wavelet family is given by $\{\sqrt{s}\,\psi[s(x-u)]\}_{(s,u)\in R^2}$. Analytically, the continuous wavelet transform of a function $f(x) \in \mathbf{L}^2(\mathbf{R})$ is defined by

$$Wf(s, u) = \int_{-\infty}^{+\infty} f(x)\sqrt{s}\,\psi[s-(x-u)]\, dx \tag{8.5}$$

It has been shown that a wavelet transform has a constant resolution on a logarithm scale in both spatial and frequency domains. This is to say, if the scale s is small, the resolution is coarse in the spatial domain and fine in the frequency domain, and if the scale s increases, the resolution increases in the spatial domain and decreases in the frequency domain.

A very important class of discrete wavelet transforms was found by Meyer and Stormberg. They showed that there exist some wavelets $\psi(x) \in \mathbf{L}^2(\mathbf{R})$ such that $\{\psi_{2^j}[x-(n/2^j)]\}_{(n,j)\in Z^2}$ is an orthogonal basis of $\mathbf{L}^2(\mathbf{R})$. These particular wavelets are called *orthogonal wavelets*. In [64] Mallat developed an iterative algorithm for calculating the discrete wavelet transform of a signal. In this chapter we restrict ourselves to a class of discrete wavelet transform (DWT) developed by Daubechies [66]. This class includes members ranging from highly localized to highly smooth. The simplest (and most localized) member, often called *DAU4*, has only four coeffi-

cients, c_0, c_1, c_2, and c_3. A discrete wavelet transform using $DAU4$ can be expressed as

$$\mathbf{Y} = \mathbf{CX} \tag{8.6}$$

where

$$\mathbf{C} = \begin{bmatrix} c_0 & c_1 & c_2 & c_3 & & & & & & & & \\ c_3 & -c_2 & c_1 & -c_0 & & & & & & & & \\ & & c_0 & c_1 & c_2 & c_3 & & & & & & \\ & & c_3 & -c_2 & c_1 & -c_0 & & & & & & \\ \vdots & \vdots & & & & & \ddots & & & & & \\ & & & & & & & c_0 & c_1 & c_2 & c_3 & \\ & & & & & & & c_3 & -c_2 & c_1 & -c_0 & \\ c_2 & c_3 & & & & & & & & c_0 & c_1 & \\ c_1 & -c_0 & & & & & & & & c_3 & -c_2 & \end{bmatrix}$$

$\mathbf{X}$ is the input vector and $\mathbf{Y}$ is the wavelet output vector. From the structure of the matrix, the coefficients c_0, c_1, c_2, c_3 can be thought of as the coefficients of a smoothing (lowpass) filter H_0. The odd rows in the matrix are used to complete the lowpass filtering on the input signal, which results in low frequency component of the original signal. On the other hand, the coefficients $c_3, -c_2, c_1, -c_0$ can be thought of as the coefficients of a highpass filter H_1 and the even rows are used to complete the highpass filtering on the input signal, resulting in high frequency component of the original signal. From a multirate signal processing point of view, the filters H_0 and H_1 are equivalent to a QMF bank. High order DWT using 12 ($DAU12$) or 20 ($DAU20$) Daubechies wavelet coefficients have a similar format as in (8.6).

The DWT can be applied to a signal vector *hierarchically* as shown in Eqn.(8.7). Consider an input vector of length N with N being some power of 2. First the DWT

is applied to the entire vector. After downsampling the resulting vector yields a "smoothed" vector of length $N/2$. The DWT is applied then to this $N/2$-dimensional vector to obtain a further smoothed vector of $N/4$ after downsampling. This DWT-subsampling process continues as necessary. This process is the same as the tree-structure decomposition in the subband coding of a speech signal [8] as illustrated in Fig. 8.11.

$$\begin{bmatrix} x_1 \\ x_2 \\ x_3 \\ x_4 \\ x_5 \\ x_6 \\ x_7 \\ x_8 \\ x_9 \\ x_{10} \\ x_{11} \\ x_{12} \\ x_{13} \\ x_{14} \\ x_{15} \\ x_{16} \end{bmatrix} \quad (8.6) \quad \begin{bmatrix} s_1 \\ d_1 \\ s_2 \\ d_2 \\ s_3 \\ d_3 \\ s_4 \\ d_4 \\ s_5 \\ d_5 \\ s_6 \\ d_6 \\ s_7 \\ d_7 \\ s_8 \\ d_8 \end{bmatrix} \quad \text{permute} \quad \begin{bmatrix} s_1 \\ s_2 \\ s_3 \\ s_4 \\ s_5 \\ s_6 \\ s_7 \\ \underline{s_8} \\ d_1 \\ d_2 \\ d_3 \\ d_4 \\ d_5 \\ d_6 \\ d_7 \\ d_8 \end{bmatrix} \quad (8.6) \quad \begin{bmatrix} S_1 \\ D_1 \\ S_2 \\ D_2 \\ S_3 \\ D_3 \\ S_4 \\ \underline{D_4} \\ d_1 \\ d_2 \\ d_3 \\ d_4 \\ d_5 \\ d_6 \\ d_7 \\ d_8 \end{bmatrix} \quad \text{permute} \quad \begin{bmatrix} S_1 \\ S_2 \\ S_3 \\ \underline{S_4} \\ D_1 \\ D_2 \\ D_3 \\ \underline{D_4} \\ d_1 \\ d_2 \\ d_3 \\ d_4 \\ d_5 \\ d_6 \\ d_7 \\ d_8 \end{bmatrix} \quad \cdots \quad \begin{bmatrix} S_1 \\ \underline{S_2} \\ D_1 \\ \underline{D_2} \\ D_1 \\ D_2 \\ D_3 \\ \underline{D_4} \\ d_1 \\ d_2 \\ d_3 \\ d_4 \\ d_5 \\ d_6 \\ d_7 \\ d_8 \end{bmatrix} \quad (8.7)$$

8.3.2 Image Compression Using DWT

A 2-D wavelet transform can be performed separably by applying 1-D wavelet transforms to the row and column components of an image successively. In this case a 2-D wavelet decomposition structure is the same as the 2-D separable subband decomposition structure shown in Fig. 8.12 (a), except that the filter coefficients are the

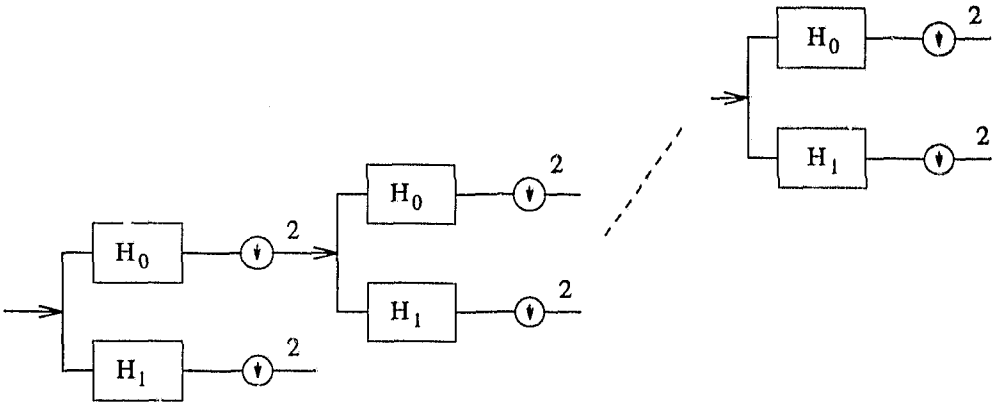

Figure 8.11: The tree-structure decomposition.

wavelet coefficients satisfying certain regularity or orthogonality conditions. This leads to the decomposition of an image into uncorrelated subimages. Fig. 8.12 (b) shows the spectrum partition by one stage separable subband decomposition. It consists of one low-frequency band "LL" and three high-frequency bands "LH", "HL" and "HH". This process can be repeated to further decompose the "LL" frequency band *hierarchically* like the tree-structure in the 1-D signal decomposition.

Fig. 8.13 shows a decomposed image "Lenna" of size 512×512 after two-stage wavelet decomposition. The low-frequency-band image is at the upper left corner and high frequency bands from different decomposition stages are shown in the rest part of the figure. It can be observed that the low-frequency bands image is the most important since it is in fact a low resolution version of the original image. On the other hand, subimages in the high-frequency bands contain only the edge and contour information of the original image. In order to achieve a high compression ratio while minimizing visible distortion in the reconstructed image, more bits should be allocated for encoding the low-frequency-band subimage. For the examples shown later, we apply a four-stage DWT decomposition using *DAU12*

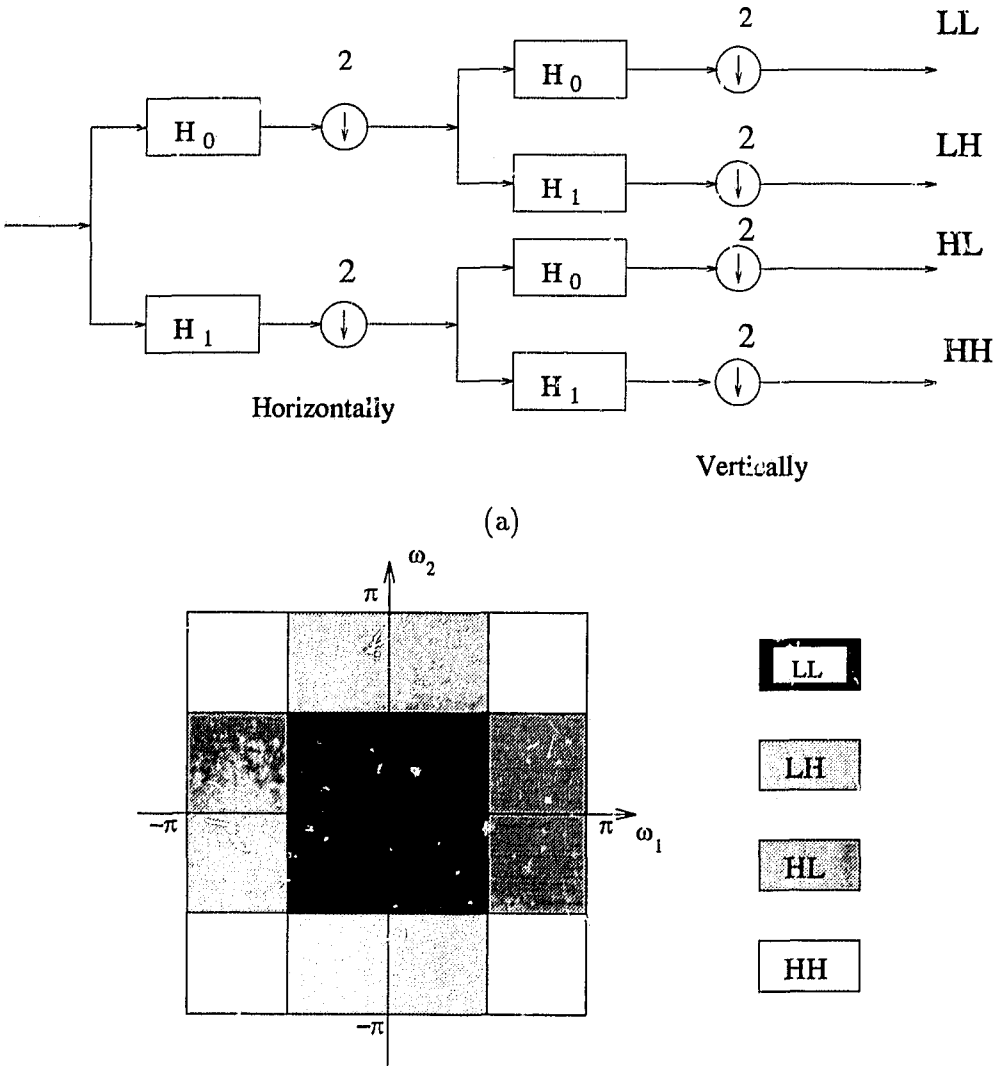

Figure 8.12: (a) One stage of 2-D separable subband decomposition. (b) Spectrum partition from one-stage subband decomposition.

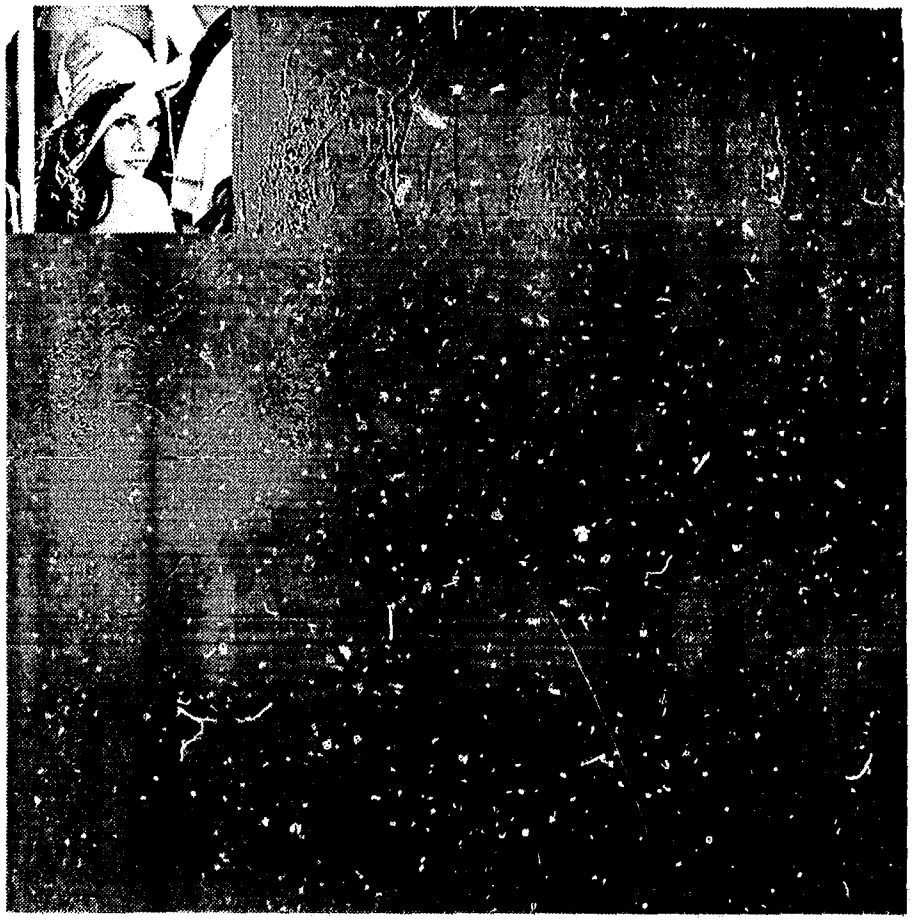

Figure 8.13: Two-stage decomposition of "Lenna" by DWT.

on the images and leave the low-frequency band subimage uncoded. For subimages in the high-frequency bands, a threshold is set and only those above the threshold are preserved.

The program that implements the encoder is written in C with some subroutines from [67]. The two images used here are: "Lenna" and "baboon". Both are 256×256 images with 8-bit grayscale. For comparison, the two images are encoded by a JPEG encoder as well. The bits per pixel (bpp) rates and SNR are given in

Table 8.2: Bit allocation and SNR for examples.

	DWT		JPEG	
	bpp	SNR (dB)	bpp	SNR (dB)
Lenna	0.44	25.06	0.44	25.72
baboon	0.29	16.65	0.28	15.30

Table 8.2. Fig 8.14 (a), (b) and (c) shows the original, the reconstructed "Lenna" from JPEG and from DWT, respectively. Fig. 8.15 shows the images for "baboon". From Table 8.2, the difference in SNR values when the same bpp rates are achieved by DWT and JPEG can hardly be observed. However from the figures shown, differences of subjective performance can be easily observed. Both images reconstructed from JPEG show block effects because of the use of the 8×8 DCT, while the images reconstructed using DWT show no such effects. As reported in the literature, our observation leads to a similar conclusion that in general DWT-based coding is superior to JPEG coding.

8.4 Conclusions

In this chapter we have constructed a nonseparable quincunx subband coding scheme by using the 2-D nonseparable diamond-shaped filter bank designed in Chapter 6. Two examples have been presented to show the coding results. Moreover, the DWT has been used to compress sample images and the results are compared with those from JPEG coding. It has been observed that DWT-based coding is in general superior to JPEG coding.

(a)

(b)

(c)

Figure 8.14: (a) Original "Lenna". (b) Reconstructed image from JPEG. (c) Reconstructed image from DWT.

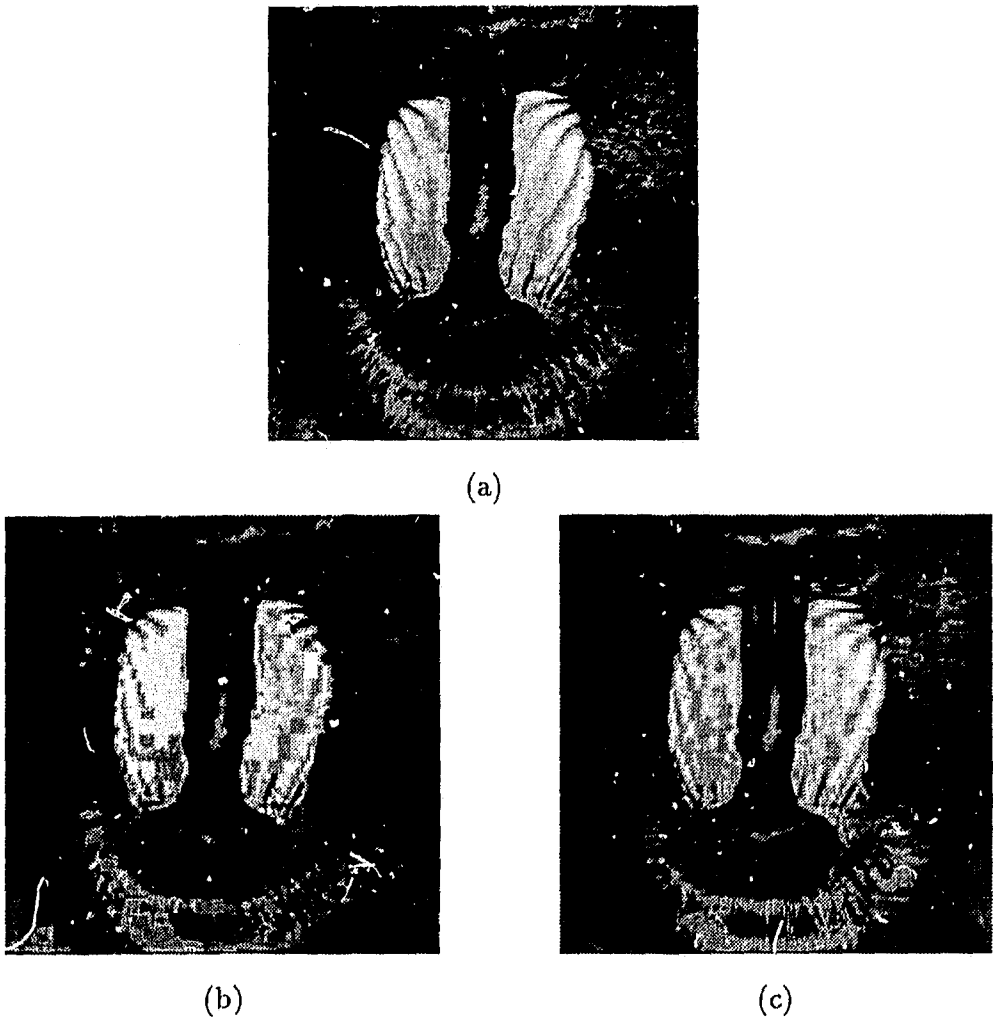

(a)

(b) (c)

Figure 8.15: (a) Original "baboon". (b) Reconstructed image from JPEG. (c) Reconstructed image from DWT.

Chapter 9

Conclusions

In this chapter the contributions of each chapter are summarized and recommendations for future research are proposed.

9.1 Summary of Contributions

Chapters 2 to 5 have concentrated on the design of a variety of 1-D and 2-D filter banks. In Chapter 2 an improved version of an iterative method for the design of two-channel conventional QMF banks has been proposed. A simple and explicit formula for the precise evaluation of the integrals involved in the objective function has been derived. This significantly reduces the design complexity and improves the performance of the QMF banks designed. A new method for the design of two-channel QMF bank with low reconstruction delay has then been proposed. Comparisons of the filter bank designed with an existing method have been made, which indicates that the proposed method has improved design efficiency and leads to low-delay QMF banks with better performances. In a case study a family of low-delay filter banks have been designed which can be used in various applications.

In Chapter 3, a new time-domain approach for the design of the same type of

QMF banks as in Chapter 2 has been proposed. Compared with the method in [12] the proposed method reduces the computational complexity significantly since no discretization is needed in the frequency-domain. This new time-domain approach has been extended to design two-channel low-delay QMF banks.

A null-space projection approach has been proposed in Chapter 4 for the design of two-channel linear phase *perfect reconstruction* QMF banks. In this approach the analysis lowpass filter was first designed by a conventional filter design method and the synthesis lowpass filter was then obtained by solving a constrained optimization problem by the null-space projection method. In addition, the null-space projection approach has been extended to design low-delay QMF banks.

In Chapter 5 a new iterative algorithm has been proposed for the design of conventional cosine-modulated QMF banks. Since the need of standard constrained or unconstrained optimization is eliminated, the algorithms have reduced computational complexity considerably. The design example presented has demonstrated that high stopband attenuation and low aliasing and amplitude distortions can be achieved by the proposed method. Furthermore, a general design method which can be used in the design of low-delay cosine-modulated QMF banks has been proposed. Again, the iterative method has been used in the design of such filter banks.

In Chapter 6 the designs of nonseparable 2-D four-channel hexagonal QMF banks and two-channel diamond-shaped QMF banks have been considered. Two design approaches have been proposed for the design of hexagonal QMF banks with improved performance. An iterative method and its improved version for the design of 2-D diamond-shaped QMF banks have been described. The method is flexible in the sense that a weighting can be adjusted to control the tradeoff between the degree of the perfect reconstruction and the frequency response of the individual

filters.

Chapters 7 and 8 of the thesis are concerned with applications of filter banks in audio and image coding. In Chapter 7 a 32-band filter bank has been designed using the iterative method proposed in Chapter 5. On comparison with the current MPEG filter bank, the filter bank designed is superior in terms of reconstruction performance and stopband attenuation. In addition, a QMF bank with about a half of reconstruction delay needed by the MPEG filter bank has been designed and evaluated. It is interesting to note that the efficient polyphase implementation can also be made available to construct a low-delay MPEG audio codec.

In Chapter 8, the diamond-shaped filter bank designed in Chapter 6 has been used to construct a subband image coding system, and several test images have been compressed using this coding system. Daubechies wavelet transform has been used in a 2-D separable multi-stage image coding system. It has been observed that in general the wavelet transform method is superior to the current JPEG standard as it eliminates the block effects on the images reconstructed.

9.2 Recommendations for Future Research

The iterative methods have been successfully used in this thesis for the design of various types of 1-D and 2-D filter banks. From the many designs carried out we are convinced that the methods are efficient, robust and lead to satisfactory designs. However, a rigorous proof of the convergence of such algorithms is still not available. We believe the search of a convergence proof is meaningful as it would provide more confidence in the algorithms and lead to insights into the quantitative relation between the convergence rate and the smoothing parameter τ used.

The low-delay QMF banks designed for 1-D two-channel and multi-channel cases are believed to be useful for real-time applications such as speech coding. In the 2-D case, low reconstruction delay can also be a useful feature in applications such as real-time image coding or progressive image transmission. The design of 2-D low-delay filter banks is believed to be an interesting topic to investigate.

In Chapter 7 it has been shown that a low-delay cosine-modulated QMF bank allows a polyphase implementation similar to the one suggested by the MPEG standard. It will be interesting to construct a MPEG audio codec using a low-delay QMF bank designed to evaluate the real compression ratio that the system can achieve and the subjective performance of the reconstructed audio signal.

Two-dimensional nonseparable filter banks have been successfully used in image and video compression. Wavelet transforms appear to be a more powerful tool for signal decomposition and coding due to their orthogonality property and available fast algorithms. However, most applications on image coding utilize *separable* 2-D wavelet transforms. Since nonseparable 2-D wavelets have more degrees of freedom they should be more efficient than their 1-D counterparts in image and video decompositions. Studies on lower-order nonseparable 2-D DWT's and their application to image coding should, therefore, be explored.

References

[1] R. E. Crochiere and L. R. Rabiner, *Multirate Digital Signal Processing.* Englewood Cliffs, NJ: Prentice-Hall, 1983.

[2] L. Rabiner and R. Schafer, *Digital Processing of Speech Signals.* Prentice-Hall, Englewood Cliffs, NJ. 1978.

[3] C. Puckette and T. Marshall, Jr, editors, Special Issue on Transmultiplexers, *IEEE Trans. on Comm*, vol. COM-30, July 1982.

[4] M. Portnoff, "Time-frequency representation of digital signals and systems based on short-time fourier analysis," *IEEE Trans. on Acoust., Speech, Signal Processing*, vol. ASSP-28, pp. 55-69, Feb. 1980.

[5] R. E. Crochiere, S. A. Webber, and J. L. Flanagan, "Digital coding of speech in subbands," *Bell Sys. Tech. J.*, vol. 55, pp. 1069-1085, Oct. 1976.

[6] A. Croisier, D. Esteban, and C. Galand, "Perfect channel splitting by use of interpolation, decimation and tree decomposition techniques," in *Proc. IEEE Int. Conf. on Information Science/Systems*, pp. 443-446, Aug. 1976.

[7] M. G. Bellanger and M. Coudreuse, "Digital filtering by polyphase network. Application to sample-rate alteration and filter banks," *IEEE Trans. on Acoust.*

Speech. and Signal Processing, pp. 109-114, April 1976.

[8] D. Esteban and C. Galand, "Application of quadrature mirror filter to split-band voice coding schemes," in *Proc. IEEE Int. Conf. Acoust., Speech, Signal Processing*, pp. 191-195, May 1977.

[9] J. D. Johnston, "A filter family designed for use in quadrature mirror filter banks," in *Proc. IEEE Int. Conf. Acoust., Speech, Signal Processing*, pp. 291-294, Mar. 1980.

[10] T. P. Barnwell, "Subband coder design incorporating recursive quadrature filters and optimum adpcm coders," *IEEE Trans. on Acoust. Speech, and Signal Processing*, vol. ASSP-30, pp. 751-765, Oct. 1982.

[11] V. K. Jain and R. E. Crochiere, "Quadrature mirror filter design in the time domain," *IEEE Trans. on Acoust., Speech, Signal Processing*, vol. ASSP-32, pp. 353-361, Apr., 1984.

[12] C.-K. Chen and J.-H. Lee, "Design of quadrature mirror filters with linear phase in the frequency domain," *IEEE Trans. Circuits Syst.*, vol. 39, pp. 593-605, Sept. 1992.

[13] M. J. T. Smith and T. P. Barnwell, III, "A procedure for designing exact reconstruction filter banks for tree structured subband coders," in *Proc. IEEE Int. Conf. Acoust., Speech, Signal Processing*, pp. 27.1.1 - 27.1.4, March 1984.

[14] M. J. T. Smith and T. P. Barnwell, "Exact reconstruction techniques for the tree structured subband coder," *IEEE Trans. on Acoust., Speech, Signal Processing*, vol. ASSP-34, pp. 434-441, June 1986.

[15] F. Mintzer, "Filters for distortion-free two-band multirate filter banks," *IEEE Trans Acoust., Speech, Signal Processing*, vol. ASSP-33, pp. 626-630, June 1985.

[16] M. J. T. Smith and T. P. Barnwell, III, "A unfying framework for maximally decimated analysis/synthesis systems," in *Proc. IEEE Int. Conf. Acoust., Speech, Signal Processing*, pp. 521-524. 1985.

[17] M. J. T. Smith and T. P. Barnwell, "A new filter bank theory for time-frequency representation," *IEEE Trans. on Acoust., Speech, Signal Processing*, vol. ASSP-35, pp. 314-327, March 1987.

[18] M. Vetterli, "Filter banks allowing perfect reconstruction," *Signal Processing*, vol. 10, pp. 219-244, April 1986.

[19] P. P. Vaidyanathan, "Theory and design of M-channel maximally decimated quadrature mirror filters with arbitrary M, having perfect reconstruction property," *IEEE Trans. on Acoust., Speech, Signal Processing*, vol. ASSP-35, pp. 476-492, Apr. 1987.

[20] T. Q. Nguyen and P. P. Vaidyanathan, "Maximally decimated perfect-reconstruction FIR filter banks with pairwise mirror-image analysis (and synthesis) frequency response," *IEEE Trans. on Acoust., Speech, Signal Processing*, vol. 36, pp. 693-705, May 1988.

[21] P. P. Vaidyanathan, T. Q. Nguyen, Z. Doganata, and T. Saramaki, "Improved techniques for design of perfect reconstruction property," *IEEE Trans. on Acoust., Speech, Signal Processing*, vol. ASSP-37, pp. 1042-1056, July 1989.

[22] B.-R. Horng and A. N. Willson, Jr., "Lagrange multiplier approaches to the design of two-channel perfect-reconstruction linear-phase FIR filter banks," *IEEE Trans. on Signal Processing*, vol. 40, pp. 364-374, Feb. 1992.

[23] P. Chu, "Quadrature mirror filter design for an arbitrary number of equal bandwidth channels," *IEEE Trans. on Acoust., Speech, Signal Processing*, pp. 203-218, Feb. 1985.

[24] R. E. Crochiere, R. Cox, and J. Johnston, "Real-time speech coding," *IEEE Trans. on Communications*, vol. COM-30, pp. 621-634, April 1982.

[25] H. Nussbaumer, "Pesudo QMF filter bank," *IBM Technical Disclosure Bulletin*, 1981.

[26] J. H. Rothweiler, "Polyphase quadrature filters — A new subband coding technique," in *Proc. IEEE Int. Conf. ASSP* (Boston, MA), pp. 1280-1283, 1983.

[27] ISO/IEC 11172-3, "Coding of moving pictures and associated audio for digital storage at up to about 1.5 Mbit/s - Part 3: Audio," ISO/IEC, Switzerland, Aug. 1993.

[28] J. Mason and Z. Picel, "Flexible design of computationally efficient nearly perfect QMF filter banks," *IEEE Int. Conf. ASSP* (Tampa, FL), pp. 14.7.1-14.7.4, Mar. 1985.

[29] P. P. Vaidyanathan, *Multirate Systems and Filter Banks*. Englewood Cliffs, NJ: Prentice Hall, 1993.

[30] R. D. Koilpillai and P. P. Vaidyanathan, "A spectral factorization approach to pseudo-QMF design," in *Proc. Int. Symp. Circuits Syst.*, Singapore, May 1991.

[31] R. D. Koilpillai and P. P. Vaidyanathan, "Cosine-modulated QMF banks satisfying perfect reconstruction," *IEEE Trans. Signal Processing*, vol. 40, pp. 770-783, April 1992.

[32] H. S. Malvar, "Extended lapped transforms: properties, applications, and fast algorithms," *IEEE Trans. Signal Processing*, vol. 40, pp. 2703-2714, Nov. 1992.

[33] T. Q. Nguyen, "Near-perfect-reconstruction pseudo-QMF banks," *IEEE Trans. on Signal Processing*, vol. 42, pp. 65-75, Jan. 1994.

[34] K. Nayebi, T. P. Barnwell, III, and M. J. T. Smith, "Time-domain filter bank analysis: A new design theory," *IEEE Trans. on Signal Processing*, vol. 40, pp. 1412-1429, June 1992.

[35] K. Nayebi, T. P. Barnwell, III, and M. J. T. Smith, "Low delay QMF banks: design and evaluation," *IEEE Trans. on Signal Processing*, vol. 42, pp. 24-31, Jan. 1994.

[36] T. Q. Nguyen, "A class of generalized cosine-modulated filter bank," in *Proc. Int. Symp. Circuits Syst.*, San Diego, pp. 943-946, May 1992.

[37] K. Nayebi, T. P. Barnwell, III, and M. J. T. Smith, "On the design of FIR analysis-synthesis filter banks with high computational efficiency," *IEEE Trans. on Signal Processing*, vol. 42, pp. 825-833, April 1994.

[38] M. Vetterli, "Multi-dimensional sub-band coding: some theory and algorithms," *Signal Processing*, vol. 6, pp. 97-112, April 1984.

[39] J. W. Woods and S. D. O'Neil, "Subband coding of images," *IEEE Trans. Acoust., Speech, Signal Processing*, vol. ASSP-34, pp. 1278-1288, Oct. 1986.

[40] M. J. T. Smith, R. M. Mersereau, and T. P. Barnwell, III, "Exact reconstructing recursive filter banks for subband image coding," in *Proc. Miami Technicon*, pp. 121-124, Oct. 1987.

[41] T. Ramstad, "IIR filterbank for subband coding of images," in *Proc. IEEE Int. Sym. Circuits and Systems* pp. 827-830, 1988.

[42] M. J. T. Smith and S. L. Eddins, "Analysis/synthesis techniques for subband image coding," *IEEE Trans. on Acoust., Speech, Signal Processing*, vol. 38, pp. 1446-1456, Aug. 1990.

[43] E. P. Simoncelli and E. Adelson, "Non-separable extension of quadrature mirror filters to multiple dimension," *Proc. IEEE*, vol.78, pp. 652-663, April 1990.

[44] R. Ansari, H. P. Gaggioni, and D. J. LeGall, "HDTV coding using a non-rectangular subband decomposition," *SPIE Visual Communication and Image Processing'88*, vol. 1001, pp. 821-825, 1988.

[45] J. W. Woods ed., *Subband Image Coding.* Kluwer Academic Publishers, 1991.

[46] I. A. Shah and A. A. C. Kalker, "Theory and design of multidimensional QMF sub-band filters from 1-D filters and polynomials using transforms," *IEE Proceedings-I*, vol. 140, no. 1, pp. 67-71, Feb. 1993.

[47] D. B. H. Tay and N. G. Kingsbury, "Flexible design of multidimensional perfect reconstruction FIR 2-band filters using transformations of variables," *IEEE Trans. Image Processing*, vol. 2, pp. 466-481, Oct. 1993.

[48] E. Viscito and J. P. Allebach, "Design of perfect reconstruction multi-dimensional filter banks using cascaded Smith form matrices," in *Proc. IEEE*

Int. Symp. Circuits and Systems, pp. 831-834, June. 1988.

[49] E. Dubois, "The sampling and reconstruction of time-varying imagery with application in video systems," *Proc. of IEEE*, vol. 73, pp. 502-522, April 1985.

[50] R. M. Mersereau and T. C. Speake, "The processing of periodically sampled multidimensional signals," *IEEE Trans. Acoust., Speech, Signal Processing*, vol. ASSP-31, pp. 188-194, Feb. 1983.

[51] E. Viscito and J. P. Allebach, "The analysis and design of multidimensional FIR perfect reconstruction filter banks for arbitary sampling lattices," *IEEE Trans. Acoust., Speech, Signal Processing*, vol. 38, pp. 29-41, Jan. 1991.

[52] H. Scheuermann and H. Gockler, "A comprehensive survey of digital transmultiplexing methods," *Proc. IEEE*, vol. 69, pp. 1419-1450, Nov. 1981.

[53] Y. C. Lim, J.-H. Lee, C.-K. Chen, and R. H. Yang, "A weighted least squares algorithm for quasi-equiripple FIR and IIR digital filter design," *IEEE Trans. Signal Processing*, vol. 40, pp. 551-558, Mar. 1992.

[54] Y. C. Lim, R. H. Yang, and S.-N. Koh, "The design of weighted minimax quadrature mirror filters," *IEEE Trans. Signal Processing*, vol. 41, pp. 1780-1789, May 1993.

[55] A. Antoniou, *Digital Filters: Analysis, Design, and Applications.* Second Edition, New York : McGraw-Hill, 1993.

[56] T. Q. Nguyen and P. P. Vaidyanathan, "Two-channel perfect-reconstruction FIR QMF structures which yield linear-phase analysis and synthesis filters,"

IEEE Trans. on Acoust., Speech, Signal Processing, vol. 37, pp. 466-690, May 1989.

[57] R. Fletcher, *Practical Methods of Optimization.* Second Edition, New York: John Wiley, 1987.

[58] C. Charalambous, "The performance of an algorithm for minimax design of two-dimensional linear phase FIR digital filters," *IEEE Trans. Circuits and Syst.*, vol. CAS-32, pp. 1016-1028, Oct. 1985.

[59] W.-S. Lu and A. Antoniou, *Two-Dimensional Digital Filters.* New York : Marcel Dekker,Inc., 1992

[60] K. Brandenburg and G. Stoll, "The ISO/MPEG-audio codec: A generic standard for coding of high quality digital audio," 92nd AES Convention, Vienna (March 1992). Preprint 3336.

[61] P. Noll, "Wideband speech and audio coding," *IEEE Communication Magazine*, pp. 34-44, Nov. 1993.

[62] W. F. Schreiber, C. F. Knapp, and N. D. Kay, "Synthesis highs, an experimental TV bandwidth reduction system," *Journal of the SMPTE*, vol. 68, pp. 525-537, Aug. 1959.

[63] H. Gharavi and A. Tabatabai, "Subband coding of monochrome and color images," *IEEE Trans. on Circuits and Systems*, vol. 35, pp. 207-214, Feb. 1988.

[64] S. G. Mallat, "A theory for multiresolution signal decomposition: the wavelet representation," *IEEE Trans. Pattern Anal. Machine Intell.*, vol. 11, pp. 674-693, July 1989.

[65] S. G. Mallat, "Multifrequency channel decompositions of images and wavelet models," *IEEE Trans. Acoust. Speech, Signal Processing*, vol. 37, pp. 2091-2110, Dec. 1989.

[66] I. Daubechies, "Ten Lectures on Wavelets," SIAM, CBMS series, April 1992.

[67] W. H. Press, S. A. Teukolsky, W. T. Vetterling and B. P. Flannery, *Numerical Recipes in C*. Second Edition, Cambridge University Press, Cambridge, UK, 1992.

[68] A. E. Cetin, "A multiresolution monrectangular wavelet representation for two-dimensional signals," *Signal Processing*, vol. 32, pp. 343-355, June 1993.

[69] R. H. Jonsson and R. M. Mersereau, "Efficient motion-oriented filter banks for video coding," in *Proceedings of ISCSSP 93*, pp. 639-642, Chicago 1992.

[70] G. Karlsson and M. Vetterli, "Three dimensional subband coding of video," *Proceedings of ICASSP 88*, New York, Apr. 1988, pp. 1100-1103

[71] E. Chang and A. Zakhor, "Subband video coding based on velocity filters," *Proceedings of ISCSSP 92*, pp. 2288-2291, 1992.

[72] M. G. Bellanger and J. L. Daguet, "TDM-FDM transmultiplexer: Digital polyphase and FFT," *IEEE Trans. Commun.*, vol. COM-22, pp. 1199-1204, Sept. 1974.

[73] Z. Doganata, P. P. Vaidyanathan, and T. Q. Nguyen, "General synthesis procedure for FIR lossless transfer matrices, for perfect reconstruction multirate filter bank applications," *IEEE Trans. on Acoust., Speech, Signal Processing*, vol. ASSP-36, pp. 1561-1574, Oct. 1988.

[74] Y. F. Dehery, M. Lever, and P. Urcun, "A MUSICAM source codec for digital audio broadcasting and storage," in *Proc. IEEE Int. Conf. on Acoust. Speech and Signal Processing*, pp. 3605-3608, 1991.

[75] K. Konstantinides, "Fast subband filtering in MPEG audio coding," *IEEE Signal Processing Letters*, vol. 1, No. 2, pp. 26-28, Feb. 1994.

[76] M. Rabbani and P. W. Jones, *Digital Image Compression Techniques*. Bellingham, 1991.

[77] J. Kovacevic, M. Vetterli, and G. Karlsson "Design of multidimensional filter banks for non-separable sampling," in *Proc. IEEE Int. Conf. Circuit and System*, pp. 2004-2007, 1990.

[78] J. Kovacevic and M. Vetterli, "Nonseparable multidimensional perfect reconstruction filter banks and wavelet bases for R^n," *IEEE Trans. Info. Theory*, vol. 38, pp. 533-554, March 1992.

[79] U. Heute and P. Vary, "A digital filter bank with polyphase network and FFT hardware: measurements and applications," *Signal Processing*, vol. 3, pp. 307-319, 1981.

[80] G. Pirani and V. Zingarelli, "An analytical formula for the design of quadrature mirror filters," *IEEE Trans. on Acoust., Speech, Signal Processing*, vol. ASSP-32, pp. 645-648, June 1984.

[81] M. J. T. Smith and S. L. Eddins, "Subband coding of images with octave band tree structures," in *Proc. IEEE Int. Conf. Acoust., Speech, Signal Processing*, pp. 1382-1385, April 1987.

[82] S. Sunder and R. P. Ramachandran, "A least-square design of nonrecursive filters satisfying prescribed magnitude and phase specifications," *IEEE Int. Sym. Circuits and Sys.*, Chicago, Michigan, pp. 335-338, May 1993.

[83] P. P. Vaidyanathan, "Multirate digital filters, filter banks, polyphase network, and applications: A tutorial," *Proc. IEEE*, vol. 78, pp. 56-93, Jan. 1990.

[84] M. Vetterli, "Perfect transmultiplexers," in *Proc. IEEE Int. Conf. Acoust., Speech, Signal Processing*, pp. 2567-2570, April 1986.

VITA

Surname: Xu | Given Name: Hua

Place of Birth: Hangzhou, China | Date of Birth: August 27, 1964

Educational Institutions Attended:

University of Victoria, Canada	1991 to 1995
Southeast University, China	1988 to 1991
Tsinghua University, China	1983 to 1988

Degrees Awarded:

M.Eng.	Southeast University, China	1991
B.Eng.	Tsinghua University, China	1988

Publications:

Refered journal publication

1. H. Xu, W.-S. Lu, and A. Antoniou, "Improved iterative methods for the design of quadrature-mirror filter banks," Accepted by *Trans. on Circuits and Systems, part II.*

2. H. Xu, W.-S. Lu, and A. Antoniou, "Efficient design of cosine-modulated QMF banks by an iterative method," Under second review by *Trans. on Signal Processing.*

3. H. Xu, W.-S. Lu, and A. Antoniou, "A direct method for the design of 2-D nonseparable diamond-shaped filter banks," *submitted to IEE*, Jan. 1995.

Refered conference publications

1. H. Xu, W.-S. Lu, and A. Antoniou, "A new approach for the design of FIR analysis-synthesis filter banks with short reconstruction delays," *Proc. of Canadian Conf. on Elec. and Comp. Eng.*, pp. 31-34, Sept. 1993.

2. H. Xu, W.-S. Lu, and A. Antoniou, "A new design of 2-D nonseparable hexagonal quadrature-mirror filter banks," *Proc. of Canadian Conf. on Elec. and Comp. Eng.*, pp. 35-38, Sept. 1993.

3. H. Xu, W.-S. Lu, and A. Antoniou, "Improved methods for the design of 1-D and 2-D QMF banks," *Proc. IEEE Int. Symp. Circuits and Syst.*, Vol. 2, pp. 153-156, May 1994.

4. H. Xu, W.-S. Lu, and A. Antoniou, "An iterative algorithm for the design of 2-D nonseparable diamond-shaped filter banks," *Proc. of 37th Midwest Symp. Circuits and Syst.*, pp. 785-788, Aug. 1994.

5. H. Xu, W.-S. Lu, and A. Antoniou, "A novel time-domain approach for the design of quadrature mirror filter banks," *Proc. of 37th Midwest Symp. Circuits Syst.*, pp. 1032-1035, Aug. 1994.

6. H. Xu, W.-S. Lu, and A. Antoniou, "A New approach for the design of low-Delay quadrature mirror filter banks," *Proc. of 28th Asilomar Conf on Signals, Syst. and Computers*, pp. 1001-1004, Oct. 1994.

7. H. Xu, W.-S. Lu, and A. Antoniou, "Design of perfect reconstruction QMF banks by a null-space-projection method," *Proc. of IEEE Int. Symp. Circuits and Syst.*, pp. 965-968, May, 1995.

8. H. Xu, W.-S. Lu, and A. Antoniou, "An efficient algorithm for the design of multi-channel pseudo cosine modulated FIR filter banks," *accepted by 38th Midwest Symp. Circuits and Syst.*, Aug. 1995.

9. H. Xu, W.-S. Lu, and A. Antoniou, "low-delay QMF banks with equiripple complex reconstruction error," *accepted by 38th Midwest Symp. Circuits and Syst.*, Aug. 1995.

10. W.-S. Lu, H. Xu, and A. Antoniou, "An algebraic method for the design of generalized QMF banks," *accepted by 29th Asilomar Conf on Signals, Syst. and Computers.*, Oct. 1995.

PARTIAL COPYRIGHT LICENSE

I hereby grant the right to lend my dissertation to users of the University of Victoria Library, and to make single copies only for such users or in response to a request from the Library of any other university, or similar institution, on its behalf or for one of its users. I further agree that permission for extensive copying of this dissertation for scholarly purposes may be granted by me or a member of the University designated by me. It is understood that copying of this dissertation for financial gai' shall not be allowed without my written permission.

Title of Dissertation :

EFFICIENT DESIGN METHODS FOR MULTIRATE FILTER BANKS AND THEIR APPLICATIONS

Author: _____

Hua Xu

August 22, 1995